THE PROCEEDINGS OF
THE PHYSICAL SOCIETY
Section A

VOL. 64, PART 4 1 April 1951 No. 376 A

The Slip, Twinning, Cohesion, Growth and Boundaries of Crystals

By H. WILMAN
Imperial College, London

MS. received 26*th July* 1949, *and in amended form* 15*th September* 1950

ABSTRACT. The nature and stability of intercrystalline boundaries are discussed and conclusions as to preferred relative orientations are illustrated by ball-bearing and bubble-raft models.

Electron-diffraction evidence from crystals of layer-lattice, ionic, metallic and van der Waals (organic molecular) types is presented, showing that crystal pairs and symmetrical or unsymmetrical triplet or multiplet crystal groupings occur, having a common lattice row, but in relative azimuthal orientations at intervals agreeing with the predictions. The component crystals were thus in coherent metastable contact of the type discussed, and in some cases strong secondary elastic scattering showed that the crystals were extensively superposed on the plane which was normal to the common row.

The seven types of electron-diffraction pattern observed from such groupings, and the nature of the specimen preparation, suggest that the origin of these groupings is a mechanical deformation of the crystals during or after growth, by a process of 'rotational slip' which has not hitherto been explored or defined in nature. Such slip is directly demonstrated macroscopically as a deformation process in potassium ferrocyanide trihydrate and gypsum, the slip being produced on the planes parallel to the highly perfect cleavage.

The relation between rotational slip and the known types of translational slip and dislocation theory is indicated, and in particular the 'deformation bands' investigated especially by Barrett and his collaborators are concluded to be essentially rotational slip bands initially at low deformation, though modified by translational types of slip at higher deformation.

A valuable new insight is also provided into many observations on crystal growth and properties, especially the nature, determining conditions, stability and disorientation of crystals growing epitaxially on single crystal substrates, and into the nature of the deformation caused by unidirectional abrasion of crystals.

§ 1. INTRODUCTION

The following electron-diffraction and other results, already partly reported (Wilman 1950), lead to new considerations of the nature and origin of certain types of intercrystalline boundaries and to the macroscopic demonstration of a hitherto unexplored type of deformation of crystals, best called 'rotational slip'. Such slip can be defined as the slipping of one part of a crystal on a neighbouring part so that the two atomic or molecular sheets which slide over one another are parallel to densely populated net planes, as in translational slip, but rotationally displaced about an axis normal to their plane (with or without simultaneous translational displacement) to one of a series of definable new azimuths where metastable equilibrium can occur. These results provide an interpretation of several types of electron-diffraction patterns, an explanation of many observations on the growth and properties of crystals, and especially a new and fundamental insight into (i) the nature of epitaxial crystal growth (see also Evans and Wilman 1950), (ii) the nature of 'deformation bands' in crystals, and (iii) the deformation caused by unidirectional abrasion of a crystal.

§ 2. THEORETICAL CRYSTAL ORIENTATIONS CORRESPONDING TO METASTABLE INTERCRYSTALLINE BOUNDARIES

The lattices of two crystals of the same species, if not in the same orientation, are related by a rotation through an angle δ about a common lattice direction. The present work concerns primarily those boundaries where two crystals meet at a plane which is (*a*) normal to the common lattice direction, or (*b*) parallel to it.

(*a*) *Superposition of two crystals in different azimuths on a similar boundary face.*

One of the simplest types of intercrystalline boundary is a plane such that the net planes parallel to it in the two crystals are of the same form, though the crystals are rotated relative to each other about the common lattice direction normal to this plane. In this case a proportion of the atoms (or ions or molecules) in the contacting planes lie in potential troughs similar to those they would occupy if the two planes were superposed in the same azimuth, as in the single crystals, but most of the atoms are raised partly out of such potential depressions (Figures 1 and 2).

As Figure 2 illustrates, the atoms in one sheet which coincide with the potential troughs in the neighbouring sheet lie on a two-dimensional network. If the atomic lattice is rectangular with axes a, b, and if the two superposed sheets are rotated in opposite directions by $\delta/2$ from the parallel azimuth so that the $[u_1 v_1]$ and $[u_1 \bar{v}_1]$ rows coincide along the initial a axis direction (Figure 3 (*a*)), then

$$\tan \delta/2 = v_1 b/u_1 a; \quad D_1 = (u_1^2 a^2 + v_1^2 b^2)^{1/2} = v_1 b \operatorname{cosec} \delta/2. \qquad \ldots\ldots(1)$$

At the same time two rows $[u_2 v_2]$ and $[\bar{u}_2 v_2]$ will coincide along the initial b direction, thus

$$\tan \delta/2 = u_2 a/v_2 b; \quad D_2 = (v_2^2 b^2 + u_2^2 a^2)^{1/2} = u_2 a \operatorname{cosec} \delta/2. \qquad \ldots\ldots(2)$$

The axial ratio of the coincidence lattice is therefore

$$D_2/D_1 = (u_2/v_1)(a/b); \qquad \ldots\ldots(3)$$

thus if $v_1 = u_2 = 1$ this ratio becomes a/b, i.e. the reciprocal of that of the atomic lattice, so that the coincidence lattice is similar to the atomic lattice in each sheet but enlarged by a factor cosec $\delta/2$ and rotated by 90° from the initial azimuth of superposition. In other cases the axes D_1 and D_2 are further multiplied by v_1 and u_2 respectively. The condition for the two types of coincidences to occur simultaneously is that $u_1 u_2/v_1 v_2 = b^2/a^2$.

It will be seen that the two lattices are reflection twins of each other across their $(v \bar{u} 0)$ or $(v u 0)$ planes respectively, though the crystals themselves will only be twins if their symmetry of atomic arrangement is appropriately high.

Since the number of coincidences per unit area is a measure of the relative stability (potential energy of fitting together of the two sheets) it may be concluded that metastable equilibrium will be possible with a high order of stability at discrete relative azimuths δ corresponding to small (integral) values of u_1, v_1, u_2 and v_2. The potential energy of fitting together of the two crystals is of course partly determined by the local atomic distributions in addition to the factor expressing the effect of the relative lattice periodicities.

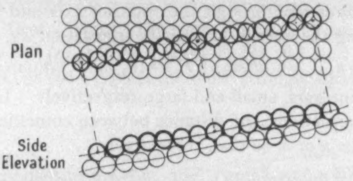

Figure 1. Fitting between an atom row forming part of an upper layer, on a similar lower layer which is in an azimuthally rotated position in which many atoms no longer lie at potential minima.

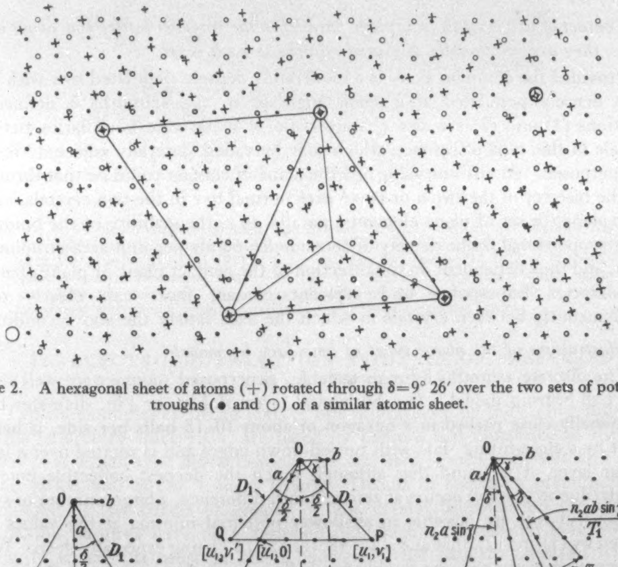

Figure 2. A hexagonal sheet of atoms (+) rotated through $\delta = 9° 26'$ over the two sets of potential troughs (● and ○) of a similar atomic sheet.

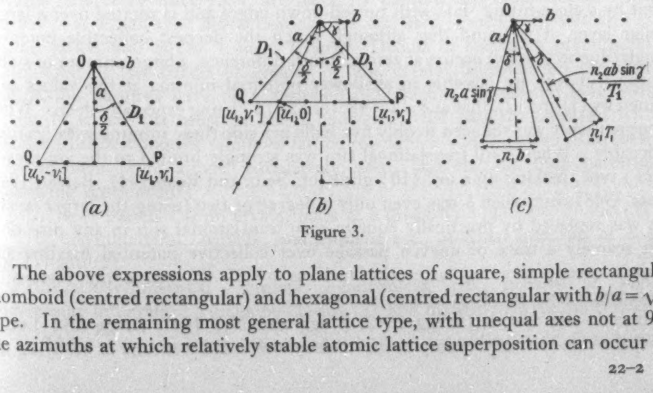

(a) (b) (c)

Figure 3.

The above expressions apply to plane lattices of square, simple rectangular, rhomboid (centred rectangular) and hexagonal (centred rectangular with $b/a = \sqrt{3}$) type. In the remaining most general lattice type, with unequal axes not at 90°, the azimuths at which relatively stable atomic lattice superposition can occur are less easily defined. If any two rows in the plane lattice are at 90° to each other or very close to it, the above expressions can be applied. If not, then even if exact coincidences are rare there may for certain values of δ be rows of approximate coincidences moderately closely distributed in the interface. At small angles δ such approximate coincidences will occur (cf. Figure 3 (*c*)) at a spacing $(n_2 ab \sin\gamma)/T_1$ in a direction through the rotation axis and normal to it in the plane of contact, along the normal to a lattice translation T_1, when

$$\delta \simeq n_1 T_1/\{(n_2 ab \sin\gamma)/T_1\} \simeq (n_1/n_2) T_1^2/ab \sin\gamma, \qquad \ldots\ldots(4)$$

where n_1 and n_2 are integers, small and large respectively. If the axes a or b are the smallest lattice translations, the distance between coincidence points is lowest when T_1 is taken to be a or b, so that, respectively,

$$\delta \simeq n_1 b/(n_2 a \sin\gamma), \quad \text{or} \quad \delta \simeq n_1 a/(n_2 b \sin\gamma). \qquad \ldots\ldots(5)$$

Green and Weigle (1948) have stated somewhat similar expressions for the *moiré* pattern of two superposed sets of parallel lines, differing slightly from the above results applicable to lattices.

(*b*) *Contact of two crystals on a plane parallel to the common lattice row about which they are rotationally displaced relative to each other.*

Provided the common axis c is a moderately densely populated row with none more densely populated at a small angle to it, the azimuths δ defined by equations (1) and (2) are also characteristic of metastable boundaries between crystals in this type of contact, which may be called 'laterally adjacent' instead of superposed. At any one value of δ the plane of contact could be that through c and the bisector of the two a or two b axes normal to c in the two crystals, or any other plane (or set of plane elements) parallel to c, the stability of the boundary being proportional to the density of coincidence points per unit area of boundary plane, and thus dependent on the direction of the contact plane or plane elements of contact. Superposed and adjacent contact faces can clearly occur simultaneously between crystals in which the axes satisfy the above conditions.

(*c*) *Illustrations of the above types of boundary by models.*

The discrete azimuths δ for metastable 'superposed' contact are well shown by a ball-bearing model. If a horizontal layer of $\frac{5}{8}$ in. or $\frac{1}{4}$ in. diameter balls, hexagonally close packed in a hexagon of about 10–15 balls per side, is held as a unit by a close-fitting 'lid' with turned-down edges and is rotated over a larger similar layer, it is found that although much the deepest collective potential trough (due to gravity) occurs at zero azimuth difference, a large number of stable positions of rest are possible in shallower potential minima at the values of δ defined by (1) and (2), that at $\delta = 27°\,48'$ (or $32°\,12'$) being especially deep. When the upper layer was reduced to only five balls per side these minima were scarcely noticeable. When $\delta = 0$ translational slip was strongly limited to the zig-zags of $\frac{1}{3}\langle 21\rangle$ type, making up a net $\langle 10\rangle$ glide (cf. Seitz and Read 1941, Barrett 1943, Zener 1948); but when δ was even only a degree or two (using the larger layers) this was replaced by practically equally easy translational slip in any direction, with scarcely a trace of uneven passage over collective potential maxima and minima except at a few azimuths such as $\delta = 27°\,48'$ where the regions of coincidence were relatively closely spaced.

Bubble-raft models (Bragg 1942, Bragg and Nye 1947, Bragg and Lomer 1949) provide not only examples of 'dislocations' and a means of studying the effect of these on electron-diffraction patterns (Dyson 1949) but also, as Figure 4 shows, illustrate well the preferred discrete azimuths at which the more stable 'laterally adjacent' intercrystal boundaries occur, and the way in which these are compatible with curved or irregular contact surfaces. In Figure 4 (ii), for example, $\delta = 22°$ (or 38° or 82°), and owing to the hexagonal symmetry there are coincident orthohexagonal $\langle 21 \rangle$ lattice translations in a collinear series IJ, JK, KL, LM and also CD of $\langle 51 \rangle$ or $\langle 13 \rangle$ type, RS of $\langle 21 \rangle$ and OQ of $\langle 10{\cdot}2 \rangle$ type. In Figure 4 (iii) $\delta = 28°$ (or 32° etc.) and CE, HJ, KL and OP are of $\langle 12 \rangle$ type and GI, HK and MO of $\langle 61 \rangle$ type at the more strongly curved general boundary.

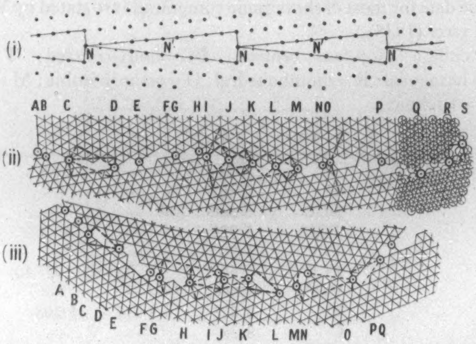
(i)
N
N
N
N
N
AB C D E FG HI J K L M NO P Q R S
(ii)
(iii)
A B C D E FG H I J K L MN O PQ

Figure 4. (i) A plane 'surface of misfit', suggested by G. I. Taylor; (ii) and (iii) bubble-raft 'crystal' junctions, drawn from Dyson's (1949) Figures 13 (*a*) and 11 (*a*) respectively ($\delta \simeq 38\frac{1}{8}°$, $[uv]=[21]$, [51], [91] or [13]; and $\delta \simeq 28°$, $[uv]=[71]$, [61] or [12] respectively, relative to orthohexagonal axes). In (iii) the lattices have a slight elastic shear causing curvature of the rows. A very small shear of this kind may occur in 'soft' crystals combined with partial relative rotational slip between successive layers.

§ 3. ELECTRON-DIFFRACTION EVIDENCE OF PREFERRED INTERCRYSTALLINE BOUNDARIES AND ROTATIONAL SLIP

Typical examples recorded (except one of graphite) by the author and others in this laboratory since 1934, are listed in Table 2 and illustrated in Figures 5 to 55*. A Finch-type diffraction camera was used (Finch and Wilman 1937) at about 60 kv. and 50 cm. camera length. Details of specimen preparation and discussion of the effects of greater or less crystal thickness on the electron-diffraction patterns have been supplied but are not reproduced here owing to limits of space. It must be stated, however, that patterns obtained with the electron beam along the common lattice row which was the axis of the rotational displacement were almost exclusively used, and that of such patterns the following types occur:

(i) Spot patterns from crystal pairs at δ given by equations (1) and (2).

(ii) 'Symmetrical' triplets, quadruplets, etc., at equal intervals of δ given by (1) and (2).

(iii) 'Unsymmetrical' triplets, quadruplets, etc., usually at regularly decreasing intervals of δ given by (1) and (2), and usually with the spots becoming progressively fainter apparently indicating thinner or laterally smaller crystal regions, or both.

---

* Most of these Figures are reproduced in the Plates, inserted at the end of the issue.

(iv) As (i) or (ii) but with additional spots due to strong secondary scattering, showing that the component crystal sheets are extensively superposed (Figures 26 (*a*) and 31) (cf. Wilman 1940).

(v) As (i) to (iii) but short or long arcs instead of spots, in (iii) often ending in a 'tailed' arc.

Table 1. Lattice constants of the materials investigated (in A. where in thick type, otherwise left in kx. where accuracy is low or doubtful). Sources of these data for most of the organic compounds are stated by Warren (1936) and Tyson (1938)

C = cubic; FC = face centred; BC = body-centred; T = tetragonal; H = hexagonal; R = rhombohedral; O = orthorhombic; M = monoclinic; Tri = triclinic

Material	Symm.	*a*	*b*	*c*	β
CdI_2	H	4·24	—	6·84	—
Graphite	H	**2·461**	—	—	—
NaCl	FCC	**5·640**	—	—	—
PbS	FCC	**5·929**	—	—	—
MgO	FCC	4·203	—	—	—
$NaNO_3$	FCR	6·48		$\alpha = 102° 40'$	
As_4O_6	FCC	11·046	—	—	—
CuO	M	4·563	5·910	5·108	99° 29′
Pb ferrocyanide	C	8·28	—	—	—
Cu, Ag, Au, Al, Pd, Pt	FCC	—	—	—	—
n–$C_{32}H_{66}$	O	7·416	4·958	∼80	—
n–$C_{20}H_{42}$	O	—	—	—	—
n–$C_{16}H_{33}OH$	M	8·80	4·90	44·2	56° 40′
n–$C_{18}H_{37}OH$	M?; O?	—	—	—	—
n–$C_{17}H_{35}I$	O?	—	—	—	—
A long-chain wax	O?	—	—	—	—
Methyl stearate	O	7·48	5·02	—	—
Stearic acid	M	—	—	—	—
Elaïdic acid	T	26·5	—	10·3	—
Ferric stearate	—	—	—	—	—
Ba stearate	H	4·85	4·85	—	—
Urotropine	BCC	7·02	—	—	—
Anthracene	M	8·58	6·02	11·18	125°
Naphthacene	Tri	7·94	6·02	13·5	67° 50′
(2.3 benzanthracene)		$\alpha = 80° 40'$		$\gamma = 92° 40'$	
1 : 2 benzanthracene	M	7·92	6·42	23·68	99°
	O				
5 Me, 1 : 2 B.A.	M	8·21	6·53	48·4	90°
	O	8·88	12·08	24·8	
5 : 6 cyclo-penteno-1 : 2 B.A.	M	12·02	8·61	13·78	103°
1 : 2, 5 : 6 dibenz-anthracene	M	6·59	7·84	14·17	103·5°
	O				
Chrysene	M	8·34	6·18	25·0	115·8°
1 : 2 benzpyrene	M	4·52	20·32	13·47	97·4°
	O	7·59	7·69	22·38	—
Me-cholanthrene	M	4·86	11·31	27·7	116·5°
	O	8·90	13·10	12·3	—

(vi) Single-crystal type of pattern but with tailed arcs extending from the spots or replacing them, showing a range of orientation of the crystals about an axis parallel to the electron beam.

(vii) Patterns of long arcs which decrease in intensity from a well-defined head and are interrupted by clear-cut gaps which correspond to a main δ interval (satisfying equations (1) or (2)) between crystal sheets meeting at a boundary of the above type (Figures 45 and 49).

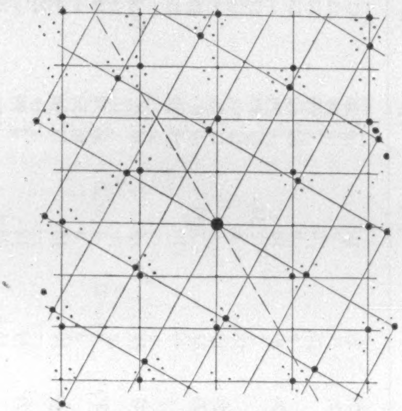

Figure 26 *b*. $C_{32}H_{66}$ doublet pattern and the spots due to secondary scattering (those not lying on the two large rectangular spot patterns).

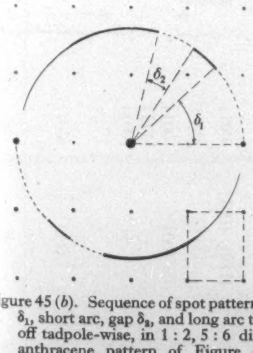

Figure 45 (*b*). Sequence of spot pattern, gap δ_1, short arc, gap δ_2, and long arc tailing off tadpole-wise, in 1 : 2, 5 : 6 dibenzanthracene pattern of Figure 45 (*a*) (inner part only, shown).

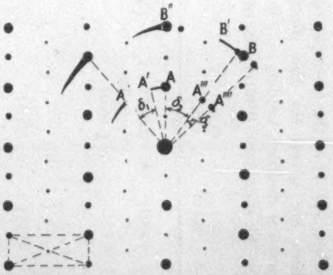

Figure 49 (*b*). Main centred-rectangle spot pattern and typical members of the rotationally displaced arcs such as AA′, BB′, tadpole-shaped arcs such as beyond A″ and B″, and displaced pattern of spots such as A‴ and A⁗.

As would be expected (cf. the familiar case of diffraction by twinned crystals), the patterns from the two crystals in contact do not differ much from the superposition of the patterns the two would yield independently, with the addition of diffracted beams attributable to secondary scattering. Even in the superposed type of contact the resulting small atomic displacements in the

Table 2. The rotational slip plane S_r and the angles δ_{obs} observed by electron diffraction in various materials, with the corresponding values of u_1/v_1 (or u_1 when $v_1 = 1$) of the lattice rows $[u_1, v_1]$ and $[u_1, -v_1]$ which coincide along the **a**′ direction in S_r at this δ; and v_2/u_2 (or v_2 when $u_2 = 1$) of the rows $[u_2, v_2]$, $[-u_2, v_2]$ which coincide along the **b**′ direction in S_r. For comparison the theoretical values are given for the more symmetrical crystals, and also the indices of the translational-slip plane S_t. A symmetrical doublet, triplet, . . . is marked by (2), (3) . . . after the mutual δ; unsymmetrical sequences are denoted by + before the successive δ intervals, otherwise each line refers to one photograph only, except where stated.

Material	S_t	S_r	δ_{obs}	u_1/v_1	v_2/u_2	δ_{calc}	Fig. No.	Nature of Specimen
Layer lattices								
CdI_2	(0001)	(0001)	6° 40′ (2)	30	10	6° 36′	11	SC
		($b' = \sqrt{3}a$	9° 27′ (2)	21	7	9° 26′	12	
		⊥ to a)	7° 14′	27	9	7° 20′	13	
			32°	6	2	32° 12′	15	
			6° 36′ (2)	30	10	6° 36′	—	
			28°	7	2·33	27° 48′	17	
			+11°	18	6	11° 0′	17	
			11° (2)	18	6	11° 0′	16	
			+ 9° 0′ (2)	22	7·33	9° 0′	16	
Graphite	(0001)	(0001)	6° 38′	30	10	6° 36′	—	Flakes
		($b' = \sqrt{3}a$						
		⊥ to a)	11° 10′ (2)	18	6	11° 0′	H. & B.	
Other ionic lattices								
NaCl	{110}, {001}	{001}	37° (or 53°)	3 (or 2)	3 (or 2)	36° 52′	18	SC
			37°	3	3	36° 52′	—	
			+11° 30′	10	10	11° 26′	—	
$NaNO_3$	{001}	{001}	—	—	—	—	25	SC
As_4O_6	—	{111}	3° 39′ (2)	54	18	3° 40′	—	E
CuO	—	{001}	5° 29′	15·0	28·4	—	19	
			+ 5° 24′	15·3	29·0	—	19	
			+ 5° 11′	15·4	29·2	—	19	
			+ 4° 49′	17·2	32·5	—	19	
			+ 5° 3′	16·3	31·0	—	19	
			6° 24′	12·9	24·5	—	19	
			+ 8° 16·5′	10·0	18·9	—	19	
Pb ferro-cyanide	—	{001}	—	—	—	—	—	SC

Material	S_t	S_r	δ_{obs}	u_1/v_1	v_2/u_2	δ_{calc}	Fig. No.	Nature of Specimen
Metals								
Cu	{111}	{001}	28°	4	4	28° 4′	—	F
			6° 41′ (4)	17	17	6° 44′	5	
			+ 9° 37′	12	12	9° 32′	5	
			9° 30′	12	12	9° 32′	—	
			+ 8°	14	14	8° 10′	—	
			8° 44′	13	13	8° 48′	8	
			+ 8° 10′ (2)	14	14	8° 10′	8	
Ag	{111}	{001}	37°	3	3	36° 52′	—	F
			37°	3	3	36° 52′	—	
			7° 5′	16	16	7° 10′	24	E
			+ 6° 24′	18	18	6° 22′	24	
Au	{111}	{001}	37°	3	3	36° 52′	—	F
Al	{111}	{001}	22° 48′	5	5	22° 38′	23	F
			+ 28°	4	4	28° 4′	23	
			14° 6′	8	8	14° 14′	22	
Pd	{111}	{001}	37°	3	3	36° 52′	20	F
			28°	4	4	28° 4′	—	
			37°	3	3	36° 52′	—	
			19°	6	6	18° 56′	—	
			9° 30′	12	12	9° 32′	—	
			16°	7	7	16° 14′	—	
			19°	6	6	18° 56′	—	
			13° (2)	9	9	12° 40′	—	
Pt	{111}	{001}	—	—	—	—	—	F
Long-chain paraffins and their derivatives								
n-$C_{32}H_{66}$	(001) ?	(001)	61° 0′	1·14	2·52	—	26*a, b*	SC
n-$C_{20}H_{42}$	(001) ?	(001)	61°	1·14	2·52	—	—	SC
n-$C_{16}H_{33}OH$	(001) ?	(001)	4° 36′ (2)	$17{\cdot}1_7$	$35{\cdot}9_8$	—	31	SC
			+ 3° 49′	20·76	43·5	—	31	
			4° 34′	17·0	36·6	—	33	
			+ 5° 55′	13·2	28·4	—	33	
			11° 56′	6·55	$13{\cdot}9_5$	—	32	
			30° 50′	2·48	5·30	—	—	

Table 2 (*cont.*)

Material	S_t	S_r	δ_{obs}	u_1/v_1	v_1/u_2	δ_{calc}	Fig. No.	Nature of Specimen
Long-chain paraffins and their derivatives (cont.)								
n–$C_{18}H_{37}OH$	(001) ?	(001)	7° 19′	10·55	22·9	—	35	SC
			40° 8′	1·87	4·00	—	—	
			40°	1·88	4·00	—	36	
			40°	1·88	4·00	—	—	
			+ 2° 38′	29·8	63·4	—	—	
			30°	2·54	5·47	—	37	
n–$C_{17}H_{35}I$	(001)	(001)	8° 28′	10·25	22·0	—	34	SC
A long-chain wax	(001)	(001)	28° 44′	2·56	6·04	—	39	SW
			+21° 34′	2·91	8·02	—	39	
			11° 20′	7 45	15·05	—	40	
			+ 8° 6′	$10{\cdot}5_8$	21·1	—	40	
Methyl stearate	(001)	(001)	(61°)	—	—	—	—	SC
Stearic acid	(001)	(001)	—	—	—	—	—	SC
Elaïdic acid	—	(001)	5° 56′	$12{\cdot}7_3$	29·0	—	41	SC
(or a long-chain		of a cell like	+ 8° 34′	8·9	$20{\cdot}1_5$	—	41	
paraffin impurity ?)		paraffins have	+33° 8′ (2)	2·22	$5{\cdot}0_6$	—	41	
Ferric stearate	(001)	(001)	—	—	—	—	42	SC
Ba stearate		(001)	—	—	—	—	—	
Other alkyl compounds								
Urotropine		{110}	10° 0′	7·98	4·03	—	43	SC
(Hexamethylene-tetramine)		(a, $b=\sqrt{2}a$ ⊥ to a)	+ 7° 58′	$10{\cdot}0_5$	$5{\cdot}07_5$	—	43	
Aromatic compounds								
Anthracene		(001)	29°	2·72	5·45	—	44	V
Naphthacene		(001)	6° 10′	$(n_1/n_1'=14{\cdot}0;\ n_2/n_2'=24{\cdot}5_2)$			48	SC
		($\gamma=92°\ 40'$)	+ 7° 14′	$(n_1/n_1'=11{\cdot}9_9;\ n_2/n_2'=20{\cdot}8_5)$				SC
1 : 2 benzanthracene (monoclinic)		(001)	3° 44′	26·0	36·5	—	—	SC
5Me, 1 : 2 benzanthracene		(001)	8° 54′	9·52	15·9	—	47	SC
5 : 6 cyclo-penteno 1 : 2 benzanthracene (monoclinic)		(001)	11° 55′	7·25	13·0	—	51	SC

Material	S_t	S_r	δ_{obs}	u_1/v_1	v_2/u_2	δ_{calc}	Fig. No.	Nature of Specimen
Aromatic compounds (cont.)								
1 : 2, 5 : 6. dibenz-	—	(001)	43°	3·02	2·13	—	45 *a*, *b*	SC
anthracene (monoclinic)			22° 20′	6·05	4·31	—	45	
Chrysene	—	(001)	—	—	—	—	46	SC
1 : 2 benzpyrene	—	(001)	3° 16′	34·9	35·3	—	43	SC
(rhombic)			+ 3° 30′	32·5	33·0	—	43	
			19° 20′	5·96	5·96	—	54	
			+ 1° 42′	(67·0)	(67·0)	—	54	
			+ 2° 8′	(53·6)	(53·6)	—	54	
			+ 3° 30′	(33·7)	(32·7)	—	54	
Methyl-cholanthrene (rhombic)	—	(001)	—	—	—	—	—	SC
" Dispersol Fast	—	—	26° 36′	1·52	$11{\cdot}4_7$	—	49 *a*, *b*	SC
Scarlet "		($a' \perp b'$,	+38° 2′	1·07	7·97	—	49 *a*, *b*	
		$a'/b' = 2{\cdot}713$)	+ 9° 16′	4·53	(33·6)	—	49 *a*, *b*	

F = beaten foil, thinned by etching.
SC = crystallized from solution on a collodion film.
SW = crystallized from solution on a water surface.
V = condensed from the vapour.
E = epitaxial orientated deposit, after substrate was dissolved.

Note 1.—Wesselowski and Wassiliew (1934) observed x-ray arc patterns from graphite indicating a mean 30° notation (0001).

Note 2.—Figure 27 is analogous to Figure 26 but arced, and illustrates the true origin of the pseudohexagonal arc patterns like Figure 28 by rotational slip; cf. earlier attempts to account for these, by Garrido and Hengstenberg (1932), Charlesby (1945), Brummage (1947); and see Germer and Storks (1938) and Coumoulos and Rideal (1941) on esters and salts. See also Hubbard (1945).

H. & B. = Hillier and Baker (1946).

contact region are likely to be mainly normal to the contact plane (Figure 1 and §2), i.e. parallel to the electron beam in the cases investigated here, thus causing no appreciable change in the diffraction pattern near the undeflected-beam spot. Extensive superposition of the component crystal sheets is proved in at least two cases (Figures 26(*a*) and 31) by the unusually strong spots also present due to secondary scattering, but when such spots are not detected the contact is still not necessarily (or may not be entirely) of the laterally adjacent type, and it may be partly of superposed type or even entirely so, the lack of secondary scattering being then merely due to the thinness of the two layers or their small proportion of overlap. Diffuse regions of increased intensity surrounding the arcs in intense patterns from beaten metal foils also appear to be largely due to such secondary scattering in superposed component crystal sheets.

The nature of the patterns and the observed values of δ prove that crystal groupings in contact, of one or both types considered in §2, often occur in the case of crystals grown from solution (CdI_2, NaCl, $NaNO_3$ and the organic materials), cleaved crystal flakes (graphite and CuO), single-crystal films floated off soluble substrates (As_2O_3, Ag and Pd, prepared by sublimation on to an NaCl cleavage face), beaten metal foils (Cu, Ag, Au, Al, Pt, Pd), and rolled or beaten metal surfaces after recrystallization at bright red heat (Cu, Ag, Al).

In all the examples observed the crystals had been subjected to deforming forces either deliberately (graphite, CuO, beaten or rolled metals) or inadvertently during growth (e.g. by surface tension and currents in solution, acting on tabular or dendritic crystals or growth layers on crystal faces) or after growth (for example, by forces on thin films due to contact with liquids, or by shearing of metal gauze supports, in As_2O_3, Ag and Pd). These facts and the occurrence of the above seven types of pattern all point to the conclusion that the observed crystal groupings are most simply explained as more or less extensively superposed and cohering lamellae azimuthally displaced by a rotational slip of either symmetrical or unsymmetrical type, with some simultaneous or subsequent translational slip generally also present.

Such a rotational slip, demonstrated macroscopically in §4, provides also a natural explanation of the origin of the nuclei which give rise at about 900° c. to secondary recrystallization in heavily cold-rolled sheets of metals like copper and aluminium, as observed in the present results and also those of Kronberg and Wilson (1949), who showed, indeed, that such secondary recrystallization in preferred orientations was associated with mechanical deformation at the sheared edges of their specimen sheets (cf. Evans, Layton and Wilman 1951). The cooperative small movements of atoms round the undisturbed coincident atoms which they suggested as origin (somewhat similar to those in the α–β quartz transformation which have been not very aptly referred to as a 'Drehgleitung' (Tertsch 1949)), seem much less probable than a rotational slip of lamellae as a whole.

Further support for the present rotational-slip explanation of the crystal groupings illustrated is provided by the adhesion and continued growth of two pre-existing crystals in preferred azimuths when they come together on plane faces, as was observed by Gaubert (1896) and especially by Schaskolsky and Schubnikow (1933). The last two authors shook small octahedra or cubes of alum into saturated alum solution in which a large octahedral alum crystal was immersed with one face horizontal, and found that the small octahedra sometimes adhered and continued to grow parallel to the substrate crystal and sometimes in the 60°-rotated {111}-twin position, while the small cubes tended to grow with a diagonal of the contact face parallel to an octahedral edge of the substrate crystal. Deicha (1948) reported similar groupings in NaCl crystallized from supersaturated solution.

§4. DIRECT DEMONSTRATION OF ROTATIONAL SLIP AS A DEFORMATION PROCESS IN CRYSTALS

(*a*) *Macroscopic demonstration in potassium ferrocyanide trihydrate and gypsum.*

The results of §3 not only indicate the common occurrence of rotational slip in many types of crystals—especially by the observations of symmetrical and unsymmetrical triplets and multiplets, the clear evidence of superposition of the layers in some of these cases, and the often effectively continuous sequences (sometimes interrupted) in azimuth—but they also show that it occurs on densely populated planes which are often cleavage planes or else those planes which develop in contact with and parallel to the substrate during growth of crystals from solution, and which then also usually develop as main growth faces on the crystals. Cleavage and orientation faces are largely an expression of the cohesional anisotropy, in that the binding of the atoms or molecules is particularly strong laterally within each sheet parallel to these planes, and is weaker between atoms or molecules in neighbouring sheets. In rotational slip, as in cleavage, there is a step-by-step disengagement (cf. a 'zip-fastener') of the atoms of one sheet from the potential depressions of the neighbouring sheet, beginning with the atoms furthest from the rotation axis, but the neighbouring sheets are not pulled apart (or only slightly so) and retain mutual coherence such that many of the atoms again lie in or partly in potential troughs of the adjacent sheet.

Potassium ferrocyanide trihydrate $K_4Fe(CN)_6 . 3H_2O$ and gypsum, $CaSO_4 . 2H_2O$ were therefore chosen as especially suitable for a macroscopic demonstration of rotational slip deformations, since highly perfect crystals 1–2 cm. in diameter and several millimetres thick were available and both have only one nearly perfect cleavage face (cf. Buckley 1934), while the easy translational slip and flexure parallel to these cleavage planes is already known. The transparent yellow $K_4Fe(CN)_6 . 3H_2O$ is monoclinic, $a:b:c = 0{\cdot}3936:1:0{\cdot}2943$, $\beta \doteq 90° 2'$, pseudotetragonal with base (010), and exceptionally perfect (010) cleavage (Groth 1906). Gypsum is also well known to be monoclinic with (010) as highly perfect cleavage, and its structure has been determined by x-ray diffraction (Wooster 1936, cf. de Jong and Bouman 1938).

A shear couple was applied in the suggested optimum direction, i.e. about an axis normal to the cleavage face. The couple was exerted by a frictional grip over the opposite faces held between two metal flats (paper or pitch covered) mounted in a lathe normal to the lathe axis. Figures 56 and 57 show typical results.

The transparency of the crystals was practically unimpaired except where some fractures or surface abrasion occurred locally, and where the rotation had caused a large overhang of some parts of the crystal and led to slight curving over of these regions, which tended to develop small cleavage areas between layers having different flexure. The main area of the cleavage faces remained substantially flat and the detail of initial small steps remained sharp. In the plan views of Figures 56 and 57, taken with a black glass or paper background, the step edges on the upper and lower faces can be seen inclined at the angle of rotation of the faces, but both sets are not in focus at once. Initially smooth side faces remained practically as glassy as before, to the eye, but had developed a regularly twisted shape (Figure 56(a')). This crystal shape cannot be accounted for except by a uniform relative rotational slip over each other of successive layers parallel to the cleavage plane, since the crystals were still cleavable easily on the planes parallel to the upper and lower faces, these cleavages being as smooth as initially though slightly undulating in crystals subjected to large shear (~40°/mm.).

Crystals cut to roughly cylindrical shape to avoid overhang developing during shear also showed, after the rotation, a regular plastic rotational slip, so that shallow scratches initially parallel to the cylinder axis became inclined lines at practically constant inclination to the vertical (Figures 56 (*c*) and 56 (*d*)). No appreciable change from this form of slip was noticed over a wide range of speed of shear.

A striking difference of ease of rotation was found between the ferrocyanide and the gypsum. In the ferrocyanide, pieces of the order of 1 cm. square by 2–4 mm. thick could be rotated easily with the thumb, applying only about 10 kg/cm^2 pressure to obtain the necessary frictional torque. In gypsum a much higher pressure approximately 350 kg/cm^2 had to be applied before the frictional force was sufficient to cause appreciable rotation. In still harder crystals such as mica, calcite, zinc blende, quartz, sapphire, etc. rotational slip must be correspondingly more difficult to produce.

(*b*) *Interpretation of 'deformation bands' as initially rotational-slip lamellae.*

The lamellar 'deformation bands' or 'etch bands' observed microscopically in metals are less sharply defined at low deformation than normal translational-slip bands or twin bands and are best made visible by very slow etching. They have been investigated in detail by Elam (1935, 1936), Barrett (1939, 1940, 1943, 1949), Barrett and Levenson (1939, 1940, 1941), Greninger (1938), Brick (1940), Brick and Williamson (1941), Crussard (1949) and Honeycombe (1950).

Barrett, and Barrett and Levenson demonstrated the form of these bands especially clearly and showed that (i) they are parallel to densely populated net planes, e.g. (100) and (111) in Fe, (100) and (110) in Al and Cu, which are not the normal transitional slip planes—(110), (221) or (321) in Fe, (111) in Al and Cu —nor the twin planes—(221) in Fe, (111) in Cu; (ii) when the bands are first observed their lattice is rotated by several degrees about an axis normal to the plane of the lamellae (see Barrett and Levenson 1940*); (iii) at high deformation the bands show much flexure and their relative orientations become more complex; (iv) the sub-division of crystals into such lamellae, and the changes of orientation in these, are processes which tend to lead to development of preferred orientations in heavily cold-worked metal wires or sheets.

Although Barrett and subsequent authors appear to have discussed these deformation bands only in terms of multiple translational slip on systems of the crystallographically equivalent planes (cf. Wood 1940) the author's results above (§§ 2, 3, 4(*a*)) lead to the logical conclusion that these bands originate as rotational-slip bands before translational slip has caused much orientation change, though subsequent flexure and other complex forms of translational slip modify their form and orientation extensively at high deformation. Clearly, a crystal in a polycrystalline aggregate will be liable to be acted on by non-homogeneous shear couples, and if these cause rotational slip any subsequent translational slip, being stopped at the boundary rotational-slip planes of the deformation bands, must cause lattice rotation relative to these boundaries and soon hinder further subdivision by rotational slip; thus such bands would be expected to be formed mainly in the initial stages of deformation, as is observed.

---

* They state that at 28% reduction of an Al single crystal by compression they observed "bands parallel to (010) planes, and the orientation difference across a band boundary was 3°", increasing to 8° at 50% reduction. "For both compressions the two orientations have the [010] axis in common; that is, the pole of the plane of the bands."

§ 5. THE RELATION OF ROTATIONAL SLIP TO THE FORMS OF TRANSLATIONAL SLIP AND TO DISLOCATION THEORY

From §§ 3 and 4 rotational slip is seen to be analogous in form to translational slip in that (i) it occurs on densely populated net planes, not necessarily only on the usual translational-slip planes but particularly easily on cleavage planes (cf. also Evans and Wilman 1950, Evans, Layton and Wilman 1951); (ii) as in flexural translational slip, at the end of the slip a proportion of the atoms at the interface are again in potential troughs similar to those they occupied before; (iii) the slip lamellae, as indicated by the above electron-diffraction patterns are often only about 100 A. thick (cf. also Heidenreich and Shockley 1947, 1948); and (iv) the primary slip planes tend to be regularly spaced and the slip displacements equal, i.e. 'symmetrical slip' (cf. Andrade 1935, Treuting and Brick 1942, Barrett 1944, 1947), though (v) unsymmetrical slip sometimes occurs under conditions which are at present uncertain.

With respect to translational slip, as Barrett (1939) pointed out, the development of striations on some crystal faces is not in itself a criterion for pure translational slip, since it may be due to 'deformation bands'. The unsymmetrical type of translational slip has not yet received much attention but seems to be well shown (with flexure finally, however) in a single-crystal rod of tin shown in Figure 58, illustrated by Masing and Polanyi (1923) and Polanyi (1928, Figure 7). Schmid and Boas (1935) state that the extension of the crystal was very slow. The regular decrease of thickness of the slip blocks and the extent of slip are strikingly analogous to the typical decrease of spot intensity and azimuth intervals in the asymmetrical rotational slip in § 3 (though in those of the latter examples which relate to growth from solution an explanation may also be possible in terms of dendritic growths subjected to forces which deflect the narrower growing tip progressively by rotational slip).

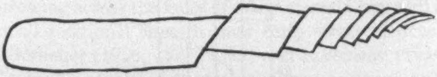

Figure 58. Form of slip bands in tin in an example observed by Polanyi (1928).

It is of interest that in the frictional analogy of slip in a pile of cards an unsymmetrical distribution of translational or rotational slip displacements can be produced in a pile of similar superposed glazed cards (or even one of crêpe paper sheets) subjected to only light normal pressure and slow displacement by tangential frictional force on the end faces; but in this case the thinner 'slip blocks' near the moving face are displaced furthest, which is opposite to the results of § 3 (unless the most displaced layers are also smaller in lateral extent) and the above example of tin. Larger pressures and speeds of slip led to a linear variation of slip displacement with height in the pile of cards, analogous to that in Figures 56 and 57 (cf. also lamellar viscous flow in liquids).

Flexural translational slip is usually described as being characteristically about an axis F normal to the translational-slip direction T, and thus parallel to the slip plane. It must obviously be possible, however, to bend a crystal about other axes parallel to the slip plane or inclined to it, and it seems likely that when the elastic limit is exceeded there may be some plastic rotational slip as well as translational slip. This possibility has not yet been tested closely (but see Cahn 1949).

Twist slip as described by Mügge (1898), Johnsen (1914) and Buerger (1930) with the translational-slip direction T as torsion axis, appears to be a special combination of translational slip and flexure of the slip planes. Closer investigation may well show that some rotational slip is produced either on the translational slip planes or on the planes normal to T.

Kinking (Mügge 1898, Friedel 1926, Brilliantow and Obreimow 1934, 1937, Orowan 1942, 1947, Crussard 1949, Barrett 1949) appears to be purely of a flexural nature and occurs when the axis of compression is roughly along the translational slip planes. The present writer finds indeed that a close analogy to Orowan's (1942, Figure 1 (*a*)) kink pairs in cadmium can be easily produced by lengthwise compression of a pile of paper strips formed by the remaining top end of a tear-off writing pad. Crussard (1949) has suggested that the change of direction at a kink may occur sharply on an atomic scale so that preferred kink angles occur and that the kink planes in cadmium shown by Orowan's figure may be $\{10\bar{1}1\}$. However, though Orowan only stated (0001) was parallel to the wire axis, it appears that the axis must have been near $\langle 100 \rangle$, since that is the direction of fastest growth in (0001) and is the translational-slip direction. Thus the kink planes could more possibly be $\{11\bar{2}2\}$, giving a kink angle $\phi = 117° 56'$ (Figure 59), which agrees reasonably well with the estimated angle 116° (Crussard's estimate was $\phi = 113°$ on one side, 118–120° on the other).

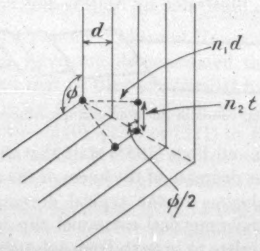

Figure 59. Possible diagrammatic section of a kink, the kink angle ϕ being then given by $\tan \phi/2 = n_1 d / n_2 t$, where n_1 and n_2 are integers.

Though kinking thus seems capable of giving rise in some cases to crystals in the 'laterally adjacent' type of contact, it seems improbable that thin but laterally extensive crystal sheets growing from solution would kink about an axis normal to their plane, except possibly in their initial stages when they were still small. Even then in many of the cases observed in §3 the rotation axes are not those which would correspond to kinking related as above to the normal translational-slip direction. Inhomogeneous shear and break up of thin crystal sheets followed by re-coalescence during growth (cf. the soap-bubble sheets, Dyson 1949) might also give 'laterally adjacent' contacts at the preferred angles defined in §2 and thus lead to electron diffraction spot patterns like some in §3, but seem unlikely to give rise to the practically continuous azimuthal sequences which yield the arc patterns observed in §3.

Like the experimental knowledge of slip, the theoretical treatment in terms of ‘ dislocations ’ also appears as yet to be rather imperfect. According to Frank (1948, 1949) the proper description for a rotation of two lattices on a like contact plane is an accumulation of screw dislocations (Cottrell 1949) in a crossed-grid array in that plane.

Van der Merwe (1950) has illustrated the necessary slight atomic displacements (laterally) from their lattice-point positions in two superposed plane atomic lattices of square type, according to such a set of dislocations. His calculation, on this basis, of the potential energy of two such superposed atomic planes in relation to the angle of displacement δ of one atomic sheet over the other, shows no minima such as were indicated by the author's ball-bearing model (§ 2) and electron-diffraction data (§ 3), and this shows that the calculations are incomplete in detail. If van der Merwe's calculated smooth variation of potential energy with δ were correct it is evident that two crystals in such superposed contact must automatically rotate into parallelism, but this is shown not to be so by the present results. It is thus suggested that two densely populated plane atomic lattices rotated over each other in contact undergo chiefly only adjustments of atomic positions normal to their initial plane array.

§ 6. THE RELATION OF ROTATIONAL SLIP TO THE GROWTH AND PROPERTIES OF CRYSTALS

(*a*) *General nature of growth.*

The results of § 3 show that rotational slip often occurs in crystals grown from solution, and is generally along the atomic or molecular layers which are first formed on the substrate and later covered by similar successive layers as main boundary faces of the growing crystals. The optically visible thick layers (cf. Bunn and Emmett 1949) growing across the faces of many crystals may well owe their origin to occasional small rotational slips in their early stages of development. The experiments of Bernauer (1926, 1927, 1929) and Rossmann (1934) on growth of ‘twisted’ and ‘spiral’ crystals suggest that vigorous stirring or agitation causes such a disturbance in the superposition of layers on the growing crystals (cf. § 3 above), which then possess abnormal optical polarization properties (as was found in paraffin crystals by Hubbard (1945), who, however, overlooked its true origin). Their illustrations appear to represent dendritic crystal forms in many cases, and it will be evident that repeated rotational slip on planes parallel to the substrate, especially across the narrow tips of the growing dendrites, could lead to the observed crystal shapes, which may correspond to the electron-diffraction patterns of ‘tailed’ arcs or spot-groups (§ 3).

In close relation to such a process, the observation by Balarew and Kolarew (1939) that a variation of rate of dissolution at crystal faces (gypsum) occurs according to the direction and speed of stirring seems explicable in terms of slip processes caused thereby (rotational or translational) in surface regions.

Some striking macroscopic twisted crystals (Spencer 1921, Frondel 1936), for example of quartz and pyrites, probably originate by a rotational-slip deformation after growth, this being made possible by the crystal being embedded in a strong retaining matrix hindering fragmentation during the torsional deformation.

Vicinal faces are explicable (Bunn and Emmett 1949) as a more or less regular terracing of superposed growth layers on main crystal faces (cf. Wyckoff 1948), but some reported cases could correspond to mosaic components related by rotational-slip contacts, e.g. (1.0.10) of galena (Hintze 1898), which is at an angle of $\tan^{-1}(1/10) \simeq 2\tan^{-1}(1/20)$ to the nearest cube face, could be really a (100) face of a mosaic component which was first formed from the main crystal by a rotational slip on (010) to the position defined by $u_1/v_1 = 20$ in equation (1).

In crystals having well-defined faces other than the rotational-slip plane, a rotational slip would cause light reflections to be elongated into streaks or, if slip were only at relatively large intervals, rows of separate reflection spots (Brilliantow and Obreimow 1934). In x-ray diffraction, similarly, the asterisms and associated trains of diffraction spots observed from some mosaic crystals (e.g. $NaNO_3$ grown from the melt, Leonhardt and Tiemeyer 1936) and in some cases of plastically deformed crystals are almost certainly due in many cases to rotational slip in the crystals.

Many other observations and properties of crystals will no doubt be clarified when considered in the light of possible presence of rotational slip.

(*b*) *Rotational slip and epitaxial crystal growth.*

The results of §§ 2–4 provide a fundamental new insight into the conditions which determine epitaxial crystal growth and its stability and degree of perfection.

(i) *The effect of cracks or steps in the substrate.* The rotational-slip results show in the clearest possible way that the existence of angles or edges of cleavage steps, whether these are macroscopic or only monatomic in height, is quite unnecessary for epitaxial orientation to occur as suggested by Thomson and Cochrane (1939) and Thomson (1948). When such steps or cracks are present they may, however, often determine the location or habit (cf. Drabble 1949) of the deposit crystals.

(ii) *The origin and nature of epitaxial growth.* The epitaxial growth of one crystal on another is thus determined by the tendency of the atoms (or ions or molecules), on arrival on the substrate, to be held in the potential troughs, which exist in a periodic array on a flat substrate crystal face, though the deposit atoms have on arrival an initial kinetic energy and they retain on the average a certain mobility over the substrate, characteristic of the nature of the deposit and substrate and the temperature of the surface. It is then to be expected that, if the temperature is not so high that recrystallization simultaneously occurs, the deposit crystals must be built up at first in a more or less strained or 'pseudomorphic' form as Finch and Quarrell (1933) found and named it. The orientation is determined by the arrangement of the first layer or so of deposit atoms or molecules in positions of lowest attainable potential energy on the substrate (Elleman and Wilman 1948) and this in turn is determined mainly but not quite entirely by that of the substrate surface layer of atoms if this is a densely populated atomic plane and other conditions are appropriate.

(iii) *Lattice relationships necessary for epitaxy.* Firstly, though crystal growth is in general a process of addition of atoms (or molecules) separately on to the first formed small groups of atoms, i.e. the crystal nuclei, whereas rotational slip involves movements of sheets of atoms (or molecules) as a whole, it is quite clear from § 3 that from the *lattice*-fitting point of view there is no hindrance to epitaxial orientations being developed which have not even one densely populated lattice row parallel to one in the substrate. However, such cases must clearly be much rarer than those with at least one densely populated row in the deposit crystal parallel to one in the substrate, as is found in practice. As Elleman and Wilman (1949) emphasized, the epitaxial orientation is in general determined by two distinct factors—initially by the fitting of the deposit atom groups with the *local* atomic distribution in the substrate surface so that low mutual potential energy is attained, then by the tendency to satisfy as far as possible the mutual fitting together of the longer range *lattice* periodicities. The above rarer case will thus mainly be expected only when the substrate and deposit crystal lattice periodicities are large and small respectively, so that the deposit crystal orientation is initiated as usual by the *local* substrate–surface atomic distribution and the crystals can grow big enough to be relatively immobile before the stresses caused by the lattice misfits tend to modify the initial nucleus orientation.

(iv) *Expitaxy of pre-existing crystals.* The rotational-slip results are largely analogous to, and further supported by, the observations of preferred azimuths of adhesion and further growth (from solution) of pre-existing crystals which had plane faces in contact with a like or unlike plane face of a larger crystal (see § 3). The necessity of considering such an origin in some cases of epitaxial growth, such as (001) KCl growth on (001) of mica, reported by Deicha (1946), has been pointed out by Royer (1948), though the present rotational-slip results show that it is in general unlikely that only one azimuthal type of orientation would result by this process.

(v) *Stability of expitaxially orientated crystals: lattice dimension relationships.* The degree of strain and stability of orientation of an epitaxial growth depends partly on the nature and degree of the lattice fitting and partly on the local atomic fitting (see (iii) above). As in the case of rotational slip, the larger the density of coincidence points (or close approximations to such) of the substrate and deposit lattices, per unit area of the interface, the stronger the adhesion of the crystal to the substrate crystal and also the more stable its orientation since there will be less strain (or more evenly distributed strain) due to the atomic misfits, and thus less tendency to disorientation by plastic deformation or by recrystallization.

Clearly from this point of view, high stability and perfection of the orientation (without recrystallization occurring) are not associated with the existence of a lattice row in the deposit crystal with a periodic spacing which is *roughly* the same as (say within 15% of) that of the parallel lattice row in the substrate. It must, on the other hand, be associated with the occurrence of rows such that x unit translations of one row *closely* approximate to y units of the parallel row, x and y being small integers. Numerous cases of this last type have been observed in this laboratory, and others have been noted occasionally elsewhere.

(vi) *Release of expitaxial strain by slip deformations.* When the deposit-crystal thickness and extent reach a certain value, dependent on the lattice constant difference, the strain must be relieved by slip at the junction region, as Frank and van der Merwe (1949) and van der Merwe (1950) pointed out and discussed. The normal crystal structure thus tends to be attained though, as is now seen more clearly, in some cases at the expense of perfection of orientation or the development of mechanical twinning, the crystals, then usually still quite small, continuing growth in the modified orientations.

The {111}-twinning in face-centred-cubic metals such as silver, formed from the vapour on alkali-halide {001} substrates of NaCl type and on metal substrates by electro-deposition, may thus arise in a sudden release of strain in the thin initially pseudomorphic crystals if these were in parallel {001} orientation. In

PbS deposits on {001} NaCl (Elleman and Wilman 1948) the {111} and {332} twinnings observed were also types which have been observed to be producible by mechanical deformation and may have arisen in this way.

Since this paper was first submitted for publication the first example of rotational slip (again on cleavage planes, cf. §4) due to expitaxial stresses has been found by Evans and Wilman (1950) in ZnO formed on zinc-blende {110} cleavage faces at 520° c. in air. At red heat no such disorientation was observed, probably because at this temperature the ZnO crystals formed underwent slip more easily, thus giving earlier releasing of the strain (and/or a recrystallization readjustment of atomic positions to more normal structure in the pseudomorphic nucleus) before the crystal size became large and much stress accumulated. A similar lack of disorientation was observed in Cu_2O formed anodically at room temperature in parallel growth on a Cu (110) face (Goswami 1950).

Other examples of directed disorientation about well-defined axes have now been found in this laboratory with the collaboration of Dr. A. Goswami (1950), Dr. M. K. Gharpurey (1950), Dr. D. M. Evans and Dr. K. Leu. In many other cases the electron-diffraction patterns show arcing at all azimuths because of the high symmetry of the substrate or deposit crystals, which leads to many different but equivalent azimuthal orientations in the deposit, or several equivalent but differently orientated possible rotational slip planes.

(*c*) *Deformation of crystals by unidirectional abrasion.*

Results indicating prominent rotational slip caused by unidirectional abrasion of crystals have been noted (Wilman 195(, Evans and Wilman 1950). A fuller description of the new results from copper and iron is given by Evans, Layton and Wilman (1951).

ACKNOWLEDGMENTS

The author wishes to thank Professor G. I. Finch for his kindness in permitting discussion of some of the electron-diffraction photographs taken in this laboratory since 1932, in addition to those recorded by the author. Acknowledgments and thanks are also especially due to Dr. J. B. Warren and Dr. J. T. Tyson for many of the photographs from organic materials and to Mr. M. M. Bluhm for Figures 12 and 16, Dr. J. R. Drabble for Figure 18, and to Mr. D. P. D. Webb for allowing reference to be made to a photograph recently obtained from arsenious oxide.

REFERENCES

ANDRADE, E. N. da C., 1935, *Report of International Conference on Physics* (London: Physical Society), **2,** 173.

BARLAREW, D., and KOLAREW, N., 1939, *Z. Kristallogr.*, **101,** 156.

BARRETT, C. S., 1939, *Trans. Amer. Inst. Min. Metall. Engrs.*, **135,** 296; 1940, *Ibid.*, **137,** 128; 1943, *The Structure of Metals* (New York and London: McGraw-Hill); 1944, *Trans. Amer. Inst. Min. Metall. Engrs.*, **156,** 62; 1947, *Phys. Rev.*, **72,** 245; 1949, in *Cold Working of Metals* (Cleveland, Ohio: Amer. Soc. Metals), p. 65.

BARRETT, C. S., and LEVENSON, L. H., 1939, *Trans. Amer. Inst. Min. Metall. Engrs.*, **135,** 327; 1940, *Ibid.*, **137,** 112; 1941, *Ibid.*, **145,** 281.

BERNAUER, F., 1926, *Z. Kristallogr.*, **64,** 505; 1927, *Fortschr. Min. Krist. Petr.*, **11,** 293; 1929, '*Gedrillte' Kristalle* (Berlin: Borntraeger).

BRAGG, W. L., 1942, *J. Sci. Instrum.*, **19,** 148.

BRAGG, W. L., and NYE, J. F., 1947, *Proc. Roy. Soc.* A, **190,** 474.

BRAGG, W. L., and LOMER, W. M., 1949, *Proc. Roy. Soc.* A, **196,** 171, 182.

Brick, R. M., 1940, *Trans. Amer. Inst. Min. Metall. Engrs.*, **137,** 193.

Brick, R. M., and Williamson, M. A., 1941, *Trans. Amer. Inst. Min. Metall. Engrs.*, **143,** 84.

Brilliantow, N. A., and Obreimow, I. W., 1934, *Phys. Z. Sowjet*, **6,** 587; 1937, *Ibid.*, **12,** 7.

Brummage, K. G., 1947, *Proc. Roy. Soc.* A, **188,** 414.

Buckley, H. E., 1934, *Z. Kristallogr.*, **89,** 221, 410.

Buerger, M. J., 1930, *Amer. Mineral.*, **15,** 45, 174, 226.

Bunn, C. W., and Emmett, H., 1946, *Nature, Lond.*, **158,** 164; 1949, *Discussions of the Faraday Society*, **5,** 132.

Cahn, R. W., 1948, *Report of Conference on Strength of Solids* (London : Physical Society), p. 46; 1949, *J. Inst. Metals*, **76,** 121.

Charlesby, A., 1945, *Proc. Phys. Soc.*, **57,** 496, 510.

Cottrell, A. H., 1949, *Progress in Metal Physics*, ed. by B. Chalmers (London : Butterworth's Scientific Publications), p. 77.

Coumoulos, G. D., and Rideal, E. K., 1941, *Proc. Roy. Soc.* A, **178,** 421.

Crussard, C., 1949, *Bull. Soc. Franc. Min.*, **68,** 174.

Deicha, G., 1946, *C. R. Acad. Sci., Paris*, **223,** 1155; 1948, *Experimentia*, **4,** 67.

Drabble, J. R., 1949, *Ph.D. Thesis* (London).

Dyson, J., 1949, *Proc. Roy. Soc.* A, **199,** 130.

Elam, C. F., 1935, *Distortion of Metal Crystals* (Oxford : Clarendon Press); 1936, *Proc. Roy. Soc.* A, **153,** 273.

Elleman, A. J., and Wilman, H., 1948, *Proc. Phys. Soc.*, **61,** 164; 1949, *Ibid.*, **62,** 344.

Evans, D. M., and Wilman, H., 1950, *Proc. Phys. Soc.* A, **63,** 298.

Evans, D. M., Layton, D. N., and Wilman, H., 1951, *Proc. Roy. Soc.* A, **205,** 17.

Finch, G. I., and Quarrell, A. G., 1933, *Proc. Roy. Soc.* A, **141,** 400.

Finch, G. I., and Wilman, H., 1937, *Ergebn. exakt. Naturw.*, **16,** 353.

Frank, F. C., 1948, *Report of Conference on Strength of Solids* (London: Physical Society), p. 46; 1949, *Discussions of the Faraday Society*, **5,** 48.

Frank, F. C., and van der Merwe, J. H., 1949, *Proc. Roy. Soc.* A, **198,** 205, 210.

Friedel, G., 1926, *Leçons de Cristallographie* (Paris : Berger–Levrault).

Frondel, C., 1936, *Amer. Mus. Novit.*, No. 829.

Garrido, J., and Hengstenberg, J., 1932, *Z. Kristallogr.*, **82,** 477.

Gaubert, P., 1896, *Bull. Soc. Franc. Min.*, **19,** 431.

Germer, L. H., and Storks, K. H., 1938, *J. Chem. Phys.*, **6,** 280; 1939, *Phys. Rev.*, **55,** 648.

Gharpurey, M. K., 1950, *Ph.D. Thesis* (London).

Goswami, A., 1950, *Ph.D. Thesis* (London).

Green, T. A., and Weigle, J., 1948, *Helv. Phys. Acta*, **21,** 217.

Greninger, A. B., 1938, *Trans. Amer. Inst. Min. Metall. Engrs.*, **128,** 369.

Groth, P., 1906, *Chemische Kristallographie*, I (Leipzig : Engelmann), p. 325.

Heidenreich, R. D., and Shockley, W., 1947, *J. Appl. Phys.*, **18,** 1029; 1948, *Report of Conference on Strength of Solids* (London : Physical Society).

Hillier, J., and Baker, R. F., 1946, *J. Appl. Phys.*, **17,** 12.

Hintze, C., 1898–1905, *Handbuch d. Mineralogie*, **1**/1, 460.

Honeycombe, R. W. K., 1950, *Proc. Phys. Soc.* A, **63,** 672.

Hubbard, B., 1945, *Amer. Mineral.*, **30,** 645.

Johnsen, A., 1914, *Jahrb. Radioaktivität u. Elektronik*, **11,** 226.

de Jong, W. F., and Bouman, J., 1938, *Z. Kristallogr.*, **100,** 275.

Kronberg, M. L., and Wilson, F. H., 1949, *J. Metals*, **1,** 501.

Leonhardt, I., and Tiemeyer, R., 1936, *Z. Phys.*, **102,** 781.

Masing, A., and Polanyi, M., 1923, *Ergebn. exakt. Naturw.*, **2,** 177.

van der Merwe, J. H., 1950, *Proc. Phys. Soc.* A, **63,** 616.

Mügge, O., 1898, *Neues Jahrb. Mineral. Geol. Palaeont.*, **1,** 71.

Orowan, E., 1942, *Nature, Lond.*, **149,** 643; 1947, *Symposium on Internal Strains in Metals and Alloys* (London : Institute of Metals), p. 47.

Polanyi, M., 1928, *Trans. Faraday Soc.*, **24,** 72.

Rossmann, E., 1934, *J. Soc. Chem. Ind., Lond.*, **53,** 135.

Royer, L., 1948, *C.R. Acad. Sci., Paris*, **226,** 262.

Schaskolsky, M., and Schubnikow, A., 1933, *Z. Kristallogr.*, **85,** 1.

SCHMID, E., and BOAS, W., 1935, *Kristallplastizität* (Berlin: Springer); English translation 1950, *Plasticity of Crystals* (London: Hughes), p. 151.
SEITZ, F., and READ, T. A., 1941, *J. Appl. Phys.*, **12**, 100, 170, 470, 538.
SPENCER, L. J., 1921, *Mineral. Mag.*, **19**, 263.
TERTSCH, H., 1949, *Die Festigkeitserscheinungen der Kristalle* (Vienna: Springer).
THOMSON, G. P., 1948, *Proc. Phys. Soc.*, **61**, 403.
THOMSON, G. P., and COCHRANE, W., 1939, *Theory and Practice of Electron Diffraction*, (London: Macmillan), p. 175.
TREUTING, R. G., and BRICK, R. M., 1942, *Trans. Amer. Inst. Min. Metall. Engrs.*, **147**, 128.
TYSON, J. T., 1938, *Ph.D. Thesis* (London).
WARREN, J. B., 1936, *Ph.D. Thesis* (London).
WESSELOWSKI, W. S., and WASSILIEW, K. W., 1934, *Z. Kristallogr.*, **89**, 494.
WILMAN, H., 1940, *Proc. Phys. Soc.*, **52**, 323; 1950, *Nature, Lond.*, **165**, 321.
WOOD, W. A., 1940, *Proc. Phys. Soc.*, **52**, 110.
WOOSTER, W. A., 1936, *Z. Kristallogr.*, **94**, 375.
WYCKOFF, R. W. G., 1948, *Acta Cryst.*, **1**, 292.
ZENER, C., 1948, *Elasticity and Anelasticity of Metals* (Chicago: University Press).

The Variation with Temperature of the Electrical Properties of a Degenerate Electronic Semiconductor as exemplified by Cadmium Oxide*

BY R. W. WRIGHT
Physics Department, University College, Ibadan, Nigeria

Communicated by J. P. Andrews; MS. received 20th April 1950, and in amended form 13th September 1950

ABSTRACT. Strong strip specimens are prepared from CdO powder such that they possess an electrical conductivity of the order of 300 $\mathrm{ohm^{-1}cm^{-1}}$ at room temperature. Simultaneous measurements of the Hall constant R and the electrical conductivity σ are made throughout the temperature range 0–500° C., and the thermoelectric power dE/dT is measured immediately afterwards on the same specimen. The properties are found to resemble those of a metal: R is found to have a constant value independent of the temperature. dE/dT is approximately 60 μv/deg. C. at room temperatures, whilst σ decreases with temperature, its value at 500° C. being roughly half that at 0° C.

The theory of degenerate semiconductors is developed, and since the values of R indicate that there is a constant number of free electrons in each specimen, this result is incorporated into the comparison of the theory with the experimental results. Satisfactory agreement is obtained between theory and experiment. Agreement is also obtained when the theory is compared with results obtained by another investigator for the thermoelectric power of CdO. The approximate form of the theory predicts that the thermoelectric power and the resistivity should be directly proportional to the absolute temperature. The experimental results are found to confirm this. CdO behaves as an excess degenerate semiconductor, with properties strongly resembling those of a metal.

§1. INTRODUCTION

SEMICONDUCTORS may be defined as " materials whose conductivity is due to impurities or non-stoichiometric excesses of one or other of the components of the crystal lattice ". Purification (removal of defects from the lattice) causes the conductivity to decrease. This definition covers a very wide range of substances which possess very varied properties. It therefore seems necessary, in this paper, to subdivide electronic semiconductors, as defined above, into two groups : (*a*) semiconducting materials which have so few electrons that the classical distribution of energy amongst the electrons may be used with an accuracy closer than 5% will be termed ' classical semiconductors ' ; (*b*) semiconducting materials which have so many free electrons that the Fermi–Dirac statistics must be applied to the electrons, will be termed ' degenerate semiconductors '.

---

* The major part of the subject matter of this paper formed part of a thesis which was accepted by London University for the degree of Ph.D.

The simple theory of semiconductors as developed by Wilson (1931 a, b, 1939) and Fowler (1933 a, b, 1936) is applicable only to classical semiconductors. It has been shown that substances such as germanium, silicon, tellurium, silicon carbide, lead sulphide, and cadmium oxide, under certain conditions must be included in amongst the degenerate semiconductors. Busch and his collaborators (1946–1947) have shown that where the free electron density in their specimens of silicon carbide causes appreciable degeneracy, the employment of the Fermi–Dirac statistics brings theory into line with experiment. Similarly, Putley's measurements (1948, 1949) on very degenerate specimens of germanium and silicon were found to be consistent with the theory, provided that the approximations of the classical theory were not introduced.

Because of its interesting electrical properties, which are totally different from those of the majority of investigated semiconductors, cadmium oxide has already been the subject of several investigations. In the majority of these only one electrical property, either conductivity or thermoelectric power, has been measured (Fischer *et al.* 1932, Andrews 1947, Andrews and Hogarth 1949). Hogarth (1948) studied both these properties, but not simultaneously, nor upon the same specimen. General conclusions drawn from such incomplete data must always remain doubtful, since the properties may vary greatly from specimen to specimen, depending upon their origin and heat treatment, and discussions of measurements on two specimens, whether of the same property or of two separate properties, must remain inconclusive.

The need for a more comprehensive investigation of cadmium oxide led to the present work, in which the Hall constant, the specific conductivity, and the thermoelectric power, with their variations with temperature, were measured, all upon the same specimen, and as far as possible simultaneously. In this way it was hoped that correlations between the properties might be attempted, and also that the theory might be developed to account for the variations. Measurements of the Hall constant especially were aimed at, since they give direct information about the conduction, and no previous account of any measurements could be found.

§ 2. PREPARATION OF THE SPECIMEN

Cadmium oxide crystals were not available for the investigation ; furthermore, cadmium forms a protective layer of oxide when oxidized, preventing further oxidation. It is possible to evaporate a thin film of cadmium upon a surface, and then oxidize it, but such a process would give all the added complications of working with thin films. It was therefore decided that a compressed and sintered specimen of CdO powder should be the subject of this investigation. The specimen was made rectangular in shape, approximately 7 cm. × 1·25 cm. × 0·1 cm., by compression in an appropriately shaped steel mould. The compression was performed by a hydraulic press, which would produce a force of about 7 tons. The powder, the purest obtainable, bound together well though the specimens produced were necessarily very brittle due to their thinness. The specimens were then sintered in the atmosphere, inside an electrical furnace, at about 720° c., for one or two days. The resultant strips of the oxide were quite strong, and gave a definite metallic ring when dropped. Furthermore, as will be shown later, the specimens, formed as above, consisted of some stable structure Cd_xO, where x is slightly greater than unity. The densities of the specimens were of the order of 6 gm/cm^3, whilst the crystal density is 8 gm/cm^3.

§3. METHOD OF MEASURING HALL CONSTANT AND CONDUCTIVITY

The apparatus used was essentially the same as that described in a previous paper (Wright and Andrews 1949) and found very successful for use in similar work upon nickel oxide. The flat specimen was held against a plate of 'Syndanio' (a type of asbestos slate) by means of the platinum electrical contacts, which consisted of two current leads at the ends of the specimen, two potential probes about 5 cm. apart on either side of the centre of the specimen along the length of the specimen, and two Hall E.M.F. point contacts on either side laterally of the centre of the specimen, about 1·25 cm. apart. The ratio of the distances apart of the potential probes and the Hall effect contacts, 4 : 1, is sufficient to eliminate the effect of size upon the Hall E.M.F. measured. The temperature was measured by means of two thermocouples, one in contact with each potential probe. The system, fixed upon a holder, between nichrome ribbon heaters, was less than 1 cm. thick, so that the poles of the water-cooled electromagnet between which it was inserted could be close together, and a magnetic field of 12·5 kilo-oersteds, virtually constant over a region 3 cm. wide, could be maintained.

The current through the specimen was produced by a source of E.M.F. in series with the specimen, a variable resistance, and a standard 0·01 ohm resistance. The current could be varied from 0·1 to 2·0 amp., but normally a current of 0·8 amp. was used, which caused very little heating in the specimen.

All air currents were carefully shielded from the specimen by enclosing the whole apparatus. To perform the measurements, the system is first allowed to attain thermal equilibrium at the required temperature, then the potential across the standard resistance is measured with the potentiometer, giving a value for the current flowing in the circuit; the potential across the potential probes is also measured and the specific conductivity calculated. The magnetic field is switched on, and the E.M.F. across the Hall effect probes is measured using the potentiometer. This is composed in the main of two components, one due to the Hall effect, and the other due to the fact that it is impossible to set the probes exactly upon an equipotential surface; the E.M.F. is therefore again measured with the magnetic field reversed, when the former contribution is reversed, but not the latter. The Hall constant may be calculated from the readings and the dimensions of the specimen.

A slow continuous change of potential of a few microvolts between the Hall contacts was found to occur after the field was reversed. The change was so very small and very slow, however, that by making instantaneous readings of the potential difference when the field is reversed this source of potential, which is due to the Ettinghausen effect, was virtually eliminated.

§4. METHOD OF MEASURING THE THERMOELECTRIC POWER

The thermoelectric power was measured by inserting the specimen unsymmetrically in a horizontal tubular furnace, so that a temperature difference of 20–40° c. existed between the ends of the specimen, as recorded by thermocouples held in firm contact with the specimen beneath the platinum potential probes, across which the thermoelectric E.M.F. was measured by the potentiometer. In obtaining reproducible results it was found to be extremely important that all air currents were excluded from the specimen by enclosing the furnace, and before any measurements were made, time had to be allowed for complete thermal equilibrium to be attained.

§5. RESULTS AND COMMENT ON THE METHOD

The essential differences between the apparatus described above and that described in a previous paper (Wright and Andrews 1949) are due to the very great differences in the specimens which were used. The specimens of CdO had resistances of about 1 ohm at room temperature, whilst at similar temperatures the specimens of NiO had resistances of the order of 10^{10} ohms. Thus the electrostatic instruments which had to be used for measuring potentials with NiO could be discarded in favour of the more accurate and easily usable potentiometer for CdO.

The object of this investigation was to take a specimen of CdO with a constant composition, i.e. constant impurity content of interstitial Cd atoms, and to examine its electrical properties. It was known, however, that CdO was unstable at about 600° c. and above ; the temperatures of the measurements were therefore restricted to below about 550° c. Above this temperature it was considered that a gradual change in the composition of the CdO would occur, a certain amount of the oxygen content being driven out of the lattice, leaving a greater excess of Cd atoms, or impurity centres. Such a change appears to be reversible, and upon cooling oxygen is replaced in the lattice from the atmosphere; this is indicated by the fact that above 600° c. the CdO changes colour to black, and upon cooling the original light brown colour returns. Thus no permanent change will be produced, and the variation of the constitution will be very difficult to allow for in the interpretation of the results. By limiting the temperature to 550° c. this difficulty is not allowed to arise.

Preliminary experiments upon the mode of conduction, by Mr. E. W. Bastin (private communication) verified the fact that the conduction in CdO obeys Ohm's law, so long as the specimen is dry; this was taken to indicate electronic conduction in the dry state. To ensure that the specimens were completely dry when used, before a series of experiments was begun, the specimen was heated to a temperature in excess of 100° c. for about 24 hours. The actual series of readings was then performed at temperatures from 0–550° c. and the readings were repeated as the specimen cooled down to room temperatures. No permanent changes were found to have resulted from an experimental run.

Two specimens were investigated thoroughly, and the results were so similar and easily reproducible, that it was considered unnecessary to repeat upon more specimens, particularly since initial measurements made upon two other specimens, which were later broken before the series could be completed, yielded similar results.

The direction of the Hall E.M.F. and the thermoelectric E.M.F. were such as to indicate conduction by negatively charged carriers, i.e. electrons. The results of the measurements of the Hall constant, specific conductivity, and thermoelectric power at various temperatures are shown graphically in Figures 1, 2, and 3.

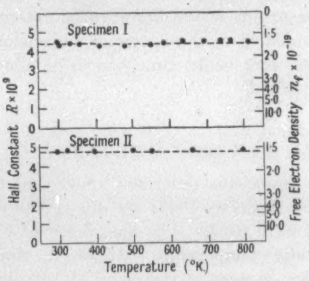

Figure 1. Values of Hall constant obtained upon two specimens of CdO at various temperatures. Corresponding values of the free electron density are shown.

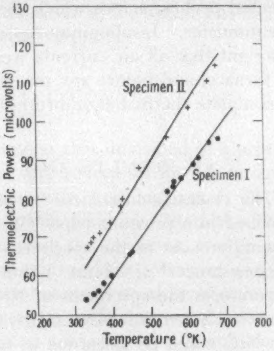

Figure 3. Values of the thermoelectric power obtained from two specimens of CdO at various temperatures. Curve for specimen I shows prediction from theory for $n_f/G^{3/2} = 7 \cdot 6 \times 10^{20}$; that for specimen II for $n_f/G^{3/2} = 5 \cdot 6 \times 10^{20}$.

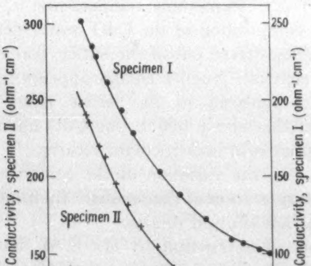

Figure 2. Values of specific conductivities of two specimens of CdO obtained at various temperatures. Curve for specimen I shows prediction from theory for $n_f/G^{3/2} = 7 \cdot 5 \times 10^{20}$; that for specimen II for $n_f/G^{3/2} = 5 \cdot 5 \times 10^{20}$.

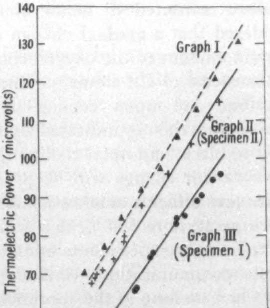

Figure 4. *Graph I.* The experimental values for the thermoelectric power obtained by Andrews are shown in relation to predicted curve for $n_f/G^{3/2} = 4 \cdot 9 \times 10^{20}$.

Graphs II, III. Experimental points obtained for the thermoelectric power of two specimens of CdO are shown in relation to the values predicted by theory from the conductivity measurements.

§6. DEVELOPMENT OF THE THEORY OF ELECTRONIC CONDUCTION IN AN IONIC LATTICE

(i) *Concentration of Free Electrons*

Consider the free electrons in the conduction band of a substance with an ionic lattice. The number of states with energies between E and $E+dE$ above the bottom of the conduction band (Seitz 1941) is

$$N(E)dE=\frac{4\pi(2m^*)^{3/2}}{\boldsymbol{h}^3}E^{1/2}dE.$$

where m^* is the effective mass of the electrons. Thus the number of free electrons with energy between E and $E+dE$ is given by $N(E)f(E)dE$, where $f(E)$ is the Fermi–Dirac function representing the probability of an electron occupying a state of energy E. The total number of free electrons present is therefore

$$n_{\mathrm{f}}=\int_0^\infty N(E)f(E)dE=\frac{4\pi(2m^*)^{3/2}}{\boldsymbol{h}^3}\int_0^\infty\frac{E^{1/2}dE}{e^{(E-E^*)/\boldsymbol{k}T}+1},$$

where E^* is the normalizing parameter of the Fermi–Dirac function, and is the chemical potential of the free electrons. Let the reduced energies be $\eta=E/\boldsymbol{k}T$, and $\eta^*=E^*/\boldsymbol{k}T$, then

$$n_{\mathrm{f}}=\frac{4\pi(2m^*\boldsymbol{k}T)^{3/2}}{\boldsymbol{h}^3}F_{1/2}(\eta^*), \qquad \ldots\ldots(1)$$

where

$$F_m(\eta^*)=\int_0^\infty\frac{\eta^m d\eta}{e^{\eta-\eta^*}+1}. \qquad \ldots\ldots(2)$$

(ii) *Mean Free Path of the Electrons*

If $1/\tau(E)$ is the probability that an electron with energy E above the bottom of the band will suffer deflection in the next unit time, then $\tau(E)$ is termed the relaxation time, and it has been shown (Fröhlich 1937, Mott and Fröhlich 1939, Davydov and Shmushkevitch 1940) that for electrons with energies E greater than $\boldsymbol{h}\nu$, where ν is the frequency of the characteristic vibrations of the lattice,

$$\tau(E)=\frac{CE^{1/2}}{e^{\boldsymbol{h}\nu/\boldsymbol{k}T}-1}, \qquad \ldots\ldots(3)$$

where

$$C=\left(\frac{2}{m^*}\right)^{1/2}\frac{\boldsymbol{h}Dva^3}{2\pi\boldsymbol{e}^4} \quad\text{and}\quad \frac{1}{D}=\frac{1}{D_+}+\frac{1}{D_-},$$

where D_+ and D_- are the masses of the positive and negative ions of the lattice, respectively, and a is the lattice constant.

The mean free path of an electron with energy E is therefore given by

$$l(E)=(2/m)^{1/2}E^{1/2}\tau(E)=l_0B\eta, \qquad \ldots\ldots(4)$$

where l_0 is a constant, and $B=\dfrac{2\boldsymbol{k}T/h\nu}{1+2/\{e^{\boldsymbol{h}\nu/\boldsymbol{k}T}-1\}}$.

The term B varies very slowly with the temperature, provided that $\boldsymbol{h}\nu/\boldsymbol{k}T$ is less than unity. For values of T much greater than $\boldsymbol{h}\nu/\boldsymbol{k}$, $B=1$ and is constant. When $T=\boldsymbol{h}\nu/\boldsymbol{k}$ then $B=1{\cdot}08$. Thus, for temperatures which are greater than $\boldsymbol{h}\nu/\boldsymbol{k}$, we may consider B as approximately constant and equal to unity.

If we further restrict ourselves to cases in which the distribution of free electrons is such that the vast majority have energies greater than $\boldsymbol{h}\nu$, as may be caused by a high concentration of free electrons, or high temperatures, or a combination of both, then we may consider that equation (4) may be used as a reasonable approximation for all the electrons.

(iii) *Electrical Conductivity*

From the Sommerfeld–Lorentz theory of electronic conduction in solids (Seitz 1941) the following expression may be obtained for the specific conductivity:

$$\sigma = -\frac{16\pi m^* \mathbf{e}^2}{3\mathbf{h}^3}\int_0^\infty lE\frac{df(E)}{dE}\,dE\,;$$

substituting for l from equation (4) and expressing in reduced energies

$$\sigma = -\frac{16\pi m^* \mathbf{e}^2 \mathbf{k} T l_0 B}{3\mathbf{h}^3}\int_0^\infty \eta^2\frac{df(\eta)}{d\eta}\,d\eta = \sigma_0 B T F_1(\eta^*). \qquad \ldots\ldots(5)$$

(iv) *Thermoelectric Power*

The Sommerfeld–Lorentz theory also leads to the following expression for the thermoelectric power Θ using reduced energies:

$$\Theta = \frac{\mathbf{k}}{\mathbf{e}}\left\{-\eta^* + \frac{\int_0^\infty l\eta^2(df/d\eta)d\eta}{\int_0^\infty l\eta(df/d\eta)d\eta}\right\}. \qquad \ldots\ldots(6)$$

Substituting from equation (4) for the mean free path we may show that

$$\Theta = \frac{\mathbf{k}}{\mathbf{e}}\left\{\frac{3}{2}\frac{F_2(\eta^*)}{F_1(\eta^*)} - \eta^*\right\}. \qquad \ldots\ldots(7)$$

(v) *The Hall Constant*

The Sommerfeld–Lorentz theory leads to the following expressions for the Hall constant R and the conductivity $\sigma(H)$ in a magnetic field H,

$$R = \frac{3}{\mathbf{e}^2}\left(\frac{m^*}{2}\right)^{1/2}\frac{1}{H}\frac{L_2}{L_1{}^2+L_2{}^2} \qquad \sigma(H) = -\frac{\mathbf{e}^2}{3}\left(\frac{2}{m^*}\right)^{1/2}\frac{L_1{}^2+L_2{}^2}{L_1},$$

where $L_1 = \frac{4\pi(2m^*)^{3/2}}{\mathbf{h}^3}\int_0^\infty \frac{El(df/dE)dE}{s^2+1}$ and $L_2 = \frac{4\pi(2m^*)^{3/2}}{\mathbf{h}^3}\int_0^\infty \frac{Els(df/dE)dE}{s^2+1}$

and $s = -\mathbf{e}lH/m^*v$ where v is the velocity of the electrons. Therefore $R\sigma(H) = -L_2/L_1H$. For weak magnetic fields s^2 is much less than 1, and $\sigma(H)$ approaches σ. Thus neglecting terms in s^2, using reduced energies, substituting from equation (4) for l, from equation (5) for σ, and introducing the number of free electrons n_f from equation (1)

$$R = \frac{1}{n_f\mathbf{e}}\frac{15}{16}\frac{F_{1/2}(\eta^*)F_{3/2}(\eta^*)}{[F_1(\eta^*)]^2} = \frac{A}{n_f\mathbf{e}}. \qquad \ldots\ldots(8)$$

(vi) *Conclusions*

Equation (1) gives the number of free electrons in any electronic semiconductor. Equations (5), (7), and (8) for the conductivity, thermoelectric power and Hall constant are applicable to conduction by electrons in ionic lattices, with the restrictions that must be applied to the use of equation (4) for the mean free path, viz. that the concentration of free electrons and the temperature must be such as to cause the majority of electronic energies to exceed $\boldsymbol{h}\nu$, and that the temperature is equal to or greater than $\boldsymbol{h}\nu/\boldsymbol{k}$, so that the factor B is approximately constant. No derivation of the equations has been previously given, but Shifrin (1944) has quoted similar results.

§7. DISCUSSION OF THE HALL CONSTANT RESULTS AND THE THEORY

Values of $F_{1/2}(\eta^*)$ and $F_{3/2}(\eta^*)$ have been tabulated by McDougall and Stoner (1938) for various values of η^*, and the author has tabulated $F_1(\eta^*)$ and $F_2(\eta^*)$ over the same range and at the same intervals. Values of the latter integrals for integral values of η^* are shown in Table 1.

Table 1. Calculated values of $F_1(\eta^*)$ and $F_2(\eta^*)$ for integral values of η^*, with the calculated values of the thermoelectric powers as predicted for 'high temperatures' from equation (8), and for 'low temperatures' from equation (11).

η^*	$F_1(\eta^*)$	$F_2(\eta^*)$	Θ_{high} (μV/°K.)	Θ_{low} (μV/°K.)
−4	0·0182	0·0366	—	558·0
−3	0·0492	0·0990	515·0	474·2
−2	0·1310	0·2662	431·9	393·2
−1	0·3387	0·7050	352·8	317·9
0	0·8225	1·8030	278·8	255·5
1	1·8062	4·3282	222·0	209·9
2	3·5135	9·5128	172·7	178·0
3	6·0957	18·9686	142·8	157·8
4	9·6267	34·529	118·5	144·0
5	14·1382	58·130	99·77	135·0
6	19·6424	91·744	86·24	128·5
7	26·144	137·364	75·39	123·1
8	33·645	196·987	67·25	120·0
9	42·145	272·609	60·04	—
10	51·645	368·232	54·59	116·5
11	62·145	479·856	49·72	—
12	73·645	615·480	46·20	—
13	86·145	774·1	42·70	111·4
14	91·645	960·7	39·98	—
15	114·145	1174·4	37·22	—
16	129·645	1418·0	34·65	107·0
17	146·145	1693·7	32·84	—
18	163·645	2003·3	31·02	—
19	182·145	2348·8	29·33	—
20	201·645	2732·7	28·13	—

From these integrals the values of the constant A in the equation (8) may be calculated for various values of η^* (Table 2).

Table 2

η^*	$-\infty$	-3	0	5	10	20	$+\infty$
A	1·1045	1·1021	1·0858	1·0221	1·0074	1·0020	1·0000

It will be seen that the values of A vary only by 10% for the whole range of η^* and the variation is extremely gradual. Furthermore, it will be shown that over the range of temperatures 0–550° c., the value of η^* appears to vary between 5 and 10 for CdO. Treatment of A as a constant and equal to unity will therefore be likely to incur an error of not more than about 2%.

The values of the Hall constant measured, and the values of the concentration of free electrons n_f, as calculated from equation (8) assuming $A=1$, are shown graphically in Figure 1. It will be seen that the concentration of free electrons in the samples is constant. This experimental result will be considered below, together with its probable explanation.

It has been suggested previously (Peierls 1937, Wilson 1939, Shifrin 1944) that the activation energy in a semiconductor should vary with the impurity content. As the concentration of impurity centres increases, they will become closer together, and interaction will occur so that the potential lattice no longer consists of wells below the conduction band at the centre, but a series of potential humps are formed between the centres. The region between the tops of the humps and the bottom of the conduction band consists of a band of discrete energy levels due to the excited states of the impurities. Thus the height of the conduction band above the ground state levels is decreased. Eventually, with a sufficiently large impurity content, the conduction band will be lowered down to the ground state, when the impurity electrons will be continuously free. Such a material will have a constant concentration of free electrons, independent of temperature, as appears to be the case in cadmium oxide. This simple picture has, however, several difficulties which more rigorous treatments have as yet failed to overcome.

Such a variation of activation energy has been observed by Pearson and Bardeen (1949) and quantitatively explained, using specimens of silicon with varying amounts of impurities. The activation energy decreases with increasing impurity content, until eventually it becomes zero, the electrons being continuously free in the ‘ impurity band ’. Thus it seems reasonable to suppose that a similar state of affairs exists in the CdO specimens investigated, there being such a concentration of excess interstitial cadmium atoms, that the ground state ‘ orbits ’ of the centres overlap, and the electrons may pass freely through the crystal lattice.

§ 8. COMPARISON OF THEORY WITH EXPERIMENTAL RESULTS

In this comparison the constancy of the electron density will be taken as proved. The comparison will not depend upon the correctness or otherwise of the explanation of this fact given in the previous section, but merely upon the interpretation of the Hall constant results.

Let the effective mass m^* of the electron be equal to $G\boldsymbol{m}$, where $\boldsymbol{m}$ is the mass of a free electron, and G is a constant. Then we may rewrite equation (1)

$$F_{1/2}(\eta^*)=\frac{\boldsymbol{h}^3}{4\pi(2\boldsymbol{mk}T)^{3/2}}\frac{n_{\mathrm{f}}}{G^{3/2}}, \qquad \ldots\ldots(9)$$

so that from a knowledge of either η^* or $n_{\mathrm{f}}/G^{3/2}$ (effective electron density), the other may be calculated at any temperature.

(i) *Thermoelectric Power Results*

The thermoelectric powers for the various values of η^* have been calculated from equation (7), and the results are shown in Table 1, and Figure 6. From a selected experimental point giving the thermoelectric power at a certain temperature, we may deduce η^* and hence $n_{\mathrm{f}}/G^{3/2}$. From this value of $n_{\mathrm{f}}/G^{3/2}$ the thermoelectric power may be calculated throughout the temperature range, and the results of such calculations are shown as the continuous lines in Figure 3. It will be seen that the theory predicts the variation of the thermoelectric power with temperature quite satisfactorily. To show that this agreement between experiment and theory was not merely true of the specimens studied by the author, a series of results by another investigator was obtained. Permission was obtained to use values measured by Andrews (1947), and these were also treated as above, and graph I of Figure 4 shows the relationship of the experimental and the theoretical curve. Once again the agreement is good.

It is of interest to note that the relationship between thermoelectric power and temperature in the range considered is practically linear, both experimentally and theoretically.

(ii) *Conductivity Results*

Assuming a value for $n_f/G^{3/2}$, we may calculate η^*, and thus $F_1(\eta^*)$ at two different temperatures T_1 and T_2. Hence the ratio of the conductivities at the two temperatures $\sigma_{T_1}/\sigma_{T_2}$ may be calculated from equation (6):

$$\sigma_{T_1}/\sigma_{T_2} = T_1 F_1(\eta_1^*)/T_2 F_1(\eta_2^*).$$

The values of this ratio for a range of values of $n_f/G^{3/2}$ and for $T_1 = 300°$ K. and $T_2 = 800°$ K. are given in Table 3.

Table 3

Log ($n_f/G^{3/2}$)	20·5	20·6	20·7	20·8	20·9	21·0	21·1
$\sigma_{300}/\sigma_{800}$	2·308	2·368	2·442	2·473	2·520	2·552	2·586

From the experimental results we may calculate a value of the ratio and thus by interpolation in Table 3 we may obtain the appropriate value for $n_f/G^{3/2}$. From this value we may calculate the variation predicted by the theory at the intermediate temperatures ; this is shown as the continuous line in Figure 2. There is seen to be close relationship between the experimental results and the predicted theoretical variation.

(iii) *Correlation of Results*

From the values of $n_f/G^{3/2}$, which were obtained from the conductivity results, the thermoelectric powers at the various temperatures may be predicted, and these are shown in relation to the experimental results in Figure 4, graphs II and III. Good agreement is obtained. From a comparison of the values of $n_f/G^{3/2}$ derived from the conductivity and the values of n_f derived from the Hall constant, values of G may be obtained, as shown in Table 4. The values of G obtained are small, and it would appear that the various approximations in the theory have been compensated by giving the electron a small effective mass.

Table 4

	Specimen I	Specimen II
$n_f/G^{3/2}$ from :		
Conductivity	$7{\cdot}50 \times 10^{20}$	$5{\cdot}50 \times 10^{20}$
Thermoelectric power	$7{\cdot}61 \times 10^{20}$	$5{\cdot}60 \times 10^{20}$
Hall constant	$1{\cdot}69 \times 10^{19}$	$1{\cdot}56 \times 10^{19}$
Mean value of G	0·080	0·093

(iv) *Approximate Formula*

From the results which have so far been analysed we may conclude that η^* is very large for all temperatures used in the experiments. This indicates that the number of carriers is sufficiently large to produce these large values of η^*. For these and any lower temperatures (since η^* increases as the temperature decreases provided the concentration of free electrons is constant), we may therefore take the equations derived for the electrical properties, and use approximate expressions for the functions $F_m(\eta^*)$ which are valid only when η^* is large.

$$R = 1/n_f\boldsymbol{e}. \qquad \ldots\ldots(10)$$

$$\rho = \rho_0 T/B. \qquad \ldots\ldots(11)$$

$$\Theta = \frac{16\pi^2 \boldsymbol{mk}^2}{3\boldsymbol{eh}^2}\left(\frac{\pi}{3}\right)^{2/3}\frac{T}{(n_f/G^{3/2})^{2/3}}. \qquad \ldots\ldots(12)$$

These relationships are only applicable in ionic semiconductors in which n_f is very large and the temperatures are not too high. The linear variation predicted for the thermoelectric power by equation (11) is clearly followed by the experimental results, as may be seen from Figures 3 and 4. It will be seen that it is much easier to calculate the values of $n_f/G^{3/2}$ from this simple formula than from equation (7).

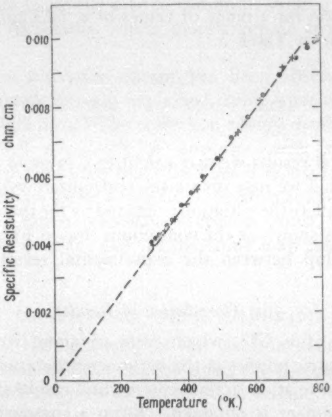

Figure 5. Graph of specific resistivity against absolute temperature for two specimens of CdO.

Figure 5 shows a graph of resistivity ρ against absolute temperature. The linearity predicted by equation (12) is quite pronounced.† At the higher temperatures, however, deviations should occur, due to the fact that η^* may no longer be sufficiently large for the approximations made to be valid. At lower temperatures the curve should again depart from linearity, and should approach a constant value as T approaches zero, due to the effect of the variation of the factor B at temperatures less than the Debye temperature. From the constant value approached as $T \to 0$, a value for the Debye temperature could be obtained.

---

† The values of $n_f/G^{3/2}$ obtained from the conductivity curve will be seen to depend on the departure of Figure 5 from linearity. The values obtained will be approximate, and the accurate agreement shown in Table 4 is probably largely fortuitous.

§9. CONCLUSIONS

As a further point of interest, the effect upon the predicted properties has been considered when the temperature is assumed to be low. Here it is assumed that the temperature and concentration of free electrons is such that a vast majority have energies less than $\boldsymbol{h}\nu$, unless they absorb a phonon of energy from the lattice. In this case it has been shown by Shifrin (1944) that

$$l(E)=l_0\{1-f(E)\}e^{\boldsymbol{h}\nu/\boldsymbol{k}T}(E/\boldsymbol{k}T)^{1/2}$$

which is very similar to that derived by Mott and Fröhlich (1939) except that it contains a factor $1-f(E)$ to allow for the cases in which degeneracy is appreciable. By substitution of this expression for the mean free path in equation (6) it follows that the thermoelectric power is given by

$$\Theta=\frac{\boldsymbol{k}}{\boldsymbol{e}}\left\{-\eta^*+\frac{5}{2}\frac{F_{1/2}(\eta^*)+\frac{2}{3}F_{3/2}(\eta^*)}{F_{1/2}(\eta^*)+\frac{1}{2}F_{-1/2}(\eta^*)}\right\}. \qquad \ldots\ldots(13)$$

The values of the thermoelectric power as predicted by this equation for various values of η^* are shown in Table 1 and Figure 6, beside those predicted by the high temperature formula (7). It will be seen that the experimental results which have been obtained could not possibly have been explained by the low temperature formula (13) since as η^* approaches infinity the theoretical thermoelectric power predicted by this equation approaches its minimum value of 86 μv/deg. c., and over a large part of the range of temperatures over which measurements were made, values less than this were obtained.

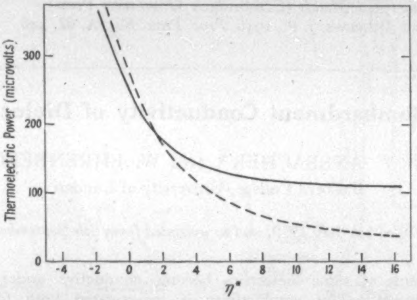

Figure 6. Calculated values of the thermoelectric power for various values of η^*. ——— Values from formula (13). – – – – Values from formula (7).

The agreement shown here between the experimental results, both of the author and of Andrews, and the theory developed appears to be very satisfactory, and may be taken as good evidence that the lines of argument leading to the theory are correct, and that the approximations made are applicable to cadmium oxide. The oxide is therefore a good example of a very degenerate electronic semiconductor possessing very metallic characteristics.

ACKNOWLEDGMENTS

The author wishes to acknowledge the very helpful advice he has received from Professor J. P. Andrews, and the encouragement given by Professor H. R. Robinson, of Queen Mary College, London. The work was carried out during the tenure of a grant from the Department of Scientific and Industrial Research.

REFERENCES

ANDREWS, J. P., 1947, *Proc. Phys. Soc.*, **59**, 990.
ANDREWS, J. P., and HOGARTH, C. A., 1949, *Phil. Mag.*, **40**, 273.
BUSCH, G., 1946, *Helv. phys. Acta*, **19**, 167.
BUSCH, G., and LABHARDT, H., 1946, *Helv. phys. Acta*, **19**, 463.
BUSCH, G., SCHMID, P., and SPÖNDLIN, R., 1947, *Helv. phys. Acta*, **20**, 461.
DAVYDOV, B., and SHMUSHKEVITCH, I., 1940, *J. Phys. U.S.S.R.*, **3**, 359.
FISCHER, F., DEHN, K., and SUSTMANN, H., 1932, *Ann. Phys., Lpz.*, **15**, 109.
FOWLER, R. H., 1933 a, *Proc. Roy. Soc.* A, **140**, 505 ; 1933 b, *Proc. Roy. Soc.* A, **141**, 56; 1936, *Statistical Mechanics* (Cambridge : University Press).
FRÖHLICH, H., 1937, *Proc. Roy. Soc.* A, **160**, 280.
HOGARTH, C. A., 1948, *Thesis*, London.
MCDOUGALL, J., and STONER, E. C., 1938, *Phil. Trans. Roy. Soc.*, **237**, 67.
MOTT, N. F., and FRÖHLICH, H., 1939, *Proc. Roy. Soc.* A, **171**, 496.
PEARSON, G. L., and BARDEEN, J., 1949, *Phys. Rev.*, **75**, 865.
PEIERLS, R. E., 1937, *Proc. Phys. Soc.*, **49**, 59.
PUTLEY, E. H., 1948, *Thesis*, London; 1949, *Proc. Phys. Soc.* A, **62**, 284.
SEITZ, F., 1941, *Modern Theory of Solids* (New York : McGraw-Hill).
SHIFRIN, K., 1944, *J. Phys. U.S.S.R.*, **8**, 242.
WILSON, A. H., 1931 a, *Proc. Roy. Soc.* A, **133**, 458; 1931 b, *Ibid.*, **134**, 277; 1939, *Semiconductors and Metals* (Cambridge : University Press).
WRIGHT, R. W., and ANDREWS, J. P., 1949, *Proc. Phys. Soc.* A, **62**, 446.

Electron-Bombardment Conductivity of Dielectric Films

BY F. ANSBACHER* AND W. EHRENBERG
Birkbeck College, University of London

MS. received 6th July 1950, *and in amended form 5th September* 1950

ABSTRACT. Films of some dielectrics become conductive under the influence of electron bombardment. This conductivity is investigated both for steady and for alternating bombardment in its dependence particularly on temperature, current density and the potential difference across the dielectric. The gain, i.e. the ratio of current through the film to the bombarding current increases strongly with temperature. On arsenic sulphide films, the gain reaches 40,000. The effect is discussed in the light of theories of conduction in dielectrics and of recent work on allied subjects.

§1. INTRODUCTION

CONDUCTIVITY in a dielectric can be induced by photons only if their energy falls into one of the bands in the absorption spectrum of the dielectric; high-speed electrons, however, should induce conductivity in any dielectric, by the production of a trail of ions and slow electrons. Early experiments indicated that dielectrics became only very weakly conducting under the influence of electron bombardment, and it is only recently that a number of authors have drawn attention to the existence of a strong electron bombardment conductivity (or E.B.C.) (McKay 1948, Rittner 1948, Ansbacher and Ehrenberg 1948, 1949, Pensak 1949). We shall report here examples of strong E.B.C. which we have observed in thin films of dielectrics.

---

* Now at H. H. Wills Physical Laboratory, Bristol.

The accepted view of electronic conduction in dielectrics leads one to expect the conductivity to be greater the more perfect the crystal and the lower the temperature, because the number of trapping centres will be smaller in more perfect crystals and because the mean free path of the electrons decreases with increasing temperature. In fact, neither of these two conclusions is borne out by our experiments. A particularly strong effect was found in amorphous arsenic sulphide, As_2S_3, and the effect increases strongly with temperature. In §§ 2–4 of this paper the experimental evidence will be given; in § 5 it will be compared with the results of other authors and its theoretical implication will be discussed.

§ 2. THE E.B.C. OF DIELECTRIC FILMS

We have observed, with electrons up to 50 kv., a strong E.B.C. effect if the electrons were directed against a film of dielectric sandwiched between two conducting electrodes (Figure 1; the galvanometer may be replaced by a resistance coupled to a cathode follower). The top layer was always thin enough not to retard the electrons appreciably. The current across the film is composed of the leakage current i_l which is normally negligible, of i_0, the fraction of the primary current penetrating the film which is observed when no field exists between the electrodes, and the E.B.C. current i_s. This was measured as a function of the following independent variables: the accelerating voltage V of the bombarding electrons, the current density I_p or the current i_p of the bombarding electrons, the 'bias' voltage v across the film, the temperature T of the film, the thickness d of the film, and the variation with time of the bombarding current density.

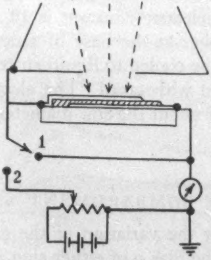

Figure 1.

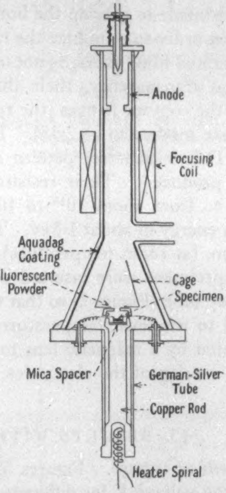

Figure 2.

The bias voltage v is called positive if it accelerates electrons in the direction of flow of the incident electrons, i.e. if the bottom electrode is positive, and i_s is called positive if it corresponds to electrons moving from top to bottom. Whenever v is different from zero the sign of i_s agrees with that of v. The ratio $i_s/i_p = g$ is called the gain, which we term positive or negative gain according to the sign of v. In most tests i_p was constant with time (D.C.–E.B.C.); in a few experiments i_p followed a square wave on–off pattern.

The preparation of the specimens, i.e. of the dielectric films, which must be uniform and free from pin holes, depends on the individual dielectric. Films of aluminium oxide can be grown by anodizing solid aluminium; the specimens are completed by thermal evaporation of aluminium on to the oxide film. Films of mica are readily obtained by cleavage, films of glass by blowing thin-walled spheres. Specimens of arsenic sulphide and antimony sulphide are obtained by thermal evaporation of the sulphides on to previously metallized (gold plated) glass. Several crucibles at different angles to the base are used successively in order to minimize the risk of pin holes. The top electrode is an evaporated gold film and is made to overlap the bottom electrode over a small region only (about 10 mm^2) in order to minimize the risk of including faults in the film.

Evaporated films of As_2S_3 not only show a very high E.B.C. but also, owing to their great transparency, their thickness can be determined very readily by counting the contour fringes (the refractive index of these films was found by an interference method to be 2·38). These films are amorphous and have the same 'liquid' Debye–Scherrer pattern as the B.D.H. 'Analar' powder from which they are produced. Their resistivity varies, between liquid air temperatures and 180° C., from about 10^{15} to 10^{11} ohm cm.; the variation corresponds to an activation energy of about 1·5 ev. The films have a breakdown strength of about 10^6 volt/cm. (at room temperature). Their dielectric constant is 10.

The specimens were inserted into a chamber at the base of a demountable cathode-ray tube (Figure 2) so that they could be cooled to liquid air temperature or heated to whatever temperature they could withstand. The electrons were concentrated by a magnetic lens to a circle of about 0·3 cm. diameter on to the region of overlap of the electrodes.

§ 3. RESULTS WITH STEADY BOMBARDMENT

The critical voltage. Figures 3, 4, 5 show the variation of the gain g with bombarding voltage V for different values of the bias v of either sign at different temperatures. The gain is here, within experimental error, independent of the polarity of the bias; and $g = 0$ for all values of v, if V is smaller than a critical voltage V_0. (The curves for $v = 0$ represent i_0, the fraction of the primary current, and not the gain; the gain at zero bias is always zero.)

The existence of a critical bombarding voltage V_0 had already been observed by Becker (1904) and has also been confirmed by Pensak. V_0^2 is proportional to d, the thickness of the film (Figure 6). This observation must be interpreted as a verification of the Thomson–Whiddington law, provided we assume that the E.B.C. begins when some primary electrons penetrate the whole film. Its thickness is equal to the range in the dielectric of electrons of energy V_0. The straight line in Figure 6 passes through the origin. This indicates that the loss of energy of the primary electrons in the top electrode is negligible.

V_0 is independent of the temperature of the specimens and of the bias, in agreement with the interpretation given above. Hence the Thomson–Whiddington law can be used to determine the thickness of films which cannot easily be measured directly (for example, antimony sulphide films are opaque, aluminium oxide films when thick are milky and do not show interference fringes, and many samples are covered by a uniform oxide film and therefore do not show contour fringes).

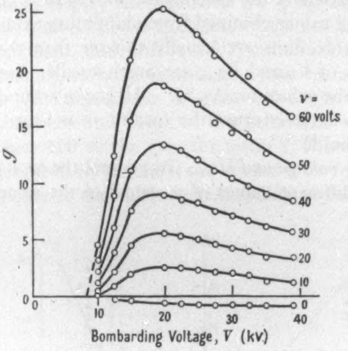

Figure 3. Variation of negative gains with bombarding voltage. As_2S_3 film, 1·2 μ thick. $I_P = 27 \times 10^{-8}$ amp/cm², $T = 26°$ c.

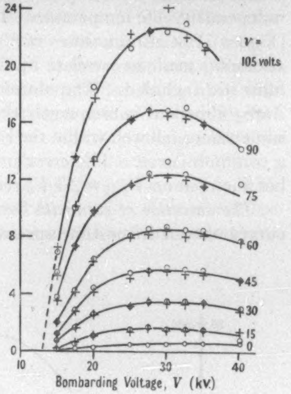

Figure 4. Positive (+) and negative (○) gain. As_2S_3 film 2·04 μ thick. $I_P = 27 \times 10^{-8}$ amp/cm², $T = 24°$ c.

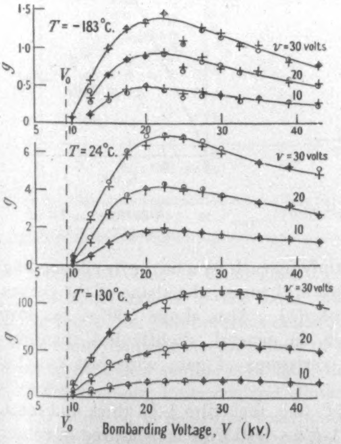

Figure 5. Positive (+) and negative (○) gain at three temperatures. $I_P = 27 \times 10^{-9}$ amp/cm². As_2S_3 film 1·2 μ thick.

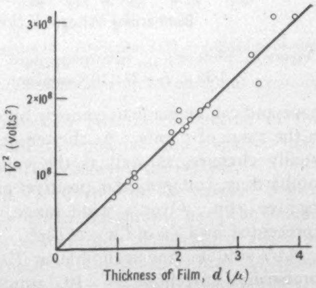

Figure 6.

The bombardment voltage for which the gain reaches a maximum. As the bombarding voltage is increased the gain at a particular bias and temperature rises to a maximum and then falls again. This maximum voltage $V_{\max}$ is independent of bias (Figures 3, 4, 5). Below room temperature, $V_{\max}$ is also independent of temperature, but for higher temperatures $V_{\max}$ increases (Figure 7); it also increases with the thickness of the specimens. In Figure 8 an attempt is made to correlate V_0 and $V_{\max}$; values obtained from aluminium oxide films are included. The aluminium oxide films are usually thinner than the As_2S_3 films and consequently the values of V_0 and $V_{\max}$ are much smaller, but some values fall well within the range of the values for As_2S_3. All group around a common curve. The error in $V_{\max}$ is large because the maximum is broad, but the relation $V_{\max} \simeq 2{\cdot}3\ V_0$ seems to hold.

The variation of gain with bombarding voltage and bias. In general the (g, V) curves obtained from one specimen at different values of v are all of the same shape and can be made to coincide by multiplying each by a factor $f(v)$ depending on the value of v only. As the temperature is changed, the shape of the curves usually changes, as well as the values of $f(v)$. Also above 100° c. for low bombarding voltages, the positive gain is, in general, slightly less than the negative gain. Over a wide range, the variations of gain with bias can be represented by $1/f = a(T)v + b(T)v^2$.

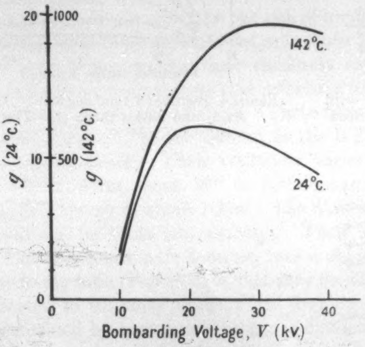

Figure 7. Shift of $V_{\max}$ with temperature. As_2S_3 film $1{\cdot}32\ \mu$, $I_P = 27 \times 10^{-8}$ amp/cm².

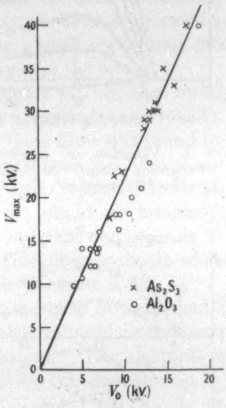

Figure 8.

At $T = 80°$ K., b is negligible, at $T = 26°$ c. (e.g. for a film $1{\cdot}2\,\mu$ thick and for a bombarding current of $2{\cdot}7 \times 10^{-7}$ amp/cm²), $b/a \sim 0{\cdot}013$ if v is measured in volts; at $T = 142°$ c. for a film $1{\cdot}32\,\mu$ thick and the same current, $b/a \sim 0{\cdot}08$. Thus the gain depends linearly on bias at liquid air temperature and becomes quadratic in bias at higher temperature. A saturation of gain with bias has not been observed.

A comparison of specimens of different thicknesses cannot be made at an arbitrary bombarding voltage. But as $V_{\max}$ is a function of the thickness alone (at least at and below room temperature) and the gain is also a function of the thickness and of the bias, it is clear that by confining attention to the maximum gains alone, samples of different thicknesses can be compared. In Figure 9 the ratio gain/field at $V_{\max}$ is plotted against field v/d for different samples at room temperature. The values for samples with highest gain are grouped around a common curve; under favourable conditions $g_{\max}$ depends on v/d only. The other values display no systematic grouping which could be related to the thickness *d*. One may attribute such loss in gain to effects of age of the specimens, previous treatment, and unfavourable conditions of evaporation of the As_2S_3 films (for instance, some specimens may have been hotter during evaporation than others).

The dependence of gain on temperature. The effect of temperature is complicated: a break in the behaviour occurs in the neighbourhood of 100° c.; below 100° c. the gain for given v, V and current density varies reversibly with temperature, that is, if the temperature returns to a certain value, the gain returns at once to the value corresponding to this temperature. Also, the E.B.C. current on reversal of bias is established instantaneously (within the period of the galvanometer) and is of the same magnitude for positive and negative bias. Above 100° c. the gain becomes dependent on the history of the sample.

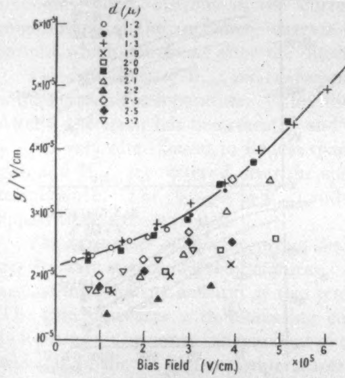

Figure 9. Gain/bias field plotted against bias field for 11 samples of As_2S_3 at $V_{\max}$. $T \sim 22°$ c. $I_p = 27 \times 10^{-8}$ amp/cm^2.

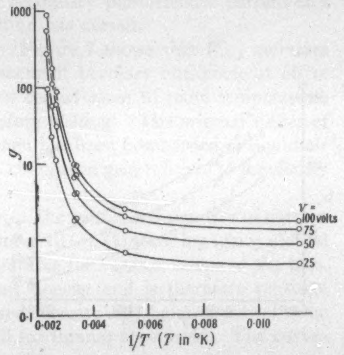

Figure 10. As_2S_3 film 2·52 μ; log (gain) plotted against $1/T$ at $V = 30$ kv. $I_p = 27 \times 10^{-8}$ amp/cm^2.

At room temperature for a field of about 9×10^5 volt/cm. the maximum gain obtained on a new sample is of the order 50. After the sample has been heated to 100° c. or more, however, and allowed to cool to room temperature, a gain of several hundred is measured for the same field. (It is possible that the initial gain may be greater, as many adjustments, such as refocusing, are necessary before the first observation.) This value is steadily reduced on bombardment and finally reaches a value about 1·3 to 1·5 times the original value. Subsequent cooling to liquid air temperature with bombardment and warming up to room temperature usually re-establishes the original gain.

For a particular bombarding current density and bias the gain rapidly increases with temperature, e.g. at $V_{\max}$ for arsenic sulphide films at $I_p = 13 \times 10^{-8}$ amp/cm^2 and fields of the order 5×10^5 v/cm. the gain at liquid air temperature is around 5, at 20° c. around 50, and at 150° c. around 500. Figure 10 shows typical curves of log (gain) plotted against $1/T$. It looks as if two processes were involved, one covering the range $-200°$ c. to about room temperature, the other applicable above room temperature. The slope of the ($\log g$, $1/T$) curve is practically independent of the current density and is also independent of the thickness of the samples.

The secondary E.B.C. *effect at high temperatures.* At elevated temperatures a phenomenon is observed which is reminiscent of the secondary photoelectric effect, and which will be called secondary E.B.C. effect.

The E.B.C. current increases at first while the bombardment is going on until after several seconds or minutes a value (the 'high' gain) is reached which may be several times the value at the beginning (the 'low' gain). Once the high gain is established for a certain bias, the E.B.C. current follows instantaneously (within the period of the galvanometer) any variations of the primary beam. If now the polarity of the bias is reversed, but the bombarding current is left on, the gain (in the reverse direction) is at first a small fraction of the previous high gain and rises slowly to about the same high value it had before the reversal of bias. The high gain is reached more quickly if the bombarding current is repeatedly interrupted, the bias being left on all the time. This 'conditioning' of the specimens does not take place, even slowly, without electron bombardment.

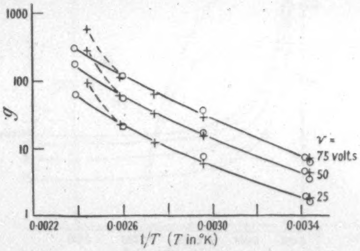

Figure 11. As_2S_3 film 2·5 μ; (+) high gain (○) low gain. V=30 kv. $I_P=27\times10^{-8}$ amp/cm².

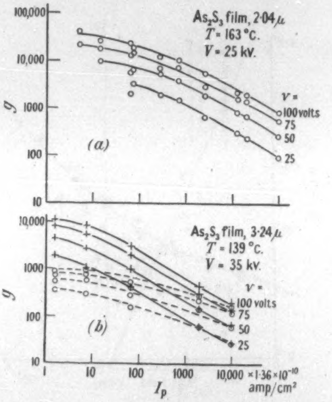

Figure 12. Variation of gain with current density. —— high gain. – – – low gain.

The difference between low gain and high gain increases with increasing bias and increasing temperature, and decreases with increasing bombardment current density and with increasing thickness of sample; for example, for 0·27 μa/cm² (the current density at which most measurements were carried out) there is no difference between low and high gain up to about 100° c., while for a current density of 0·0014 μa/cm² there is already a small difference at 20° c.

Plots of log (low gain) and of log (high gain)—dotted curve—against $1/T$ are shown in Figure 11. Over the temperature range the low gain appears to follow a simple law; the high gain deviates from this at 120° c.

The low gain values are somewhat uncertain, because they depend on the preceding conditioning of the specimen for high gain before reversal of bias. This conditioning may take several minutes for large current densities and for temperatures only slightly above 100° C.

Below 100° C. the gain for positive and negative bias is usually the same (the other variables being the same) but above 100° C. the negative high gain exceeds the positive high gain by as much as 100% at low bombarding voltages, and approaches the negative gain for large V. In some specimens the negative gain exceeds the positive gain over the whole range of V.

The highest gain ever obtained was in the neighbourhood of 40,000 for a specimen 2·04 microns thick at 163° C. The bombarding voltage was 24 kv., the bias 100 V. and the current density $6{\cdot}8 \times 10^{-11}$ amp/cm^2 (Figure 12 (*a*)). This current density was already so low that no increase in gain could be expected by further reduction. On the other hand, at higher temperatures the leakage current would have masked the E.B.C. current. It should be emphasized that the secondary E.B.C. current is the current under electron bombardment after conditioning of the specimen whereas the secondary photoelectric current is a current which continues after the illumination has ceased.

The dependence of $V_{\max}$ *on temperature.* Figure 7 shows that $V_{\max}$ increases with increasing temperature. This displacement becomes noticeable at 60° C. After a specimen has been heated and then cooled again to room temperature, $V_{\max}$ is very often found to be less than before heating. The original values of gain and $V_{\max}$ are restored after the specimen has been bombarded at liquid air temperature. The changes in $V_{\max}$ and the changes in gain referred to previously appear to be closely related.

The dependence of gain on current density. The gain is independent of current density only at very low temperatures. Figures 12 (*a*), (*b*) show log (gain) plotted against log (current density) at two temperatures for various values of the bias. The gain decreases with increasing current density and is therefore sensitive to focusing; it becomes independent of current density only below a critical value which is smaller at higher temperatures and for thinner specimens. The curves indicate $g \propto I_p^{-\alpha(T)}$; $\alpha(T)$ is very small for low T.

In Figure 12 (*b*) values both for log (high gain), full curve, and log (low gain), dotted curve, are given. For large current densities the difference between the two becomes small. Of all E.B.C. effects only the critical bombarding voltage is, within experimental error, independent of temperature.

Charges in bombarded films. At room temperature, for small bombarding voltages (just above V_0) the following ' discharge ' phenomenon is observed. If the bombardment current is switched off before the bias is reduced to zero and then switched on again with the bias at zero, a current is observed in the direction opposite to that of the previous E.B.C. current, rapidly decreasing to the normal i_0. The time integral of this current, as recorded by a ballistic galvanometer was found to be 8×10^{-9} coulomb for a bombarded area of 0·058 cm^2, for a specimen 2 μ thick. If the bias is reduced to zero before switching off the primary current, no 'discharge' current is observed on subsequently switching on i_p. The magnitude of the 'discharge' current decreases to zero as the bombarding voltage approaches $V_{\max}$.

From the 'discharge' current at low V the number of traps in the film is estimated to be not less than 3×10^{16} cm^{-3} under the assumption that on discharge the carriers traverse on the average half the film.

Experiments with films other than As_2S_3. Antimony sulphide films can be prepared in the same way as As_2S_3 films. Thin films are deep red by transmitted light and micro-crystalline. Our experiments indicate that Sb_2S_3 shows the same effect as As_2S_3 and under corresponding conditions probably a larger gain. Al_2O_3 films grown on Al show also a strong E.B.C. depending on the method of anodizing and the type of Al used. Most of our experiments were carried out on films produced by the chromic acid process. The top electrode was evaporated aluminium. These specimens have the remarkable property of changing their capacity reversibly to one-twentieth of their value in air when placed in a vacuum. Their thicknesses were obtained from E.B.C. data as mentioned above. Curves corresponding to Figure 3 are shown in Figure 13. They differ from the As_2S_3 curves in the following respects: (*a*) the gains are smaller; (*b*) the factors $f(v)$ are up to 30% different for positive and negative bias; (*c*) the negative gain seems to saturate with temperature (Figure 14): the straight portions of a (log (gain), $1/T$) curve correspond to an activation energy of 0·35 ev. for positive gains and 0·5 ev. for negative gains; (*d*) no secondary E.B.C. effect and no variation of $V_{\max}$ with temperature is observed; (*e*) the specimens show for current densities greater than 3×10^{-7} amp/cm^2 a fatigue effect at high temperature: the gain decreases with time under bombardment.

§4. EXPERIMENTS ON As_2S_3 AND Al_2O_3 SPECIMENS USING MODULATED BOMBARDING CURRENTS AND STEADY BIAS VOLTAGES (A.C. METHOD)

Experimental arrangement. The electron beam is modulated by driving the grid of the electron gun with a square-wave generator at from 22 c/s. to 66 kc/s. During one half of the cycle the bombarding current is cut off, and during the other half rises to a constant value within a small fraction of the duration of the total current pulse, so that it varies with time as shown in Figure 15 (*a*). In order to measure the E.B.C. current (A.C./E.B.C.) for this alternating bombardment the galvanometer of Figure 1 is replaced by a resistance X and the voltage developed across X is, after amplification, applied to the screen of a cathode-ray oscillograph. The amplifier had a gain of about 20,000 independent of frequency up to 0·5 Mc/s. The A.C./E.B.C. deflection is always compared with the deflection obtained by passing the bombarding current directly through X (switch in position 1, Figure 1). In addition the average primary and secondary currents are measured by a galvanometer. For comparison, a measurement of the D.C. gain is also made for a D.C. bombarding current equal to the average A.C. bombarding current.

The scope of the measurements is similar to that described for the D.C. experiments; it includes the variation of gain with bombarding voltage, bombarding current density, applied bias, temperature of the specimens and frequency of the bombarding current pulse. It includes also a comparison between the wave-form of the E.B.C. current with that of the bombarding current. As these are, in general, not identical the definition of gain becomes somewhat arbitrary. In the following, A.C. gain denotes the ratio of the amplitudes measured from peak to peak, and average A.C. gain the ratio of average secondary to average primary current. The capacity of the specimens is so large that it is necessary to allow for distortion of the signals by the measuring circuit. During the bombardment the film becomes conducting, so that the sample is equivalent to a condenser of constant capacity C shunted by a resistance $R(t)$ which varies periodically with time.

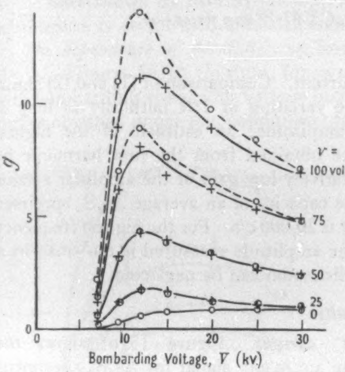

Figure 13. Positive (+) and negative (○) gain of aluminium oxide film. $I_P=13{\cdot}6\times10^{-8}$ amp/cm², room temperature.

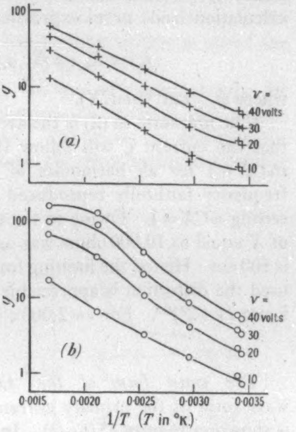

Figure 14. Positive (+) and negative (○) gain of aluminium oxide film 0·42 μ thick at $V=14$ kv.

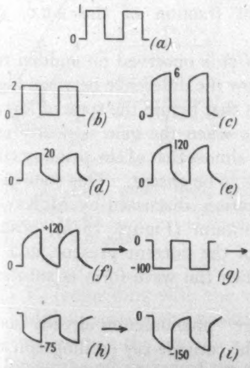

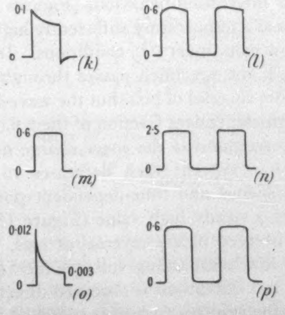

Figure 15 (*a*)–(*i*). A.C./E.B.C. (*a*) represents the bombarding current varying with time; (*b*)–(*i*) E.B.C. signal from a As_2S_3 film 1·9 μ thick, $I_P=13{\cdot}6\times10^{-8}$ amp/cm², pulse length 0·5 msec. The numbers indicate the A.C. gain; (*b*), (*c*) specimen at 26° C. small and large bias, (*d*), (*e*) specimen at 140° C., small and large bias, (*f*)–(*i*) specimen at 120° C., change of appearance of cathode-ray oscillograph trail on reversal of bias: (*f*) high A.C./E.B.C., with positive bias, (*g*) bias just reversed, (*h*) negative bias on for 1 second (low A.C./E.B.C.), (*i*) negative bias on for some time (high A.C./E.B.C.).

Figure 15 (*k*)–(*p*). A.C./E.B.C. signal from aluminium oxide film at 300° C., pulse length 5 msec. The numbers represent the A.C./E.B.C. gain in (*l*) and (*n*) ($V=20$ volts), in (*k*), (*m*), (*o*), (*p*) ($v=0$) they give the portions of the primary current reaching the bottom electrode. $I_P=0{\cdot}27$ μa/cm², (*o*) and (*p*) $I_P=2{\cdot}7$ μa/cm²; (*n*), (*l*), (*o*) $V=5$ kv.; (*m*), (*n*), (*p*) $V=10$ kv.

Let $1/R$ be represented by a Fourier series:

$$\frac{1}{R}=\frac{1}{R_0}+\sum_{-\infty}^{+\infty}{}' a_r \exp(jr\omega t), \qquad \ldots\ldots(1)$$

where Σ' means that $r=0$ is excluded from the summation. A simple calculation leads to an expression for the E.B.C. current

$$i_s=v/R_0+v\sum_{-\infty}^{+\infty}{}' a_r[1+(r\omega CX)^2]^{-1/2}\exp j(r\omega t-\psi_r) \qquad \ldots\ldots(2)$$

where $\psi_r=\tan^{-1}(r\omega CX)$.

The first term in (2) is the average current. Comparison of (1) and (2) shows that the current i_s will follow the time variation of $1/R$ faithfully as long as $r\omega CX \ll 1$ for all harmonics of large amplitude; an estimate of the highest frequency faithfully reproduced may be obtained from the first harmonic by setting $\omega CX=1$. Owing to the comparatively low gain of the amplifier a value of X equal to 10,000 ohms was used; the capacity of an average As_2S_3 specimen is 500 cm. Hence, the limiting frequency is 30,000 c/s. For the highest frequency used the distortion is appreciable and the amplitude measured is too small by a factor $(1+2^2)^{1/2}$. For $\nu=2{,}000$ c/s. the distortion can be neglected.

Results

The wave form of the A.C./E.B.C. current. Figure 15 (*a*) shows the wave-form of the primary current. The A.C./E.B.C. signal for As_2S_3 specimens is shown in Figures 15 (*b*)–(*e*). It appears that part of the E.B.C. current responds instantaneously (within the limits of observation) to variations of the primary current, but that a considerable fraction of the total A.C./E.B.C. current takes time to establish itself. This is also borne out by Figure 17 discussed below. With increasing temperature, this time-dependent fraction of the E.B.C. current increases.

An interesting behaviour (Figures 15 (*f*)–(*i*)) is observed on sudden reversal of bias at a temperature sufficiently high to show the difference between high gain and low gain under D.C. conditions. It is seen that before the state of low gain is reached, the specimen passes through a stage when the gain is nearly as large as before reversal of bias, but the wave-form is almost that of the primary current; the time-dependent fraction of the E.B.C. seems to be absent. This state of affairs may correspond to the space charge neutralization, discussed by McKay. The A.C./E.B.C. current then decreases to a minimum (Figure 15 (*h*)) with both instantaneous and time-dependent portions of the current present, and finally rises to a steady high value (Figure 15 (*i*)) when the wave-form is substantially that observed before reversal of bias.

At low bombarding voltages the ‘ discharge ’ phenomenon already observed under D.C. conditions is observed directly on the cathode-ray oscillograph screen. When the primary current is switched off, then the bias reduced to zero, then the (modulated) primary current switched on, a large A.C./E.B.C. pulse is observed in the reverse direction, which rapidly reduces to the normal fraction of the primary current reaching the bottom electrode. This shows that a large polarization exists in the insulator under bombardment and application of bias, which remains after the bombardment has ceased. At higher bombarding voltages this reversal is not observed.

The behaviour of the Al_2O_3 specimens resembles closely that of As_2S_3 samples, but on account of their large capacities, the distortion of the wave-form of the A.C./E.B.C. current is already noticeable at low frequencies. Owing to the greater strength of the Al_2O_3 films very large primary currents could be used. Figure 15 (*o*) shows clearly the build-up of internal space charge at zero bias and at very small bombarding voltages for which $i_0/i_p \ll 1$; this figure is very similar to the ones shown by McKay (1948). As the bombarding voltage is raised the equilibrium is established almost instantaneously (Figure 15 (*p*)).

The dependence of A.C./E.B.C. on bombarding voltage and current density for As_2S_3. Figures 16 (*a*), (*b*) show, for two temperatures the variation of A.C. gain with bombarding voltage for various bias voltages. The curves are similar to the curves obtained under D.C. conditions; for instance, the effect begins at a definite value of V_0 (coinciding with the value of V_0 for D.C. experiments), there exists a $V_{\max}$ and the negative and positive gains are equal. The A.C. gain is, however, always smaller than the average A.C. gain; this indicates that some E.B.C. current flows during the off period of the primary current. The A.C. gain does decrease with increasing current density, but not as rapidly as the D.C. gain.

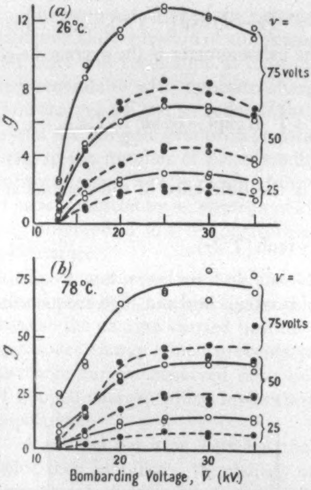

Figure 16. A.C./E.B.C. gain. As_2S_3 specimen, 1·9 μ. I_p (average) 27×10^{-8} amp/cm², pulse frequency 2×10^3 sec^{-1}. —— average A.C. gain. – – – A.C. gain.

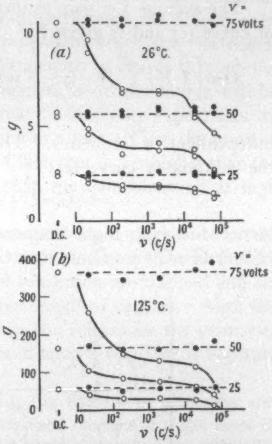

Figure 17. As_2S_3 film 1·9 μ. $V = 25$ kv., average $I_p = 27 \times 10^{-8}$ amp/cm²; variation of g with frequency. —— A.C. gain. – – – average A.C. gain.

The dependence of A.C. gain on the frequency of the primary current. Figures 17 (*a*), (*b*) show the variation of A.C. gain at two temperatures with the frequency of the primary beam. The gain is initially constant, then decreases with increasing frequency, approaching a constant value at about 500 c/s. Above 10,000 c/s. the gain drops rapidly. The second decrease must be attributed to the circuit. The D.C. gains and the average A.C. gains are also shown on the diagrams. The average A.C. gain is, throughout the frequency range, equal to the D.C. gain.

The decrease of gain with frequency and the shape of the A.C./E.B.C. current pulse can be interpreted as follows. For primary current of unit amplitude let I_1 be the time-dependent fraction of the A.C./E.B.C. current (Figure 18 (*a*)) and let I_2 be the instantaneous fraction (Figure 18 (*b*)), so that the total A.C./E.B.C. has the form shown in Figure 18 (*c*). It will be assumed that the rise and fall of the time-dependent current follows an exponential law with a relaxation time τ, so that for the rise $dI_1/dt=\gamma/\tau-I_1/\tau$, where γ/τ represents the effect of bombardment, and for the fall $dI_1/dt=-I_1/\tau$. Then for the steady periodic state (Figure 18 (*c*)) at a particular bias and bombardment voltage but for a frequency $\nu=1/2T$ the maxima B and the minima A of I_1 are related by

$$B\exp(-T/\tau)=A \quad \text{and} \quad B=\gamma-(\gamma-A)\exp(-T/\tau). \qquad \ldots\ldots(3)$$

The average A.C. gain as measured by the galvanometer is the average height of curve (*c*) and is given by

$$\overline{G}=\left[CT+\int_0^T\{\gamma-(\gamma-A)\exp(-t/\tau)\}dt+\int_0^T B\exp(-t/\tau)dt\right]\bigg/T=C+\gamma, \qquad \ldots\ldots(4)$$

independent of frequency. The A.C. gain is the difference of the maxima and the minima of curve (*c*):

$$G=C+B-A=C+\gamma\tanh(T/2\tau). \qquad \ldots\ldots(5)$$

Hence for very high frequency ($T\ll\tau$) $G=C$, and for very low frequency ($T\gg\tau$) $G=C+\gamma=\overline{G}$, so that G drops by γ between low and high frequencies.

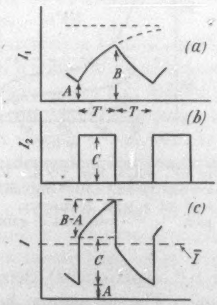

Figure 18.

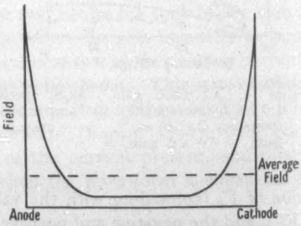

Figure 19.

Also, for $T\gg\tau$, I simply reproduces a sequence of equally long on and off periods so that then, neglecting current density effects, $G=\overline{G}=g$. This is confirmed by Figure 17.

Half way between the low and the high frequency regions $G=C+\gamma/2$. The frequency for which $G=C+\gamma/2$ can be read from Figure 17 so that τ can be found from (5):

$$C+\gamma/2=C+\gamma\tanh(1/4\nu'\tau) \qquad \ldots\ldots(6)$$

or $1/\tau = 2\nu' \ln 3$. From Figure 17 for the 75-volt bias curves

$$\text{at } 26^\circ \text{c.}, \; \overline{G} = 10{\cdot}5, \quad C = 6{\cdot}8, \quad \nu' = 30\ \text{sec}^{-1}, \quad 1/\tau = 66\ \text{sec}^{-1},$$
$$\text{at } 125^\circ \text{c.}, \; \overline{G} = 365 \quad C = 125, \quad \nu' = 27\ \text{sec}^{-1}, \quad 1/\tau = 54\ \text{sec}^{-1}.$$

With these values of $\overline{G}$ and C and an average $1/\tau = 60\,\text{sec}^{-1}$ equation (5) reproduces in fact the full curves of Figure 17 below 10^4 c/s. This shows that the value $1/\tau = 60\text{sec}^{-1}$ is independent of temperature and of bias.

These results indicate that the time-dependent part of the E.B.C. depends on an intermediate excitation. One would expect, however, the relaxation time of such an intermediate process to depend strongly on temperature. In the following brief discussion, this intermediate process will be left out of account.

§ 5. DISCUSSION OF RESULTS

The main net effect of the passage of a fast electron through an insulator is the excitation and ionization of atoms along its path. Some of the secondary electrons and holes will recombine at once, others will wander through the crystal until they recombine with opposite charges or are trapped or reach the electrodes. If no charges are lost by recombination, the total transport of charge through the crystal per ion pair produced is always **e**, and the gain, as defined above, will be equal to the number of pairs produced per primary. One may expect that an energy of about 5 ev. is required for the production of a pair. Then the number of pairs produced by an electron of 20 kv. will be 4,000, that is, far higher than the gain observed at low temperature and far less than the gain observed at high temperature.

But trapping and recombination are well illustrated by the existence of the critical voltage V_0: below V_0 the pairs produced recombine near their birthplace because the charges carried beyond the region of ionization are trapped and set up a space charge which prevents any further movement of carriers. Also, the discharge current observed must be interpreted as the release by the primaries of trapped charges which move through the film in such a way that it becomes unpolarized.

A general equation between the electric field, the density of electrons and holes, their mobilities, the density of traps and trapped charges and the rates of ionization and recombination is readily established but intractable. The far simpler and closely analogous problem, however, of the ionization chamber in which there are no traps and for which the ionization is constant through space can be solved by successive approximation (Mie 1904, Thomson 1906), and this solution should still indicate at least qualitatively the electric field in the dielectric under E.B.C.

J. J. Thomson and G. Mie have shown that the field in the ionized gas is nearly constant and small throughout a large part of the gas and rises exponentially near the electrodes (Figure 19). In the region of nearly constant field the number of recombinations of charges almost equals the number of charges produced by ionization. The narrow regions of strong field near the electrodes contribute, therefore, nearly all the current. As the applied field increases, the region of small constant electric field shrinks, until, in the limit, the field throughout the sample is nearly constant and equal to the applied field. When that happens all the charges produced in the gas are drawn to the electrodes. The strong fields near the electrodes arise from the separation by the applied field of charge carriers of opposite sign. When the carriers have equal mobility, the field distribution is symmetrical; for unequal mobilities the field is highest at the electrode which attracts the slower carriers. Figure 19 should be representative for the field in dielectric films under E.B.C.

Newton (1949) has suggested an expression for the average field E_D required to suppress recombination over a given layer of thickness D. By the use of this relation one can arrive at values for the field both in the central region and near the electrodes.

Approximate values for the rate of production of pairs and the coefficient of recombination are first obtained as follows: For a primary current density of $13{\cdot}6 \times 10^{-8}$ amp/cm^2 the number of electrons impinging on the film equals 86×10^{10} electrons/cm^2 sec. Let us assume that the electrons ionize uniformly throughout the film and completely lose their energy within the film thickness $d = 3 \times 10^{-4}$ cm., also that the ionization energy per pair is 5 ev. and the bombarding voltage is 20 kv. Then the rate of production of pairs is

$$\beta = (86 \times 10^{10} \times 20 \times 10^3)/(5 \times 3 \times 10^{-4}) \sim 12 \times 10^{18} \text{ cm}^{-3} \text{ sec}^{-1}.$$

The rate of recombination will be given by $\alpha n_+ n_-$ where n_+, n_- are the densities of positive and negative carriers and α is a factor approximately equal to the product of the velocity of the carriers and an atomic cross section, $\alpha \sim 6 \times 10^7 \times 10^{-15} = 6 \times 10^8$ cm^3 sec^{-1}, corresponding to an electron of $E_{\text{kin}} = 0{\cdot}5$ ev. One also requires values for the mobilities u_+, u_- of the carriers. Usually one reckons these to be in the neighbourhood of 100 cm^2 sec^{-1} volt^{-1}. This value refers to carriers in the free state. Here, in view of the presence of traps, it should be multiplied by the ratio of the time the carriers are free to the time they are trapped. We cannot estimate this ratio. The calculation will first be carried out for $u_+ < u_-$, $u_+ \sim 1$ cm^2 sec^{-1} volt^{-1}.. Then the time required for either charge to traverse the layer is $\tau_{+,-} < D/u_{+,-}E_D$. During this time $\beta D\tau = \beta D^2/u_{+,-} E_D$ pairs are produced in the layer. The density of free charges approximately equals the number of charges produced in the time τ divided by the thickness of the layer, $n_{+,-} \sim \beta D/u_{+,-}E_D$ and the number of recombinations per second in the layer will be smaller than $\alpha n_+{}^2 D \sim \alpha(\beta D)^2/D(u_+E_D)^2$. On the other hand, the number of electrons produced in the layer per second is βD. The number of recombinations is negligible if it is much smaller than the number of electrons produced, that is if $E_D \sim (\beta\alpha)^{1/2} D/u_+$. Hence, even in order to suppress recombination over the whole thickness d of the specimen $(3 \times 10^{-4}$ cm.), a field of only 200 v/cm. would be required. But in all our experiments the applied field exceeded 200 v/cm. by a large factor (10 to 10^3). If, therefore, the applied field existed throughout the film all liberated electrons and holes should have been drawn to the electrodes and the largest gain (in the example, 4,000) obtained, instead of the small fraction of this usually found. Hence one must conclude either that in a wide central region the field is far smaller than 200 v/cm., and very large fields at the boundary make up the total potential drop across the specimen, or that the value taken for u is far too high. Now, the thickness λ of these boundary layers and the fields E_λ there can also be estimated: for the bombarding voltage and the current density of the example and a bias of 100 v. a gain of 20, i.e. an E.B.C. current i_s of $1{\cdot}7 \times 10^{13}$ electrons/cm^2 sec. is observed. If this comes entirely from the boundary layers, $i_s = 2\beta\lambda$ or

$\lambda \sim 7 \times 10^{-7}$ cm. As further, approximately $2\lambda E_\lambda + (d-2\lambda)E_C = 100$ volts, and the field E_C in the central region must be smaller than 200 volts/cm.,

$$E_\lambda \sim [100 - (3\times 10^{-4} - 1{\cdot}5\times 10^{-6})200]/1{\cdot}5\times 10^{-6} \sim 6\times 10^{7}\ \text{v/cm.}$$

This value for E_λ is rather high although the macroscopic breakdown field strength can be exceeded in very thin layers (see, for example, Plessner 1948). But this high field would entail field emission from the electrodes which would invalidate the relation $\lambda = i_s/2\beta$. Besides, field emission can barely play an important role when the gain observed is small. Hence, one must conclude that $u \ll 1$ for the condition under examination; in order to arrive at a more reasonable value for E_λ, say 3×10^{6} v/cm., u would have to be about 6×10^{-4} cm^2 sec^{-1} volt^{-1} and $E_C \sim 3\times 10^{5}$ volt cm^{-1} so that most of the potential drop takes place in the central region.

But the mobilities as determined by the rate of release of charges from traps must increase exponentially with temperature and it appears that the resultant increase in gain is due both to the increasing width of the boundary layers and also to the increased boundary fields. Even if the entry of carriers does not take place at low gain it should do so when a high gain is observed. The main evidence for this comes from the high gains observed at high temperatures and high bias which cannot be explained by the formation of ion pairs by the incident beam alone, especially as even at the highest gains observed no trace of saturation was found.

Even higher gains than those reported here have been observed in cadmium sulphide crystals irradiated with light and with α- and β-particles. These crystals were first prepared by Frerichs (1946) and have been investigated in detail by Frerichs and Warminsky (1946), Kallmann and Warminsky (1948), Fassbender (1949) and Frerichs (1949). In particular, Kallmann and Warminsky have reported secondary currents equivalent to up to 10,000 times the number of ion pairs produced, and both these authors and Frerichs have concluded that this effect must be due to the entry of carriers. Two others processes are known which might lead to extra secondary currents, viz. ionization by collisions and an excess temperature of the electron gas over the lattice temperature (Fröhlich and O'Dwyer 1950). The first possibility has also been discussed by Kallmann and Warminsky and rejected on account of the comparatively low fields used. In the experiments reported here one can exclude ionization by collisions because of the too gradual increase of gain with bias. Again, from the figures given by Fröhlich and O'Dwyer it appears that an excess electronic temperature would not be sufficient to explain the high gain observed or extrapolated. Hence, one should conclude that the highest gains observed in E.B.C. are due to the entry of carriers. In many respects, however, the effects in CdS and those observed here are very different.

It is not yet possible to follow up in detail the related processes of formation of ion pairs, establishment of space charge and the entry of carriers. We know very little about the distribution of ionization in the dielectric, or about the variation of effective mobility with temperature and we do not know how the mobility and current density of the carriers affect the shape of the field. One would expect, however, that in the low gain region—where no entry of carriers takes place and which corresponds to the regions investigated by McKay and

Pensak—the gain roughly follows the effective mobility which should increase exponentially with temperature as it depends mainly on the activation of traps. Such traps have been studied extensively by Randall and Wilkins (1945) and Garlick and Wilkins (1945). In fact, Figure 10 suggests that there are two types of trap present: between liquid air and room temperature thermal release only takes place from shallow traps less than 0·01 volt deep; the rapid rise of gain at high temperatures is due to thermal release from deeper traps with an activation energy of 0·5 ev.

The variation of gain with current density is a complicated effect which could be explained in a number of ways. A displacement of $V_{\max}$ with temperature is not incompatible with Thomson–Whiddington's law. In view of the complexity of the process the optimum distribution of ionization throughout the layer will be sensitive to changes in mobility. It appears attractive to associate the secondary effect with the entry of carriers into the dielectric in the same way as Mott and Gurney (1949) have interpreted the secondary photoelectric effect. Also, the slow awakening of the secondary E.B.C. is analogous to the slow development of the passage of carriers observed in cadmium sulphide crystals. But the explanation given by Mott and Gurney does not provide for the instantaneous response of the E.B.C., once the dielectric films are conditioned by previous bombardment.

APPENDIX

THE PHOTOCONDUCTIVITY OF As_2S_3 FILMS

The films show photoconductivity. The currents are of the order of 10^{-6} amp. at room temperature for an illuminated area of 0·1 cm² and fields of about $0{\cdot}5 \times 10^6$ v/cm. when a 75-watt lamp is placed at 1 cm. away from specimen.

The photocurrent, similar to the E.B.C. current, increases rapidly with increasing bias and with increasing temperature. It follows the modulations of the light source (ON, OFF) without a time lag within the period of the galvanometer below 100° C. always and at higher temperatures if the sample has, for some time, been illuminated under steady bias. But for a virgin sample, at a given bias, the photocurrent reaches a maximum slowly, and on reversal of the bias starts at a much lower value and rises slowly to the value it had previously.

This behaviour differs from the secondary photoelectric current which decays or increases slowly when the light is switched on or off.

ACKNOWLEDGMENTS

The work described in this paper was carried out in the Research Laboratory, Birkbeck College, University of London (Director, Professor J. D. Bernal). It was made possible by generous grants from the Nuffield Foundation. One of the authors (F. A.) wishes to acknowledge the receipt of a maintenance grant from the Department of Scientific and Industrial Research.

The experimental part of the paper is fully described in a thesis for the Ph.D. degree submitted by F. A. which has been approved by the University of London.

REFERENCES

Ansbacher, F., and Ehrenberg, W., 1948, *Opening of Biomolecular Research Laboratory*, Birkbeck College, p. 6; 1949, *Nature, Lond.*, **164**, 144.

Becker, A., 1904, *Ann. Phys., Lpz.*, **13**, 394.

Fassbender, J., 1949, *Ann. Phys., Lpz.*, **5**, 33.

Frerichs, R., 1946, *Naturwissenschaften*, **33**, 281; 1949, *Phys. Rev.*, **86**, 1869.

Frerichs, R., and Warminsky, R., 1946, *Naturwissenschaften*, **33**, 251.

Kallmann, H., and Warminsky, R., 1948, *Ann. Phys., Lpz.*, **4**, 57, 69.

Fröhlich, H., and O'Dwyer, J., 1950, *Proc. Phys. Soc.* A, **63**, 81.

Garlick, G. F. J., and Wilkins, M. H. F., 1945, *Proc. Roy. Soc.* A, **184**, 408.

McKay, K. G., 1948, *Phys. Rev.*, **74**, 1606.

Mie, G., 1904, *Ann. Phys., Lpz.*, **13**, 857.

Mott, N. F., and Gurney, R. W., 1949, *Electronic Processes in Ionic Crystals*, 2nd Edition (Oxford : University Press) p. 186.

Newton, R. R., 1949, *Phys. Rev.*, **75**, 234.

Pensak, L., 1949, *Phys. Rev.*, **75**, 472.

Plessner, K. W., 1948, *Proc. Phys. Soc.*, **60**, 243.

Randall, J. T., and Wilkins, M. H. F., 1945, *Proc. Roy. Soc.* A, **184**, 347.

Rittner, E. J., 1948, *Phys. Rev.*, **73**, 1212.

Thomson, J. J., 1906, *Conduction of Electricity through Gases* (Cambridge : University Press), pp. 84, etc.

The Specific Heat of Liquid Helium at Temperatures between 0·6° and 1·6° K.

By R. A. HULL,* K. R. WILKINSON and J. WILKS

Clarendon Laboratory, Oxford

Communicated by F. E. Simon; *MS. received 2nd October* 1950

ABSTRACT. A detailed account is given of experiments made to measure the specific heat of liquid helium between 0·6 and 1·6° K. Below 1·4° the specific heat may be expressed as $C=0{\cdot}024T^{6{\cdot}2}$ cal/gm/deg. Some implications of this result are briefly discussed.

§ 1. INTRODUCTION

The specific heat of liquid helium below 1° K. is of some consequence in the interpretation of the properties of liquid helium and was first measured by Pickard and Simon (1939) using a sealed capsule containing paramagnetic salt and helium. This work was never fully published as the authors subsequently had reason to doubt its accuracy. Keesom and Westmijze (1941) announced that they had made similar measurements but their results have likewise never been fully published. The brief notices that have appeared show that while Keesom and Westmijze found that the specific heat varied as T^6 right down to 0·6°, Pickard and Simon found a T^3 region below 0·8°; there is also a discrepancy in the absolute magnitudes at 1·0°. This paper describes a new attempt to measure the specific heat and clear up the somewhat confused position. As no full account of measurements with a capsule has yet been published it may be useful to describe the experiments in some detail. The specific heat with which we are concerned is the specific heat of the liquid in equilibrium with the saturated vapour, though for brevity it will be referred to as the specific heat of helium.

---

* Dr. Hull was killed in an Alpine accident on 23rd August 1949.

§ 2. THE EXPERIMENT

A calorimeter containing liquid helium and some paramagnetic salt is demagnetized adiabatically from a starting temperature of about 1·0° K. As the salt cools, the thermal conductivity of the helium ensures that the calorimeter and all its contents cool down with it.* The calorimeter is then heated at a known rate and its resulting change in temperature is observed. Provided that the thermal capacities of the paramagnetic salt and the calorimeter are known, the specific heat of the helium may then be obtained. Alternatively we may get the same result by performing experiments in the same calorimeter with a constant quantity of salt but with different amounts of helium. The magnetic moment of the salt ballistically is measured, and this determines the temperature provided the dependence of its susceptibility on temperature is known below 1°. As both the specific heat and the susceptibility of iron ammonium alum have been measured at these temperatures by Kurti, Simon and Squire (Cooke 1949) we used it in all the experiments. The calorimeter was mounted inside a double walled cryostat of a Simon expansion liquefier; a general description of this, and of the technique of adiabatic demagnetization, has already been given by one of us (Hull 1947).

§ 3. THE CALORIMETER

The size of the calorimeter is limited by the requirement that the whole apparatus must fit between the poles of a magnet. Thus as the specific heats of both helium and salt are small in the region below 1°, the thermal capacity of the calorimeter and its contents will also be small; with the calorimeter finally used its minimum value at 0·6° was only about 4×10^4 erg/deg. Heat was supplied at the rate of about 1000 erg/minute so as to raise the temperature 0·1° in about five minutes, and the thermal capacity obtained by differentiating a plot of temperature against time. The heat leak due to imperfect insulation should therefore be no greater than about 100 erg/minute.

The simplest form of a calorimeter would have been a thin walled vessel fitting inside a double walled helium cryostat and communicating with the rest of the apparatus by a thin walled German silver tube passing through the cryostat. However, the existence of the helium II film leads to a heat inflow (Rollin and Simon 1939) which even with a fine capillary may amount to several hundred erg/minute.

Our measurements were made using the sealed-off 'capsule' technique first used by Kurti, Rollin and Simon (1936). Helium gas at about 120 atmospheres pressure together with the paramagnetic salt is introduced at room temperature into a thick walled calorimeter or capsule which is then completely sealed off with soft solder. The capsule is mounted on nylon threads in a cradle (Hull 1947) and placed in the cryostat (Figure 1) so that the only thermal contact with the cryostat is via the threads. On cooling the capsule the helium gas condenses producing about 1·5 cm^3 of liquid. Using this technique we have consistently obtained heat inflows of only about 70 erg/minute.

---

* Although the heat conductivity of liquid helium falls off below 1·0° (Kurti and Simon 1938 a) it should be adequate for our purpose down to at least 0·2°. Certainly there was almost no sign of any overheating occurring.

§4. THE CAPSULE

In order that there is as much helium to work with as possible the capsule (Figure 2) is made as large as will conveniently fit into the cryostat. It is machined from a rod of phosphor bronze (8% tin) which has a high tensile strength, a low electronic specific heat, and is free of superconductivity and magnetic effects at helium temperatures.

One end is closed by a screwed plug which may be removed in order to introduce the salt in the form of a powder C which is pressed down into the bottom of the capsule. The plug is then screwed and soldered in while the other end of the capsule is kept cool in a mixture of solid carbon dioxide and acetone so that the salt is not decomposed by the heat. Helium gas is introduced into the capsule through a well-cleaned copper capillary tube A soft soldered into a hole in the screw plug. In the bore of this tube is a wire of soft solder B and the gas is sealed in the capsule by hammering the capillary flat and then applying heat so that the solder runs. Finally, the capillary is cut above the solder seal.

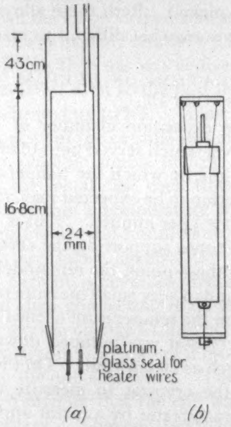

Figure 1.

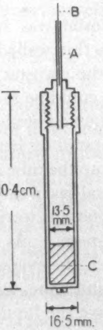

Figure 2.

After a set of experiments the quantity of helium in a capsule is determined by making a fine cut in the copper capillary tube with a razor blade, collecting the gas over water and measuring its volume. An independent result is also obtained by weighing the capsule before and after releasing the gas. The measurements of mass and volume were consistent to 1%.

An electrical heater of No. 40 S.W.G. silk-covered manganin wire was wound on to the capsule, the whole being coated with 'Demarda' bakelite varnish (supplied by Messrs. Bakelite Ltd.) and baked so as to obtain adequate thermal contact with the capsule. This was important as, if the heater or the leads to it were overheated, any gas adsorbed on them might be evolved and ruin the vacuum insulation round the capsule. However, no such trouble was encountered.

§ 5. THE MAGNETIC PROPERTIES OF SOME TECHNICAL MATERIALS

All our temperature measurements depend on accurate determinations of the susceptibility of iron ammonium alum which, like all paramagnetic susceptibilities, is small even at 4°. Therefore it is important that no other part of the apparatus should be magnetic and give effects which are superposed on those due to the salt. The parts of the apparatus most likely to give trouble in this respect are the capsule and the cryostat which both surround the salt, because a very small amount of ferromagnetic impurity in this mass (about 200 gm.) of metal would give effects comparable with those produced by our 6 gm. or so of salt. Undesirable magnetic effects were, in fact, found when using German silver cryostats and constantan resistance wire.

The reasons for this are not clear although the work of Kaufmann and Storr (1943) has shown that copper–nickel alloys can have a susceptibility which is both temperature and field dependent. Both German silver and constantan have a high nickel content so we turned to materials containing little or no nickel. For the cryostat and capsule we used phosphor bronze and for the electrical heater and leads manganin wire (about 5% nickel). Both these alloys have been entirely satisfactory* although the bronze is somewhat difficult to machine.

§ 6. THE RATE OF EVAPORATION OF HELIUM FROM THE CRYOSTAT

The cryostat was suspended below the expansion chamber of the helium liquefier by a thin walled tube of German silver which served both to introduce the liquid into the cryostat and as a pumping line by which the temperature of the helium bath could be reduced. The evaporation to be expected may, from known data, be estimated at about 6 cm^3 of gas (N.T.P.) per minute. This is made up of 2 cm^3 evaporated by heat coming down the tubes supporting the cryostat, 3 cm^3 which flows up the tube as a HeII film below the λ-point, the remainder being due to any residual gas in the vacuum insulation and in very small measure to radiation. These expectations were only borne out when the temperature of the cryostat was above the λ-point. As the helium in the cryostat was pumped down from the λ-point to 1·5° the evaporation rose to as much as 20 cm^3/min. On the occasions when a second tube was introduced into the cryostat to measure the vapour pressure above the liquid, the evaporation was greater by a factor approximately equal to the increase in the total perimeter of the tubes up which film could creep. Moreover the dependence of the amount of evaporation on the temperature of the cryostat took the same form as would be expected if it were all due to film flow. Thus it appeared that film flow of a greater magnitude than that usually reported was taking place. Subsequently, Bowers and Mendelssohn (1949) have shown that such an increased flow may be produced if the helium gas condensed into the cryostat contains impurities: such impurities are deposited as a thin layer on the inner walls of the cryostat and the tubes to it, so producing an increased flow of film. As confirmation of this we may mention that each time we condensed helium gas into the cryostat after it had been pumped down we observed a considerable increase in the evaporation.

---

* There does not appear to be a simple test which can be made at room temperature to give an indication of the low temperature behaviour. For example the constantan wire which showed much remanence was in no way attracted by a powerful permanent magnet at room temperature whereas the manganin wire whose low temperature performance was satisfactory was slightly attracted.

§ 7. THE THERMAL INSULATION OF THE SPECIMEN

To obtain accurate measurements, the heat leak to the calorimeter must be kept to a minimum, i.e. once the calorimeter has been cooled down, it must stay cold and not receive any appreciable heat from its surroundings. The problem of thermally isolating specimens at very low temperatures has been very fully treated by Cooke and Hull (1942), who showed that for good thermal insulation it is necessary to support the specimen on thin fibres and to have a minimum of residual gas* around it before demagnetization. This latter condition can be fulfilled by using a baking out technique (Hull 1947). One further precaution was necessary because of the very peculiar effect that any vibration of the specimen was accompanied by an evolution of heat, sometimes as great as 300 erg/minute. This effect is still being investigated, but in the present experiments the vibration was reduced by mounting the apparatus as rigidly as possible.

Our final practice was to magnetize the capsule at a temperature of 1·4°. The exchange gas was then pumped for an hour and then just prior to demagnetization the cryostat was pumped down as far as possible (to about 0·9°). After demagnetization the heat inflow was about 70 erg/min., most of which was probably arriving down the nylon suspension, as this had to be comparatively strong in order to hold the heavy capsule steady. The heat flow remained small to temperatures of about 1·1° but then gas was evolved and it was necessary to pump the vacuum space continually; even so the heat leak rose to a few thousand erg/min. when the capsule was heated up to 1·5°. This, however, was of no great consequence as the thermal capacity of the capsule was also rising rapidly.

Another possible source of heat inflow to the capsule is the eddy currents induced in the metal case each time the measuring field (order of 10 gauss) is reversed in taking a temperature measurement. This contribution can quite easily amount to several hundred ergs at each temperature determination unless precautions are taken against it. To make a temperature measurement the measuring current is reversed, by disconnecting the measuring coil from the battery and then connecting it up the other way round. As the eddy current heating for a given change of flux is inversely proportional to the time constant of the primary circuit, nearly all of it is occasioned by breaking the coil circuit prior to making it in the opposite sense. Therefore we used a reversing switch connected up in such a manner that the coil was always shorted before being disconnected from the battery. This ensured that the time constant was not unduly small and we were able to reduce the eddy current heating to at most 20 ergs per temperature measurement.

§ 8. THE MEASUREMENTS

After the calorimeter had been cooled down, the heat inflow to it was measured by watching the temperature drift for about ten minutes. Electrical energy was then supplied to the capsule at a rate known from measurements of the voltage across and the current in the heater. The temperature changes were observed by making ballistic determinations of the magnetic moment of the capsule at half-minute intervals for about ten minutes; the whole cycle was then repeated. A typical set of galvanometer readings is given in Figure 3; by differentiating this curve we were able to obtain values of the thermal capacity of the cryostat as a function of temperature. Values of this measured capacity (taken from a smoothed curve) are given in the Table.

---

* In order to magnetize the salt isothermally, helium exchange gas is admitted to the space surrounding the specimen so that the heat of magnetization may be carried away to the cryostat. In order to carry out the demagnetization adiabatically it is of course necessary first to pump away all this exchange gas.

As has been previously explained (e.g. Kurti and Simon 1938 b) the temperature scale T^* on which measurements are made below 1° is not the absolute scale T but one defined by assuming Curie's law to hold for the salt even at the lowest temperatures †. To convert T^* temperatures to absolute ones it is necessary to know the susceptibility of the salt as a function of temperature. We use the results of Kurti, Simon and Squire (Cooke 1949) giving T_s^* and dT_s^*/dT as functions of T to correct temperatures and specific heats to the absolute scale (see Table).

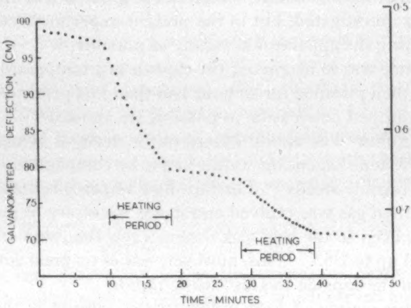

Figure 3.

T	T^*	dT/dT_s^*	Thermal Capacities (cals × 10^{-5} per deg.)					$C \times 10^4$
			Capsule	Case	Salt	Evap.	Helium	(cal/gm/deg.)
0·4	0·415	0·970	215	12	203	0	0	0
0·5	0·512	0·979	166	15	142	0	9	5
0·6	0·610	0·984	138	18	98	0	22	11
0·7	0·708	0·988	160	21	73	12	54	27
0·8	0·807	0·991	240	23	57	44	118	59
0·9	0·906	0·994	450	26	46	116	260	130
1·0	1·006	0·997	810	29	38	250	490	240
1·1	1·10	1·00	1470	32	31	430	980	490
1·2	1·20	1·00	2400	35	26	820	1520	760
1·3	1·30	1·00	3800	38	22	1310	2400	1190
1·4	1·40	1·00	5500	41	19	1950	3500	1750
1·5	1·50	1·00	7800	44	17	2800	4900	2400
1·6	1·60	1·00	10300	47	14	3600	6600	3300

The measured thermal capacity (column 4 of the Table) is made up of four components: the capacity of the liquid helium, of the iron alum, of the metal capsule and a capacity associated with the latent heat of liquid helium evaporating into the free space above the salt and liquid. The specific heat of the salt is known, the small capacity of the metal case may be estimated from the known electronic specific heats of its components while the capacity associated with helium evaporating is calculated in the Appendix. Values of these quantities for a capsule filled at room temperatures with 120 atmospheres of helium are given in the

---

† Because of demagnetization effects the measured susceptibility depends on the shape of the specimen. Following usual practice our T^* temperatures are corrected to T_s^* temperatures, the T^* temperatures that would be obtained if we were using a spherical sample of salt (Kurti and Simon 1938 b).

Table. The penultimate column in this Table gives the capacity of the helium obtained as the difference between the measured capacity of the capsule and the total capacity of all the other constituents.

Clearly below 0·6° the thermal capacity of the helium is so small a part of the total that the method becomes insensitive. As a check on the values below 1° experiments were done with the same capsule containing the same amount of salt but only 15 atmospheres pressure of helium. The difference in the thermal capacities of the capsule filled with different quantities of helium gave another set of values for the specific heat which agreed with the earlier results to within the experimental error.

The final values for the specific heat C are shown in the last column of the Table, in Figures 4(*a*) and (*b*) and as a logarithmic plot in Figure 4(*c*). The accuracy is estimated to be within $\pm 5\%$ or $\pm 3 \times 10^{-4}$ cal/gm/deg., whichever is the larger.

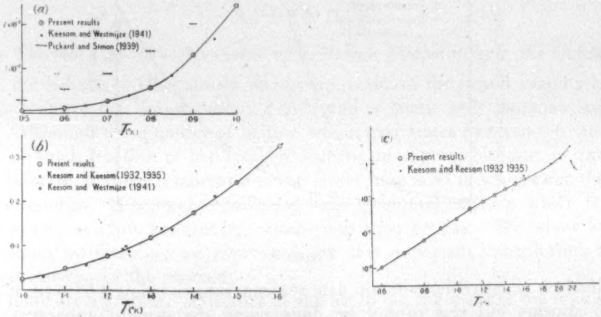

Figure 4.

§ 9. THE SPECIFIC HEAT OF LIQUID HELIUM

Between 1·4° and 0·6° we can represent the results by $C = 0{\cdot}024\,T^{6{\cdot}2}$ cal/gm/deg. which agrees closely with the values obtained by Keesom and Westmijze.

It may be of consequence to note that our measurements have been made not on bulk liquid but on liquid in the interstices of a powdered crystalline salt, and there might be some dependence of the specific heat on the degree of dispersion of the helium.* However, it has recently been shown (Frederikse 1949) that while the specific heat of thin films of helium can be much different from that of the bulk liquid the difference will be very small if the film is at least a hundred molecular layers thick (say 10^{-5} cm.). As the mean diameter of our crystals was at least 10^{-3} cm., it is apparent that these size effects would be of no importance.

It is of interest to discuss whether we may extrapolate the T^6 relation down to absolute zero. Both Landau (1941) and Tisza (1947) in their theories of liquid helium postulate that at sufficiently low temperatures the only contribution to the specific heat will be due to Debye type waves which give rise to the usual T^3 law. An estimate of the magnitude of such a term has been made (Landau 1941,

---

* This was one of the reasons why Pickard and Simon refrained from publishing their results but it now seems that the need to determine the absolute value of the energy supplied by their gamma-ray source of heat added an additional uncertainty to an already complicated experiment.

Dingle 1949) by using Debye's theory of the specific heat of a continuum but omitting transverse waves as He II has a vanishing viscosity. Using the measured value of the velocity of sound they find that the specific heat is given by $C = 4{\cdot}4 \times 10^{-4} T^3$ cal/gm/deg. which implies 0·0010 cal/gm/deg. at 0·6°. Our measured value of 0·0011 cal/gm/deg. at 0·6° does not rule out such a term but if one is present there must be an abrupt change in the index of the power law at about this temperature.

According to Landau the specific heat follows a T^3 law from absolute zero to about 0·6° when it increases more rapidly because, to use Landau's terminology, the rotons make a contribution which, though only 1% of the Debye specific heat at 0·5°, increases so rapidly that it is 400% of the Debye term at 1·0°. Values of the specific heat calculated from Landau (1947) are given in Figure 5, there is a satisfactory agreement between the theoretical and observed values.

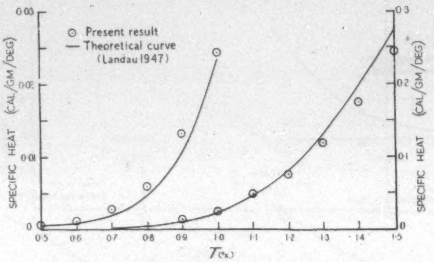

Figure 5.

Clearly it is desirable to obtain data at temperatures below 0·6° to see if the T^3 region appears but this cannot be done using the present apparatus. The difficulty is that while the thermal capacity of the salt is rising as T^{-2}, that of the helium is falling as T^6 and will soon become a very small part of the total capacity of the capsule. In fact in order to make measurements down to 0·3° we should have to increase the sensitivity by a factor of about 100. We could obtain some of this increase by using less salt and demagnetizing from a lower temperature but this would increase the difficulty of obtaining good thermal insulation at temperatures above 0·5°. Alternatively we might use salts with lower specific heats but these have smaller entropies of magnetization and so a greater quantity is needed to produce the same cooling. The best method, however, would be to use a much greater quantity of helium in the calorimeter. This does not seem possible in a capsule of practical size but Hudson, Hunt and Kurti (1949) have recently described a calorimeter into which helium may be introduced as a liquid and in which the heat inflow due to film has been reduced to a low value. It is hoped that by using such a calorimeter measurements will shortly be extended to appreciably lower temperatures.

Although our measurements were made primarily to investigate the region below 1·0° it is interesting to compare our values with those of other workers above 1·0°. Between 1·0° and 1·4° both our results and those of Keesom and Westmijze are in agreement with three points due to Keesom and Keesom (1932). Between 1·4° and 2·0° however, the position is not so satisfactory as, apart from some early work by Keesom and Clusius (1932) which show much scatter, only three points due to Keesom and Keesom (1932, 1935) are available. Although these three points do not seem self-consistent they give values appreciably higher than ours at 1·5° and 1·6°; we hope eventually to make measurements in this region to clarify the position.

As the entropy diagram for helium has already been calculated (Keesom, Bijl and Monte 1941) using Keesom and Westmijze's value, no modification to this is called for. Our results necessitate, however, a small correction to the vapour pressure curve of Bleaney and Simon (1939) which was based on the results of Pickard and Simon below 1·2°. As this correction will be of the same order as the error introduced by the uncertainty in the value of the specific heat in the region of 1·5° we do not propose to treat this until more data have been obtained in that region.

APPENDIX

The Thermal Capacity Associated with Helium Evaporating in the Capsule

As the helium in the capsule warms up, some of the liquid evaporates into the space above the liquid (about 8 cm³) and a latent heat must be supplied to it. Although the quantity of helium which evaporates between 0·6° and 1·6° is a very small fraction of the total, it absorbs an appreciable part of the heat input because at these temperatures the latent heat is so much greater than the thermal energy. The vapour will also have a thermal capacity which is small and may be taken into account by treating it as a perfect gas. We follow Pickard and Simon in obtaining an expression for this important contribution to the thermal capacity of the capsule.

If there are n gramme molecules of vapour in the space above the liquid, then the rate Y at which heat must be supplied to evaporate the liquid and heat the vapour is given by

$$Y=\lambda\frac{dn}{dT}+\frac{3}{2}n\boldsymbol{R}\ \text{erg/deg.}=\lambda\frac{d}{dT}\left[\frac{pV}{\boldsymbol{R}T}\right]+\frac{3}{2}\frac{pV}{T}$$

$$=\frac{\lambda V}{\boldsymbol{R}}\left[\frac{1}{T}\frac{dp}{dT}-\frac{p}{T^2}\right]+\frac{3}{2}\frac{pV}{T},$$

where λ = molar heat of evaporation, p = vapour pressure, V = volume of vapour. As we may write $\lambda=\boldsymbol{R}T^2[\partial(\ln p)/\partial p]$, we can evaluate ΔY from the vapour pressure curve of liquid helium (Bleaney and Simon 1939). Values of ΔY as a function of temperature are given in column 7 of the Table.

ACKNOWLEDGMENTS

The authors wish to thank Professor F. E. Simon for his continued interest and Dr. A. H. Cooke and Dr. N. Kurti for many helpful discussions. Two of them (K. R. W. and J. W.) also wish to thank the Department of Scientific and Industrial Research for maintenance grants.

REFERENCES

Bleaney, B., and Simon, F., 1939, *Trans. Faraday Soc.*, **35,** 1205.
Bowers, R., and Mendelssohn, K., 1949, *Nature, Lond.*, **163,** 870.
Cooke, A. H., 1949, *Proc. Phys. Soc.* A, **62,** 269.
Cooke, A. H., and Hull, R. A., 1942, *Proc. Roy. Soc.* A, **181,** 83.

Dingle, R. B., 1949, *Proc. Phys. Soc.*, A **62**, 154.
Frederikse, H. P. R., 1949, *Physica* **15**, 860.
Hudson, R. P., Hunt, B., and Kurti, N., 1949, *Proc. Phys. Soc.* A, **62**, 392.
Hull, R. A., 1947, *Report on Cambridge Low Temperature Conference* (London : Physical Society), p. 72.
Kaufmann, and Storr, 1943, *Phys. Rev.*, **63**, 445.
Keesom, W. H., Bijl, A., and Monte, L. A. J., 1941, *Inst. Int. du Froid, Leiden.*
Keesom, W. H., and Clusius, K., 1932, *Proc. K. Akad. wet., Amst.*, **35**, 307.
Keesom, W. H., and Keesom, A. P., 1932, *Proc. K. Akad. wet., Amst.*, **35**, 736; 1935, *Physica*, **2**, 557.
Keesom, W. H., and Westmijze, W. K., 1941, *Physica*, **8**, 1044.
Kurti, N., Rollin, B. V., and Simon, F. E., 1936, *Physica*, **3**, 266.
Kurti, N., and Simon, F. E., 1938 a, *Nature, Lond.*, **142**, 207; 1938 b, *Phil. Mag.*, **26**, 849.
Landau, L., 1941, *J. Phys. U.S.S.R.*, **5**, 71; 1947, *Ibid.*, **11**, 91.
Pickard, G., and Simon, F. E., 1939, *Abstracts of papers communicated to the Royal Society of London*, 521 (3rd April 1939).
Rollin, B. V., and Simon, F. E., 1939, *Physica*, **6**, 219.
Tisza, L., 1947, *Phys. Rev.*, **72**, 838.

The Total Cross Section of Beryllium, Aluminium, Sulphur and Lead for Neutrons of Energies from 2 Mev. to 6 Mev.

By G. H. STAFFORD[*]
Cavendish Laboratory, Cambridge

Communicated by E. S. Shire; MS. received 23rd August 1950, and in amended form 17th October 1950

ABSTRACT. The total neutron cross sections of beryllium, aluminium, sulphur and lead have been measured in the range of energies from 2 Mev. to 4 Mev. and from 5 Mev. to 6 Mev. by a transmission experiment. Resonances were observed in all four elements. The results obtained for lead and for beryllium are compared with those expected according to the one-body theory for light nuclei.

§ 1. INTRODUCTION

The technique of producing mono-energetic neutron beams has been developed considerably in recent years. Velocity selectors and filtered neutron beams are available for the range of energies below 1 kev.; the energy range from 10 kev. to 1 Mev. is obtained by a number of (γ, n) reactions, and in the energy range from 30 kev. to 6 Mev. there are such reactions as the ^{12}C (d, n), the ^{2}H(d, n), and the ^{7}Li(p, n). The parallel development in the technique of neutron detection has made accurate cross section measurements possible.

A considerable number of total neutron cross section measurements have been reported, particularly in the energy range below 1 kev. (Goldsmith, Ibser and Feld 1947). The energy range above about 1 Mev. has not been so well investigated.

Aoki (1939) studied the total neutron cross section of a large number of elements in the energy range from 2 Mev. to 3 Mev. by the use of neutrons from the ^{2}H(d, n) reaction. Many elements showed an irregular variation in cross section with neutron energy but this might have been due, in part at least, to the fact that the neutron detector responded not only to neutrons but also to any gamma radiation that was present. However, broad resonances have since been observed by Macphail (1940) in magnesium and aluminium and by Allen, Burcham and Wilkinson (1947) in beryllium and aluminium in the range of neutron energies from 2 Mev. to 4 Mev. Measurements have also recently been reported by Freier, Fulk, Lampi and Williams (1950) in the range of neutron energies from 0·60 Mev. to 1·90 Mev. and from 2·5 Mev. to 5·0 Mev. with carbon, oxygen, magnesium, silicon and sulphur. Resonances were observed in all these elements.

---

[*] Now with the South African Council for Scientific and Industrial Research at the Atomic Energy Research Establishment, Harwell.

By means of a high-pressure hydrogen-filled pulse ionization chamber it has been possible to investigate some of these broad resonances with improved resolution and to extend the measurements to the energy range between 5 Mev. and 6 Mev.

§ 2. EXPERIMENTAL

(i) *Geometrical Arrangement*

The total neutron cross section measurements were made by means of a transmission experiment similar to that used by other experimenters (see, for example, Allen, Burcham and Wilkinson 1947).

The detector was a pulse ionization chamber filled to a pressure of 89 atmospheres of hydrogen (Stafford 1948). It was placed at a distance of approximately 300 cm. from the neutron source and subtended an angle of 6 minutes at the target. Scattering from the walls, ceiling and floor was reduced by surrounding the detector on all sides with 120 cm. of paraffin wax. A collimating hole 7 cm. in diameter passed through the centre. A study of the neutrons from a monokinetic source had shown that this method of screening and collimation introduced no spurious effects. A scale diagram is given in Figure 1.

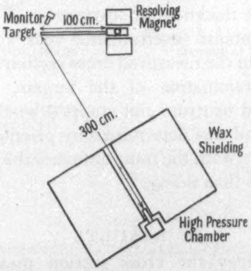

Figure 1. Experimental arrangement.

(ii) *Neutron Sources*

Monokinetic neutrons were obtained from the following reactions: (i) $^{2}\mathrm{H}(d, n)\,^{3}\mathrm{He}$, *Q* value $3{\cdot}25 \pm 0{\cdot}02$ Mev. (Livesey and Wilkinson 1948); (ii) $^{14}\mathrm{N}(d, n)\,^{15}\mathrm{O}$, *Q* value $5{\cdot}15 \pm 0{\cdot}10$ Mev. (Gibson and Livesey 1948). Thick targets mounted at the end of a brass tube 120 cm. in length were bombarded with a 930-kev. magnetically resolved deuteron beam. With each reaction the neutron energy was varied over a limited range by changing the angle between the detector and the direction of the incident deuteron beam.

(iii) *Scatterers*

The lead and the sulphur were cast into blocks, considerable care being taken to avoid air gaps inside the casting. The beryllium was in the form of an alloy (75·4% beryllium, 24·6% aluminium). Separate determinations of the cross section for aluminium were made at each neutron energy to correct in the case of the alloy for its contribution to the measured cross section. The aluminium was rolled sheet of 99·5% purity.

The scatterers were made several centimetres larger than the diameter of the detector and the collimating hole in the wax. They were mounted on a wooden stand half-way between the target and the detector. The stand was so placed that neutrons scattered off it could not enter the chamber without passing through the wax screening.

§ 3. PROCEDURE

In order to check that the attenuation of the neutron beam in passing through a thickness x of scatterer could be represented by $I=I_0 \exp(-n\sigma x)$, where I is the intensity of the neutron beam of initial intensity I_0, n the number of scattering nuclei per cm^3, and σ the total cross section, measurements were first made of the attenuation for several thicknesses of material. Once the above relation had been established the cross section was determined by a careful measurement of the attenuation for a single thickness of scatterer.

By the choice of a suitable discriminator bias voltage it was possible to eliminate the contribution to the measured cross section from low energy neutrons produced by carbon contamination of the targets. At the same time the contribution from scattered neutrons not stopped by the wax was also reduced.

The residual background was determined by placing 100 cm. of wax between the target and the detector. With the most unfavourable geometrical arrangement used it was found to be less than 0·5%.

§ 4. RESULTS

For each neutron energy the cross section measurement reported here represents the mean of fifteen independent determinations involving a total of more than 10^5 counts. In the range of energies from 2 MEV. to 4 MEV. the overall probable error is estimated at ±2%; in the range from 5 MEV. to 6 MEV. the probable error is ±3%.

Owing to the finite size of both the scatterer and the detector some neutrons were scattered into the detector; under the geometrical conditions prevailing in this experiment this correction was negligible.

A correction must, however, be applied for the spread in neutron energy introduced by the use of thick targets. This correction factor was given by Allen *et al.* (1947) as

$$\sigma(E)=\overline{\sigma(E)}+(E-\bar{E})d\overline{\sigma(E)}/d\bar{E}, \qquad \ldots\ldots(1)$$

where E is the maximum neutron energy, $\bar{E}$ is the mean neutron energy, $\sigma(E)$ is the cross section for monokinetic neutrons of energy E, and $\overline{\sigma(E)}$ is the observed cross section.

This equation assumes that the neutron spectrum has a sharp cut-off at energy E and that the absorption of the inhomogeneous neutrons is exponential so that a mean cross section can be defined.

The results are illustrated in Figures 2, 3, 4 and 5 after the above correction has been made to the experimentally determined cross section. Maxima and minima are observed in the results for each of the four elements used.

The energy resolution varies considerably with the neutron energy. At 2·2 MEV. the width at half-maximum is 0·15 MEV. and at 3·9 MEV. it is 0·5 MEV. (Livesey and Wilkinson 1948). Between 5 MEV. and 6 MEV. the width at half-maximum is 0·4 MEV. (Gibson and Livesey 1948).

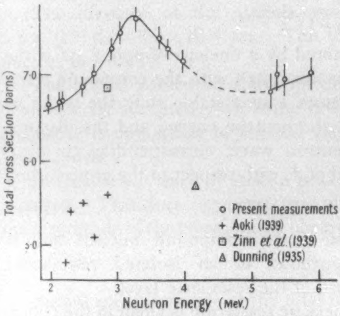

Figure 2. Variation of total neutron cross section of lead with neutron energy.

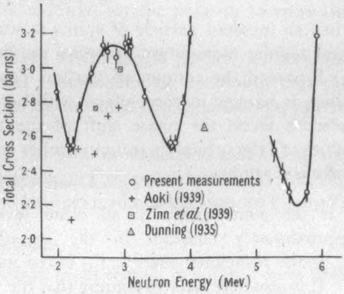

Figure 3. Variation of total neutron cross section of sulphur with neutron energy.

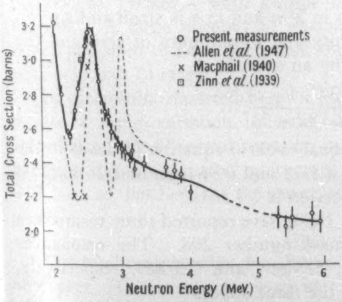

Figure 4. Variation of total neutron cross section of aluminium with neutron energy.

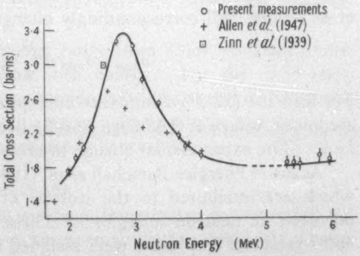

Figure 5. Variation of total neutron cross section of beryllium with neutron energy.

§ 5. DISCUSSION

(i) *Lead*

Lead is an interesting element in that the most abundant isotope of mass number 208 is made up to 82 protons and 126 neutrons, two of the so-called 'magic numbers' which may correspond to the completion of closed shells in the nucleus (Mayer 1948, Feenberg and Hammack 1949, Nordheim 1949, and others). A considerable amount of evidence has, in fact, accumulated which reveals that some of the lead isotopes behave as light elements with regard to the level spacing (see, for example, Kinsey, Bartholomew and Walker 1950, Gittings, Barschall and Everhart, 1949, Feld 1949).

If it is assumed that the observed change in cross section is not due to a number of unresolved narrow levels but to a single broad level and that the resonance occurs in only one isotope (the most abundant) it becomes possible to attempt a comparison of the experimental cross section with that expected according to the one-body theory for light nuclei (Breit and Wigner 1936, Bethe and Placzek 1937, Macphail 1940, Feshbach, Peaslea and Weisskoff 1947). According to this theory the total cross section can be represented by

$$\sigma = \frac{\lambda^2}{\pi} \sum_{lJ} \frac{2J+1}{(2s+1)(2i+1)} \sin^2 \delta_{lJ} \qquad \ldots\ldots(2)$$

when an incident particle of spin s is scattered by a nucleus of spin i. J is the total angular momentum quantum number associated with the compound state.

Provided the compound nucleus possesses a semi-stable state the width of which is narrow in comparison with both the neutron energy and the distance between levels the phase shift of the neutron wave, corresponding to given values of l the orbital quantum number and of J, with respect to the unperturbed wave is given by

$$\delta_{lJ} = \bar{\delta} - \operatorname{arc\,cot}\,[(E-E_{lJ})/\tfrac{1}{2}\Gamma_{lJ}] \qquad \ldots\ldots(3)$$

$\bar{\delta}$ is the contribution of all other levels of the compound nucleus and is approximately constant in the neighbourhood of an isolated resonance; E_{lJ} is the resonance energy; Γ_{lJ} is the width of the resonance level.

It is also necessary to assume that the inelastic scattering is small in the region of the resonance. For lead it is 1·5 barns (Feld 1949) to be compared with a total cross section at maximum of 7·7 barns. If these conditions are satisfied then on passing through the resonance the variation in λ^2/π and in $\bar{\delta}$ is small and $\sin^2 \delta_{lJ}$ will vary between a maximum value of unity and a minimum of zero and the cross section will correspondingly change by an amount

$$\sigma_{\max} - \sigma_{\min} = \frac{\lambda^2}{\pi} \frac{2J+1}{(2s+1)(2i+1)}. \qquad \ldots\ldots(4)$$

For lead 208 (52·3% abundance and spin equal to zero) equation (4) leads to the computed values of 0·42 barn or 0·84 barn if $l=1$ and 0·84 barn or 1·26 barns if $l=2$. The experimental change in cross-section is 1·1 barn.

At lower energies Barschall *et al.* (1949, 1950) have reported three resonances which are attributed to the isotope of mass number 208. The resonances occurred at neutron energies of 350 kev., 525 kev. and 720 kev. respectively, and l-values of 0, 1 and 1 were assigned to the three states.

From equations (2) and (3) it follows that the resonance energy E_{lJ} and the level width Γ_{lJ} are given by

$$E_{lJ} = \tfrac{1}{2}(E_1+E_2) + \tfrac{1}{2}(E_1-E_2)\cos 2\bar{\delta}, \qquad \ldots\ldots(5)$$

$$\Gamma_{lJ} = (E_2-E_1)\sin 2\bar{\delta}, \qquad \ldots\ldots(6)$$

where E_1 and E_2 are the neutron energies for which the cross section is a maximum and a minimum. The value of $\bar{\delta}$ is arbitrarily chosen to give the best 'shape fit' to the experimental points.

With $\bar{\delta}$ equal to $-15°$ it is found that $3{\cdot}15 \leqslant E_{lJ} \leqslant 3{\cdot}2$ Mev., $0{\cdot}8 \leqslant \Gamma_{lJ} \leqslant 1{\cdot}15$ Mev. Most of the uncertainty is in the position of the minimum.

If the resonance is assumed to be due to D-neutrons, then the reduced width γ^2 is given in terms of the natural width Γ (Feshbach, Peaslea and Weisskopf 1947) by

$$\gamma^2 = \frac{\Gamma}{2k}\left[\frac{9+3(ka)^2+(ka)^4}{(ka)^4}\right],$$

where $k=2\pi/\lambda$ and a is the nuclear radius ($9{\cdot}2\times10^{-13}$ cm.: Sherr 1945). The reduced width is found to be $1{\cdot}3\times10^{-13}\leqslant\gamma^2\leqslant1{\cdot}9\times10^{-13}$ Mev. cm. This is in reasonable agreement with the allowed maximum value of $3\hbar^2/2ma = 6{\cdot}8\times10^{-12}$ Mev. cm. to be expected if the neutron scattering is treated as a single particle interaction (Wigner 1949).

The life-time of the excited state given by $\tau=\hbar/\Gamma$ is calculated to be $5{\cdot}8\times10^{-22}\leqslant\tau\leqslant8{\cdot}2\times10^{-22}$ sec. The time required for the neutron to cross the nucleus is $7{\cdot}6\times10^{-22}$ sec.

The results presented above on the basis of the single particle model must obviously be accepted with some reserve. Moreover, the possibility that the resonance is due either to another isotope or to more than one isotope cannot be excluded.

In the earlier work of Aoki a peak in the total cross section at 2·4 Mev. was reported. This does not agree with the resonance reported here (3·2 Mev.) and the magnitude of the cross section observed by Aoki is somewhat less (see Figure 2).

(ii) *Sulphur*

Recent measurements of the total neutron cross section in sulphur have been made by Adair, Bockelman and Peterson (1949) in the energy range from 16 kev. to 250 kev. and by Freier, Fulk, Lampi and Williams (1950) from 600 kev. to 1·9 Mev. Both groups used neutrons produced by the ^{7}Li (p, n) reaction. A large number of resonance levels were observed, the density of which appeared to be so great that the resonances were not completely resolved with a 30 kev. Li target.

In the results reported here in the energy range from 2 Mev. to 6 Mev., there is also a rapid variation in cross section with energy. For the 2·85 Mev. 'resonance', the observed variation in cross section is 0·62 barn and the expected variation for an S-neutron interacting with a target nucleus of spin zero would be 0·97 barn so that here too the resonances are not fully resolved.

(iii) *Aluminium*

The total cross section for aluminium has been investigated by a number of observers. The energy range up to 1 Mev. has been studied in detail and a large number of resonances have been reported with an average level spacing of 50 kev. (see Goldsmith, Ibser and Feld 1947, p. 271, for a list of references).

Aoki (1939), Zinn *et al.* (1939), Macphail (1940) and Allen *et al.* (1947) have made measurements in the range from 2 Mev. to 4 Mev. The published curves of Allen *et al.* showed two resonances, one at 2·55 Mev. and the second at 3·0 Mev. The measurements reported here do not provide any evidence for the 3·0 Mev. resonance and while this agrees with the observations of Macphail and of Aoki, the possibility of a resonance at 3·0 Mev. cannot be ruled out because the experimental technique is not well suited to the observation of such sharp resonances.

All results on the 2·55 MeV. resonance agree very well. In the energy range from 5 MeV. to 6 MeV. no further resonances were detected.

As pointed out by Macphail (1940), the ground state of ^{27}Al has a spin of 5/2 and the scattering cross section for a given state is now determined not only by the corresponding values of the orbital quantum number but also by the transition probabilities between the various components of that state, and, as these are not known, an interpretation of the experimental results is not possible.

(iv) *Beryllium*

The results of the present experiment are illustrated in Figure 5 together with the relevant data obtained by other observers. The experimental value for the change in cross section from maximum to minimum is uncertain but probably lies between 1·8 barns and 2·1 barns. A value of $l \nless 5$ is required to explain the magnitude of this change in cross section on the basis of the single particle model and assuming the spin of the ^{9}Be nucleus to be 3/2 units (Kusch, Millman and Rabi 1939, Paul 1941). The large value obtained for l may possibly be explained (Flowers, private communication) by the fact that the odd neutron in the ^{9}Be nucleus and the incoming neutron may pair up and appear to add angular momenta. A result of this would be that waves of higher angular momenta than expected from the incident neutron energy become effective. Moreover, as the single particle model requires strong pairing between the incident neutron and the bombarded nucleus the results obtained with this model should be accepted with reserve in the case of beryllium.

The following values are obtained for the resonance energy, level width and lifetime of the excited state: $2{\cdot}70 \leqslant E_{lJ} \leqslant 2{\cdot}75$ MeV., $0{\cdot}5 \leqslant \Gamma_{lJ} \leqslant 0{\cdot}7$ MeV., $13{\cdot}1 \times 10^{-22}$ sec. $\geqslant \tau \geqslant 9{\cdot}4 \times 10^{-22}$ sec. The time required for the neutron to cross the nucleus is equal to $3{\cdot}6 \times 10^{-22}$ sec.

ACKNOWLEDGMENTS

The writer wishes to thank Professor O. R. Frisch, Dr. W. E. Burcham and Mr. B. H. Flowers for valuable advice and criticism and Mr. W. Birtwhistle for the efficient operation of the 1 million volt accelerating equipment in the Cavendish Laboratory.

REFERENCES

Adair, R. K., Bockelman, C. K., and Peterson, R. E., 1949, *Phys. Rev.*, **76,** 308.

Allen, K. W., Burcham, W. E., and Wilkinson, D. H., 1947, *Proc. Roy. Soc.* A, **192,** 114.

Aoki, H., 1939, *Proc. Phys. Math. Soc., Japan*, **21,** 232.

Barschall, H. H., Adair, R. K., and Peterson, R. E., 1950, *Phys. Rev.*, **79,** 935.

Barschall, H. H., Bockelman, C. K., Peterson, R. E., and Adair, R. K., 1949, *Phys. Rev.*, **76,** 1146.

Bockelman, C. K., Peterson, R. E., Adair, R. K., and Barschall, H. H., 1949, *Phys. Rev.*, **76,** 277.

Bethe, H., and Placzek, G., 1937, *Phys. Rev.*, **51,** 450.

Breit, G., and Wigner, E., 1936, *Phys. Rev.*, **49,** 519.

Dunning, J. R., Pegrain, G. B., Fish, G. A., and Mitchell, D. P., 1935, *Phys. Rev.*, **48,** 265.

Feenberg, E., and Hammack, K. C., 1949, *Phys. Rev.*, **75,** 1877.

Feld, B. T., 1949, *Phys. Rev.*, **75,** 1115.

Feshbach, H., Peaslea, D. C., and Weisskopf, V. F., 1947, *Phys. Rev.*, **71,** 145.

Fields, R., Russell, B., Sachs, D., and Wattenberg, A., 1947, *Phys. Rev.*, **71,** 508.

Freier, G., Fulk, M., Lampi, E. E., and Williams, J. H., 1950, *Phys. Rev.*, **78,** 508.

Gibson, W. M., and Livesey, D. L., 1948, *Proc. Phys. Soc.*, **60,** 523.

Gittings, H. T., Barschall, H. H., and Everhart, G. G., 1949, *Phys. Rev.*, **75**, 1610.
Goldsmith, H. H., Ibser, H. W., and Feld, B. T., 1947, *Rev. Mod. Phys.*, **19**, 259.
Good, W. E., and Scharff-Goldhaber, G., 1941, *Phys. Rev.*, **59**, 917.
Kinsey, B. B., Bartholomew, G. A., and Walker, W. H., 1950, *Phys. Rev.*, **78**, 77.
Kusch, P., Millman, S., and Rabi, I. I., 1939, *Phys. Rev.*, **55**, 666.
Livesey, D. L., and Wilkinson, D. H., 1948, *Proc. Roy. Soc.* A, **195**, 123.
MacPhail, M. R., 1940, *Phys. Rev.*, **57**, 669.
Mayer, Maria G., 1948, *Phys. Rev.*, **74**, 235.
Nordheim, L. W., 1949, *Phys. Rev.*, **75**, 1894.
Paul, W., 1941, *Z. Phys.*, **117**, 774.
Sherr, R., 1945, *Phys. Rev.*, **68**, 240.
Stafford, G. H., 1948, *Nature, Lond.*, **162**, 771.
Wigner, E., 1949, *Amer. J. Phys.*, **17**, 99.
Zinn, W. H., Seely, S., and Cohen, V. W., 1939, *Phys. Rev.*, **56**, 260.

New Radioactive Isotopes produced by Nuclear Photo-Disintegration

By F. D. S. BUTEMENT
Atomic Energy Research Establishment, Harwell, Berks.

MS. received 1st *August* 1950, *and in amended form* 22nd *November* 1950

ABSTRACT. Photonuclear (γ, n) and (γ, p) reactions produced by 23 Mev. x-rays from a synchrotron have been used to prepare new radioactive isotopes, the method being particularly advantageous for neutron-excess isotopes in the region $Z=63$ to 79. Whenever possible the isotopes were chemically identified. The following Table summarizes the results.

Element Irradiated	Element Chemically Identified	Half-Life	Assignment
Se	As	9 minutes	^{79}As
Sm	Sm	8 minutes	^{143}Sm or ^{146}Sm
Eu	Eu	15 hours	^{150}Eu
Gd	—	20 minutes	^{159}Eu or Gd^{m}
Dy	—	14 minutes	^{162}Tb or ^{163}Tb
Er	—	96 minutes	^{163}Er, ^{167}Ho or ^{169}Ho
Yb	—	19 minutes	^{172}Tm, ^{173}Tm or ^{175}Tm
Hf	Lu	22 minutes	^{178}Lu or ^{179}Lu
W	Ta	48 minutes	^{185}Ta
W	Ta	116 hours	^{183}Ta
Os	Re	17 minutes	^{189}Re or ^{191}Re
Pt	Ir	66 minutes	^{195}Ir or ^{197}Ir
Hg	Au	27 minutes	^{201}Au or ^{203}Au

Definite mass assignments, hitherto uncertain, have been made for 18-hour ^{159}Gd and 48-minute ^{200}Au.

§ 1. INTRODUCTION

This paper describes a search for new radioactive isotopes produced by (γ, n) and (γ, p) reactions. Inspection of an isotope chart shows that, especially in the region $Z=63$ to 79, many new neutron-excess isotopes of elements of odd atomic number Z could be made by (γ, p) reactions on the appropriate $Z+1$ targets. Some of these isotopes could not be made by any other practicable means, others might be made by (n, p) reactions, but even here the photo-disintegration method frequently has the advantage of ease of interpretation when a chemical separation is not practicable, since strong activities produced by neutron capture are precluded. Certain neutron-deficient isotopes can be most conveniently made by (γ, n) reactions. Thirteen new isotopes have been found and characterized by their half-lives, and where practicable a chemical identification.

§2. EXPERIMENTAL TECHNIQUE

Samples for irradiation were contained in a cylindrical tube 1 cm. in diameter, placed along the axis of the X-ray beam from a synchrotron and 30 cm. from the target. The X-ray energy spectrum was a continuum up to a limit at 23 MEV. The irradiation time was usually one hour, a limit imposed by the heating of the synchrotron magnet. The samples received approximately 2000 r. per hour. Photo-neutrons, both fast and of thermal energy were present, the flux of each at the sample being about 1000 $\mathrm{sec}^{-1}\,\mathrm{cm}^{-2}$. The samples were therefore screened with 1 mm. of cadmium foil to prevent activation by slow neutrons, and no half-life attributable to a product of neutron capture was ever observed, except for ^{165}Dy.

For (γ, p) products where chemical separation allows the activity to be concentrated into a small mass, 1 to 10 gm. of target material was irradiated and activities of the shorter-lived products of up to about 1,000 counts per minute obtained.

For (γ, p) products of certain rare earths, where a rapid chemical method of separation is not available, and for (γ, n) products, quantities of 0·1 to 0·2 gm. were irradiated. Activities of about 100 counts/min. were obtained. With an end-window Geiger counter there is little advantage in using larger quantities owing to self-absorption of the radiation by the sample.

The decay of the activity was followed by means of a thin-window (1·7 mg. cm^{-2}) Geiger counter. The activities found were nearly all of short half-life, since it was seldom possible to produce sufficient activity of an isotope of half-life greater than one day.

In order not to miss short activities, chemical separations were made as quickly as possible, using methods based on the assumption that only the products of (γ, n) and (γ, p) reactions were present. Activities with half-lives considerably less than the time necessary for the separation would not have been observed. When oxides were irradiated and counted without any chemical separation, half-lives less than 2 minutes would not have been observed owing to the strong 126-second ^{15}O activity. The activities available were usually too weak to permit any determination of the energy of the particles emitted.

§3. REACTION YIELDS

When an irradiation produces more than one isotope, the ratio of the yields provides a useful indication of the type of reaction occurring. This ratio (i.e. the ratio of the number of atoms of each radio-isotope produced) can be calculated from the half-lives of the isotopes, their activities measured at a known time after the end of the irradiation, and the duration of the irradiation.

The results will be fairly accurate for the thin samples of beta-emitters prepared by a chemical separation, since the unknown but small correction factors for back-scattering and window absorption will be about equal for the several activities in the sample. For thick samples, i.e. where no chemical separation is possible, there will be a larger error owing to the impossibility of correcting for the self-absorption for the new isotopes of unmeasured beta-particle or positron energy.

It has been shown (Price and Kerst 1950) that the value σ of the absolute cross section for a (γ, n) reaction is nearly the same for all isotopes of an element, and increases steadily with increase of Z. Also Hirzel and Wäffler (1947) found that the ratio $\sigma\ (\gamma, \text{p})/\sigma\ (\gamma, \text{n})$ has values about 1/30 at $Z=49$–50 and decreases as Z increases. The approximate value obtained in this work was 1/200 at $Z=78$.

Conseqnently, when two radio-isotopes of the same element are produced simultaneously (by either two (γ, n) or two (γ, p) processes) and the mass number of one of them is already known, then, if the mass number assigned to the other, new, radio-isotope is to be plausible, the ratio of the yields should approximately equal the ratio of the abundances of those stable isotopes from which the radio-isotopes were produced.

The results of irradiations are described below. Data quoted without reference are from the *Table of Isotopes* by Seaborg and Perlman (1948).

§ 4. ARSENIC

The object was to produce the unknown ^{79}As by ^{80}Se (γ, p). The stable selenium isotopes are as follows:

Mass number	74	76	77	78	80	82
Abundance (%)	0·87	9·02	7·58	23·52	49·82	9·19

The radioactive arsenic isotopes which could be produced by (γ, p) are :

Mass number	73	76	77	79	81
Half-life	90 days	26·8 hr.	40 hr.	—	<10 min.

The activity due to ^{73}As would be negligible. The half-life of ^{81}As is given by the Plutonium Project (1946) list of fission nuclei.

Ten grammes of potassium selenate was irradiated and the radio-arsenic chemically separated. The time taken for the isolation was 30 minutes. The activity showed a half-life of 9 minutes and a weak residual activity with an apparent half-life of about 31 hours. The latter may be attributed to a mixture of 26·8-hour ^{76}As and 40-hour ^{77}As. The yields of the 9-minute and '31-hour' activities were approximately equal. The 9-minute arsenic is therefore probably ^{79}As, decaying by beta-particle emission into ^{79}Se whose half-life is either very short or very long. It cannot be ^{81}As since it does not produce any 17-minute or 57-minute ^{81}Se daughter activities.

§ 5. SAMARIUM

The natural samarium isotopes are as follows:

Mass number	144	147	148	149	150	152	154
Abundance (%)	3·16	15·07	11·27	13·84	7·47	26·63	22·53

The samarium isotopes 143, 146, 151 (20-year) and 153 (46-hour) would be produced by (γ, n) reactions, and (γ, p) reactions would produce much smaller yields of seven promethium isotopes.

A sample of 200 mg. irradiated samarium oxide of over 99·9% purity showed, after the decay of the ^{15}O, two activities with half-lives of 8 minutes (Figure 1) and 46 hours. The yield (not corrected for self-absorption in the sample) of the 8-minute activity was about one-quarter that of the 46-hour activity.

These activities were both identified as samarium by irradiating samples of samarium dichloride and chemically purifying the samarium. The 46-hour activity must be ^{153}Sm. The long-lived ^{151}Sm would not be observed. Apart from possible isomerism the 8-minute activity must be ^{143}Sm or ^{146}Sm. Since one natural samarium isotope is an alpha-particle emitter, absorption measurements in aluminium were made of the 8-minute activity, which showed that the radiation detected was either positrons or electrons. With the counter employed, a samarium isotope decaying only by orbital electron capture would scarcely be detected. In view of the relative abundances of ^{144}Sm and ^{154}Sm, the yield of the 8-minute activity relative to ^{153}Sm is consistent with its assignment to a positron-emitting ^{143}Sm, decaying into ^{143}Pm, which would not be observed since its half-life is 350 days (Hicks 1949).

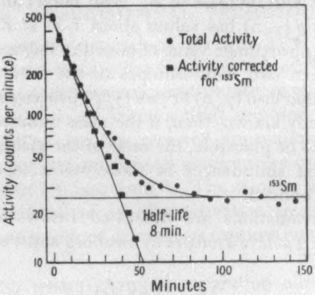

Figure 1. Decay of radioactive samarium.

§ 6. EUROPIUM

Europium has two stable isotopes of mass numbers 151 (47·8%) and 153 (52·2%). A (γ, n) reaction would produce ^{152}Eu (9·2-hour, and a 5-year isomer) and the hitherto unidentified ^{150}Eu. Pool and Quill (1938) produced a 27-hour positron activity by bombarding europium with fast neutrons and suggested an assignment to ^{150}Eu, but a chemical identification was not made. A sample of 100 mg. of 'Specpure' europium oxide was irradiated and the europium chemically purified as europous sulphate.

The activity showed a nearly logarithmic decay with an apparent half-life of 12 hours. Such a decay, resulting from two slightly different half-lives, is difficult to resolve accurately unless one component is known. By assuming one component to be 9·2-hour ^{152}Eu which must have been formed, the best value for the half-life of the other component was 15 hours, and its yield was nearly equal to that of the ^{152}Eu. The 15-hour activity must almost certainly be ^{150}Eu, and since the abundances of ^{151}Eu and ^{153}Eu are nearly equal, the relative yield indicates a high counting efficiency, so that decay is probably by positron emission. With the counter employed, a ^{150}Eu decaying only by orbital electron capture would scarcely be detected.

§ 7. LUTETIUM

The object was to prepare ^{178}Lu and ^{179}Lu by (γ, p) reactions on hafnium. The stable hafnium isotopes are as follows:

Mass number	174	176	177	178	179	180
Abundance (%)	0·18	5·3	18·47	27·10	13·84	35·11

A sample of 0·8 gm. hafnium oxide, free from zirconium, was irradiated and the lutetium chemically separated.

The half-lives found were 22 minutes, 6 days (evidently the known ^{177}Lu) and an intermediate period whose decay was not quite logarithmic, but appeared to be a mixture of periods of 3·5 hours and about 5 hours. It may therefore indicate the presence both of 3·5-hour ^{176}Lu and one of the new isotopes sought, but no certain conclusion can be reached solely on the evidence of the decay.

The 22-minute lutetium is a new isotope, and consideration of its yield (about 70% of that of the ^{176}Lu) indicates that its mass number must be 178 or 179.

§ 8. TANTALUM

The object was to prepare ^{183}Ta and ^{185}Ta by (γ, p) reactions on tungsten. The stable tungsten isotopes are as follows:

Mass number	180	182	183	184	186
Abundance (%)	0·12	25·77	14·24	30·68	29·17

In a preliminary experiment tungsten metal was irradiated. The main yield of tungsten isotopes, produced by (γ, n) reactions, will be the long-lived ^{181}W (140 days) and ^{185}W (74 days) which will show only a feeble activity, so that short-lived tantalum isotopes will be observable. The shortest half-lives shown were 17 minutes (evidently 16·2-minute ^{182}Ta) and 48 minutes. To isolate the tantalum activities 14 gm. of tungstic acid was irradiated and the tantalum chemically separated.

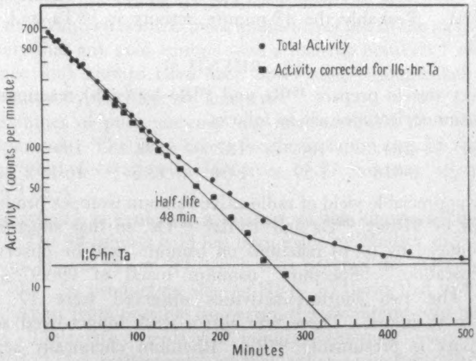

Figure 2. Decay of 48-minute tantalum.

The decay graph (Figure 2), commencing after the disappearance of the 17-minute activity, shows half-lives of 48 minutes and a long period, originally given as 6 days (Butement 1950 a), but subsequently re-determined much more accurately on a larger sample as 116 hours (Figure 3). A sample of this 116-hour activity, isolated after decay of the 48-minute activity, showed after 37 days a residual long activity of 2·7% of the initial activity, which is about that to be expected for the yield of 117-day ^{182}Ta. The 116-hour activity cannot be ^{185}Ta, since there should then have been also an additional residue of 4·9% of the initial activity, due to its daughter 74-day ^{185}W.

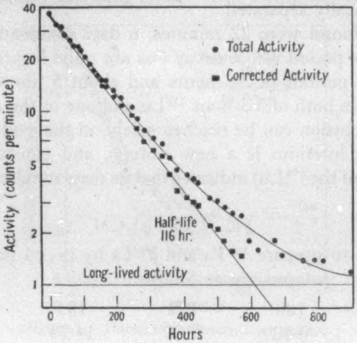

Figure 3. Decay of 116-hour tantalum.

The yields of 48-minute and 116-hour tantalums were in the ratio of 1 : 1·2 respectively, which is in conformity with the nearly equal abundances of ^{184}W and ^{186}W. Probably the 48-minute activity is ^{185}Ta and the 116-hour activity ^{183}Ta.

§ 9. RHENIUM

The object was to prepare ^{189}Re and ^{191}Re by (γ, p) reactions on osmium. The stable osmium isotopes are as follows:

Mass number	184	186	187	188	189	190	192
Abundance (%)	0·018	1·59	1·64	13·3	16·1	26·4	41·0

The only appreciable yield of radioactive osmium isotopes produced by (γ, n) reactions will be 97-day ^{185}Os and 16-day ^{191}Os, so that short-lived rhenium isotopes, produced by (γ, p) reactions on osmium, will be observable without chemical separation. 'Specpure' osmium metal of 99·997% purity was irradiated. The two shortest activities observed were 17 minutes and approximately 18 hours. There was also a weak longer-lived activity. The 18-hour activity is presumably ^{188}Re. Rhenium chemically separated from irradiated osmium showed a short period, approximately 15 minutes half-life, and a weak longer-lived residual activity, partly 18-hour ^{188}Re. Owing to the decay of activity during the time taken for chemical separation, the short rhenium half-life was more accurately determined as 17 minutes using irradiated osmium, without chemical separation.

The only radioactive rhenium isotopes which will be formed in appreciable yield will be ^{186}Re (92 hours), ^{188}Re (18 hours), and the unknown ^{189}Re and ^{191}Re. The yield of the 17-minute rhenium was slightly greater than that of the ^{188}Re. Apart from possible isomerism, therefore, the 17-minute rhenium must have a mass number of 189 or 191.

§ 10. IRIDIUM

The object was to prepare ^{195}Ir and ^{197}Ir by (γ, p) reactions on platinum. The stable platinum isotopes are as follows:

Mass number	192	194	195	196	198
Abundance (%)	0·78	32·8	33·7	25·4	7·23

Irradiated platinum metal showed activities with half-lives of 80 minutes and 18 hours, both attributable to platinum isotopes. It is unlikely that any iridium isotope with a half-life of between 1 and 20 minutes is formed, since such should have been observable.

Five grammes of chloroplatinic acid was irradiated, and the iridium isolated chemically. The iridium activity decayed with half-lives of 66 minutes and 19 hours, the latter period being evidently the known ^{194}Ir.

The yield of the 66-minute iridium was about one-fifth that of the ^{194}Ir. Apart from possible isomerism, it must be ^{195}Ir or ^{197}Ir, and the yield relative to ^{194}Ir suggests ^{197}Ir as the more probable assignment, in view of the relative abundances of the platinum isotopes 198 and 195.

§ 11. GOLD

The object was to prepare ^{201}Au and ^{203}Au by (γ, p) reactions on mercury. The stable mercury isotopes are as follows:

Mass number	196	198	199	200	201	202	204
Abundance (%)	0·15	10·1	17·0	23·3	13·2	29·6	6·7

The shortest half-life shown by irradiated mercury metal was 40 minutes, evidently due to the known isomer (mass unknown) of one of the mercury isotopes.

It is unlikely that any gold isotope with a half-life between 1 and 5 minutes is formed, since such should have been observable. Longer half-lives would have been obscured by the mercury activity.

Twelve grammes of pure mercury was irradiated and the radioactive gold chemically separated. The time taken for the isolation was 28 minutes. The activity of the gold decayed with half-lives of 27 minutes, 48 minutes, and approximately 3 days.

The 3-day activity is evidently a mixture of the known 2·7-day ^{198}Au and 3·3-day ^{199}Au. The 48-minute gold has been made by Maurer and Ramm (1942) by the reactions Hg (n, p) and Tl (n, α), thus proving the mass number to be either 200 or 202. Its production also by Hg (γ, p) shows that its mass number must be 200. Apart from possible isomerism the 27-minute gold must be either ^{201}Au or ^{203}Au. The relative yields of 27-minute : 38-minute : 3-day activities were approximately 1 : 1 : 1·5 respectively, so that either assignment appears equally probable.

§ 12. RARE EARTH ELEMENTS

With most of the rare earth elements there is no practicable method of chemically identifying weak short-lived activities, but evidence for new isotopes can be obtained by irradiating samples of the pure oxides, and measuring the decay of activity after the 126-second ^{15}O has disappeared. The oxides were ignited at 1,000° c. shortly before irradiation to eliminate possible contamination by carbonates which could yield 20-minute ^{11}C. The results are given below under the headings of the element irradiated.

§ 13. GADOLINIUM

'Specpure' gadolinium oxide showed activities with half-lives of 20 minutes and 18 hours.

The latter period is also that of the beta-emitter produced by neutron capture in gadolinium, and is therefore ^{159}Gd, produced here by the reaction ^{160}Gd (γ, n). This confirms the mass assignment suggested previously (Butement 1949).

There was no known contamination to account for the 20-minute activity. Its yield relative to the ^{159}Gd, not corrected for self-absorption by the sample, was 1/80. This is about the yield to be expected for ^{159}Eu. The activities of all the other and longer-lived europium isotopes produced would not be observable. Alternatively it may be an isomer of a stable gadolinium isotope. It is not likely to be ^{151}Gd produced by ^{152}Gd (γ, n) since bombardment of europium oxide with 10 MEV. protons, which would produce ^{151}Gd, did not yield any 20-minute rare earth activity.

§ 14. TERBIUM

A (γ, n) reaction on terbium would produce ^{158}Tb. Irradiated terbium oxide showed no significant activity, so that the half-life of ^{158}Tb is probably long.

§ 15. DYSPROSIUM

A sample of dysprosium oxide containing 0·3% Ho showed activities with half-lives of 22 minutes and 140 minutes. The latter period is evidently ^{165}Dy formed by neutron capture, since the yield was much reduced by increasing the thickness of cadmium screening. The short period, given as 22 minutes in earlier work (Butement 1950 a) might be inaccurate owing to contamination with ^{164}Ho, the half-life of which has been found to be 34 ± 1 minutes (Hicks 1949). Consequently, a sample of very pure dysprosium oxide was prepared by the ion-exchange method, and this showed a half-life of 14 minutes. The dysprosium isotopes formed by (γ, n) reactions will be the long-lived ^{159}Dy (Butement 1950 b) and negligible yields of ^{155}Dy and ^{157}Dy from the scarce stable isotopes ^{156}Dy and ^{158}Dy. The 14-minute activity is therefore probably a terbium isotope of mass number 162 or 163.

§ 16. ERBIUM

Irradiated 'Specpure' erbium oxide showed an activity with a half-life of 44 minutes (Butement 1950 a). This period is too long to be due entirely to 34-minute ^{164}Ho derived from a (γ, n) reaction on holmium contamination, but could be due to a mixture of a 34-minute and a somewhat longer half-life. An analysis of the erbium, made by using the pile-activation method and measuring the 27-hour ^{166}Ho activity produced, showed a holmium content of about 0·5%.

By adding to the erbium a trace of ^{166}Ho and then eliminating it by an ion-exchange separation, a sample of erbium oxide containing less than 0·01% of holmium was prepared. After irradiation this showed activities with half-lives of 96 minutes, 10 hours and 9 days.

The 9-day activity is evidently 9·4-day ^{169}Er produced by a (γ, n) reaction. A comparable yield of ^{165}Er will also be produced, with a half-life of 10 hours (Butement 1950 c), but this shows only a low activity since it decays by orbital electron capture, so that the counting efficiency is low. The yield of the 96-minute activity was about 1/190 that of the ^{169}Er, after making a correction for the self-absorption of the 0·33 MEV. beta-radiation from the ^{169}Er in a sample of 25 mg. cm^{-2} thickness. This activity may be ^{163}Er derived from ^{164}Er whose abundance is 1·5%, or may be ^{167}Ho or ^{169}Ho produced by a (γ, p) reaction on ^{168}Er or ^{170}Er whose abundances are respectively 26·9% and 14·2%.

§ 17. YTTERBIUM

Irradiated 'Specpure' ytterbium oxide showed activities with half-lives of 19 minutes and about 100 hours, the latter evidently ^{175}Yb. The only other ytterbium isotope which would be formed in appreciable yield is 33-day ^{169}Yb, which would not be observed. The yield of the 19-minute activity was about one-hundredth that of the ^{175}Yb, after making a correction for the self-absorption only of the 0·5 and 0·13 MEV. beta-radiations from the ^{175}Yb in a sample of 50 mg. cm^{-2} thickness. This 19-minute activity is probably a thulium isotope of mass number 172, 173, or 175.

§ 18. LUTETIUM

Irradiated lutetium oxide showed only the known 3·5-hour ^{176}Lu isomer, and the natural radioactivity of ^{176}Lu. The half-life of ^{174}Lu which must be produced by a (γ, n) reaction on ^{175}Lu is therefore probably long.

ACKNOWLEDGMENTS

Acknowledgments are made to Messrs. D. W. Fry, F. K. Goward, L. H. Metcalfe and D. J. Lees for providing facilities for synchrotron irradiations, to Mr. B. A. J. Lister for information on a method of purifying hafnium, to the Director, Atomic Energy Research Establishment, for permission to publish these results and to the Ministry of Supply for the grant of a Senior Harwell Research Fellowship.

REFERENCES

BUTEMENT, F. D. S., 1949, *Phys. Rev.*, **75**, 1276; 1950 a, *Nature, Lond.*, **165**, 149; 1950 b, *Proc. Phys. Soc.* A, **63**, 532; 1950 c, *Ibid.*, **63**, 775.

HICKS, H. G., 1949, United States Atomic Energy Commission, AECU-217.

HIRZEL, O., and WÄFFLER, H., 1947, *Helv. Phys. Acta*, **20**, 373.

MAURER, W., and RAMM, W., 1942, *Z. Phys.*, **119**, 602.

PLUTONIUM PROJECT, 1946, *J. Amer. Chem. Soc.*, **68**, 2411.

POOL, M. L., and QUILL, L. L., 1938, *Phys. Rev.*, **53**, 437.

PRICE, G. A., and KERST, D. W., 1950, *Phys. Rev.*, **77**, 806.

SEABORG, G. T., and PERLMAN, I., 1948, *Rev. Mod. Phys.*, **20**, 585.

On the Proton Component of the Vertical Cosmic-Ray Beam at Sea Level

By M. G. MYLROI and J. G. WILSON
The Physical Laboratories, University of Manchester

Communicated by P. M. S. Blackett; MS. received 23rd October 1950

ABSTRACT. Approximately 1% of the vertical cosmic-ray intensity at sea level is shown to consist of protons. These form a momentum spectrum of index $-2{\cdot}8$ in the range 10^3 Mev/c $< p < 5\times10^3$ Mev/c. and have an absorption range in lead, 160 ± 40 gm.cm^{-2}. Using existing measurements at high altitude, the attenuation in the atmosphere of protons in the spectral region investigated is found to take place with a range 140 ± 10 gm.cm^{-2}.

There is no negatively charged component of strong nuclear interaction in the vertical beam of intensity as great as 0·1% of the whole beam.

§ 1. INTRODUCTION

Experiments have been carried out to examine the absorption properties of charged cosmic-ray particles as a function of momentum, particles of measured momentum now being available in the output of the magnetic spectrograph described in an earlier paper (Hyams, Mylroi, Owen and Wilson 1950). The work was in the first place expected to give information about the range–momentum relation for μ-mesons, and to show the presence of any measurable fraction of more absorbable particles in the beam, in a manner similar to that described by Alikhanian *et al.* (1948) and by Lheritier, Peyrou and Lagarrigue (1947). Exploratory experiments showed at a very early stage that a reasonable number of more absorbable particles was in fact present, and the forms of apparatus described in the present paper were adopted for the specific purpose of studying these particles and identifying them.

§ 2. EXPERIMENTAL ARRANGEMENT

The experiments consist essentially in recording from an upper counter tray the entry of particles of measured momentum into an absorbing layer, and also from a further tray below the absorber to determine whether or not the particles emerge. Preliminary experiments indicated that the proportion of absorbable particles reaches a value which may be as large as 5% of the whole flux at momenta near 10^3 Mev/c. and falls rapidly at higher momenta, and that the absorbable component shows a strong positive excess. The apparatus was therefore dimensioned on the assumption that the main part of the absorbable component consists of protons. The absorbing thickness was made small enough for the critical momentum of penetration for mesons to be significantly less than the momentum of the anticipated maximum of a proton spectrum (set by the increase of ionization loss from an inverse power spectrum), but nevertheless larger than the collision range corresponding to the geometrical cross section of the absorbing (lead) nuclei. A 20 cm. absorbing layer of lead was adopted, which μ-mesons of momentum greater than $0{\cdot}37\times10^3$ Mev/c. should be able to penetrate, and which is about 1·5 nuclear collision lengths in thickness. The use of this, and even thicker, absorbing layers is straightforward on account of the small angular divergence of the measured particles from our instrument. Only a relatively small increase of area of the lower counter tray, which detects the emergence of particles from the absorber, as compared with the upper tray is necessary to allow both for the divergence of the entrant beam and for scattering of particles in the absorber.

The greater part of the work discussed has been carried out with the two arrangements shown in Figure 1 (*a*) and (*b*). In both arrangements the entry of measured particles to the absorbing layers was detected by tray A and final emergence at tray EFGH. The use of intermediate trays to obtain more detailed information about the absorption process is discussed below (§ 3.2).

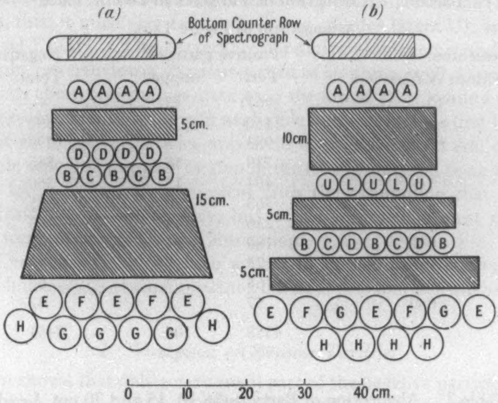

Figure 1. The absorption apparatus in relation to the bottom counter layer of the spectrograph.

2.1. *Efficiency of Detection in the Lower Counter Tray*

Since effects of the order 1% of the total beam are to be examined, it is necessary for tray EFGH to detect particles emerging from the absorber, after traversing it, with high efficiency. It accordingly consists of two tightly packed layers of counters staggered relative to each other. With this arrangement, about 75% of all particles traversing the tray pass through the sensitive region of two counters, while the remaining 25% pass, in one layer or the other, through the dead space between counters. (The insensitive space in each layer, ~12%, arises to some extent because the counter tubes (80 cm. long) are not all completely straight.) The dead-time of the individual counters, which was measured to be about 120 μsec., leads to an inefficiency per counter of about $\frac{1}{2}$%; the total inefficiency of the whole tray is thus about $\frac{1}{8}$%. This figure was checked in an experiment without absorber. Of 3,700 particles traversing the lowest tray, six failed to operate it.

It is further necessary to ensure that no significant fraction of particles is scattered in the absorber so as to miss this tray. To test this possibility, and to maintain a continuous check on the working efficiency of the various counters in the tray, the sub-groups, E, F, G, H (Figure 1(*a*)), were recorded separately. Thus the most scattered particles are recorded at H alone, and the next most scattered at EH. Of 8,000 traversals ($p > 6 \times 10^8$ ev/c.), six are of the type EH and four of type H. We therefore conclude that the cover of the tray EFGH is adequate and that scattered particles which miss this tray can hardly amount to more than 0·05% of those traversing it.

The continuous efficient operation of the various counters is checked from the actual records by the fraction of all counts which discharge only one of the subgroups G, E, F.

§ 3. RESULTS

The results of the main experiments are summarized in Tables 1 and 2.

Table 1. Absorption of Particles in 20 cm. Lead

Arrangement as Figure 1 (*a*).

Category	Momentum Mean (10^3 Mev/c.)	Positive particles Total	Positive particles Stopped	Negative particles Total	Negative particles Stopped
0	12	(967)	(3)	—	–
1	6	1150	8	888	4
2	3	983	8	799	3
3	2	739	18	566	2
4	1·5	464	15	360	1
5	1·2	363	10	285	2
6	1·0	236	14	163	2
7	0·86	180	14	147	0
8	0·75	125	7	94	1
9	0·67	65	7	67	0
10	0·60	57	5	42	1
Total		4358 +(967)	106 +(3)	3464	16

Table 2. Absorption of Particles in 10, 15 and 20 cm. Lead

Arrangement as Figure 1 (*b*).

Momentum		Positive particles				Negative particles			
Category	Mean (10^3 Mev/c.)	Total	Stopped in (cm. Pb) 0–10	10–15	15–20	Total	Stopped in (cm. Pb) 0–10	10–15	15–20
0	12	(496)	–	–	(3)	—	–	–	–
1	6	576	–	2	1	469	–	–	2
2	3	494	2	1	1	355	–	–	3
3	2	337	4	1	1	307	–	–	–
4	1·5	277	8	1	1	194	–	–	1
5	1·2	182	3	–	1	118	1	–	–
6	1·0	110	3	2	–	77	2	–	–
7	0·86	76	2	2	1	55	–	–	1
8	0·75	57	2	–	–	41	–	–	–
9	0·67	30	3	–	–	27	1	–	1
10	0·60	30	4	1	–	15	–	–	–
Total		2169 +(496)	31	10	6 +(3)	1974	4	0	8

3.1. *Instrumental Background*

We first observe that the absorption of negative particles is, in both arrangements, small and independent of momentum: we tentatively regard this apparent absorption of negative particles as representing the instrumental background. In the first experiment in which the detecting efficiency of the main discriminating tray EFGH was very carefully controlled, this background is about 0·45%. It is thus slightly higher than that calculated from the properties of individual counters (absorbing system 0·15%, spectrograph ~0·1%), and therefore indicates slight inefficiency of maintenance of the counters in tray EFGH which is not detected in the check processes outlined above. In the second experiment the negative background is rather higher, but the particular layers in which the particles appear to have stopped are very significant. The majority (0·4%) appear to stop in the last 5 cm. of lead: that is to say, the evidence that they have stopped is based only on the failure of tray EFGH to discharge. If a particle which in fact traverses the whole absorber is recorded as stopping in the first (0–10 cm.) or second (10–15 cm.) layers of lead, then it must also fail to discharge counter layers UL and BCD in addition to layer EFGH. These layers are of relatively low geometrical efficiency, about 85% only, nevertheless a spurious record of stopping in 10–15 cm. lead is to be expected only about one-sixth as often as in the lowest layer, while a corresponding spurious record should occur with negligible frequency for the first 10 cm. lead. That 0·4% of all negative particles appear to stop in the last 5 cm. of the lead absorber, while only 0·2% appear to stop in the first 10 cm., and none at all in the intermediate layer, is entirely consistent with the assumption that this 0·4% arises from instrumental inefficiency, but would represent a most remarkable property if it were interpreted as real absorption.

The four negative particles which appear to stop in the first 10 cm., about 0·2% of the whole negative beam, present a different problem and will be discussed later.

3.2. *Absorption of Positive Particles*

It has been shown that only a very small part of the negative particle beam can be considered to be absorbed in 20 cm. of lead. In contrast, considerable absorption of positive particles appears in both Table 1 and Table 2, and we proceed to examine the absorption and the total flux of these particles. To determine the total flux of absorbable positive particles, the efficiency of absorption in the experimental arrangement must be estimated, and the records of the intermediate absorbing layers, BCD in Figure 1 (*a*), UL and BCD in Figure 1 (*b*), are used for this purpose, and at the same time to give the range of the particles in lead. The relevant observations are given in Table 3, which refers only to positive particles. The records in layer BCD of arrangement (*a*) have not been given in Table 1; the corresponding intermediate values for arrangement (*b*) appear in Table 2 and are transcribed. For the reasons developed in the previous paragraph, the most significant comparison in the second experiment is between particles stopping in the first 10 cm. and in the next 5 cm. lead.

In determining absorption from the data of Table 3 it is necessary to take account of the ionization range of the particles (which we assume to be protons). The momenta of protons which in absence of nuclear interaction will penetrate respectively 5, 10, 15 and 20 cm. lead are 0·66, 0·80, 0·93 and $1{\cdot}05 \times 10^3$ MEV/c. (*Princeton Range Tables*, E. P. Gross 1947). Although each momentum category in fact includes particles of an appreciable range of momentum (Hyams *et al.* 1950), it will be sufficiently accurate to divide the measurements with arrangement (*a*) into two groups: categories 1–5, for which protons would not be stopped by ionization in the lower absorbing layer, and categories 6–9, for which all protons will be stopped in this way if they do not sooner make a nuclear collision. With arrangement (*b*) only categories 1–6 yield relevant information. The derivation of the absorption range is summarized in Table 4; the value deduced is (160 ± 40) gm.cm^{-2} (14 cm. lead).

Table 3. Absorption of Positive Particles in Lead

Momentum		Arrangement (*a*)			Arrangement (*b*)		
	Mean		Stopped			Stopped	
Category	(10^3 MeV/c.)	Total	0–5 cm.	5–20 cm.	Total	0–10 cm.	10–15 cm.
0	12	(967)	—	(3)	(496)	–	–
1	6	1150	2	6	576	–	2
2	3	983	1	7	494	2	1
3	2	739	6	12	337	4	1
4	1·5	464	6	9	277	8	1
5	1·2	363	4	6	182	3	–
6	1·0	236	3	11	110	3	2
7	0·86	180	6	8	76	2	2
8	0·75	125	2	5	57	2	–
9	0·67	65	4	3	30	3	–
10	0·60	57	2	3	30	4	1
Total		4358	37	73	2202	31	10
Estimated background		+(967)		$20 \pm 4{\cdot}5$	+(496)		

Table 4. Absorption of Protons (of spectral distribution shown in Figure 3) in Lead

(1)	(2)	(3)	(4)
(*a*) 1–5	$\dfrac{1-\exp(-5/\lambda)}{\exp(-5/\lambda)-\exp(-20/\lambda)}$	$0{\cdot}54 \pm 0{\cdot}17$	20
(*a*) 6–9	$\dfrac{1-\exp(-5/\lambda)}{\exp(-5/\lambda)}$	$0{\cdot}55 \pm 0{\cdot}17$	11·5
(*b*) 1–6	$\dfrac{1-\exp(-10/\lambda)}{\exp(-10/\lambda)-\exp(-15/\lambda)}$	$3{\cdot}0 \pm 1{\cdot}4$	19

(1) Arrangement and momentum categories considered. (2) Calculated ratio of particles stopped in successive layers as a function of range λ cm. (3) Observed value of ratio (in lead) $f_i \pm \epsilon$. (4) Deduced value of range (cm. lead).

The mean range $\bar{\lambda}$ and its standard deviation are given, writing $\epsilon(\lambda_i) = (\partial\lambda_i/\partial f_i)\epsilon(f_i)$, by $\bar{\lambda} = [\Sigma_1^3\{\lambda_i/\epsilon^2(\lambda_i)\}]/[\Sigma_1^3\{1/\epsilon^2(\lambda_i)\}]$, $\epsilon^2(\bar{\lambda}) = 3/\Sigma_1^3\{1/\epsilon^2(\lambda_i)\}$.

3.3. *Proportion of Protons in the Vertical Beam*

The value 160 ± 40 gm.cm^{-2}, referred to in the previous section, although not accurate, allows an estimate to be made of the relatively small number of protons not stopped in our absorber. We give in Table 5 the fraction of protons present in the accepted beam of our apparatus as a function of momentum. Since we are concerned here with a momentum range for which incident electrons are rare, and since (§ 4.5) we have in this work used a screen above the spectrograph for the purpose of degrading the remaining electrons; this fraction may be taken to refer to the hard component in directions within 10° of the zenith (Figure 2).

Table 5. The Proton Component of the Vertical Beam (within 10° of the zenith) as a percentage of the total hard component within the same angle

Note: The uncertainties throughout the table are regarded as purely statistical, and for convenience are only stated in the final column.

Mean momentum	Arrangement (*a*)					Arrangement (*b*)			Total		
(10^3 Mev/c.)	(1)	(2)	(3)	(4)	(5)	(1)	(4)	(5)	(1)	(6)	(7)
12	967	3	4·5	−1·5	—	496	–	—	1463	−1·5	−0·1±0·1
6	2038	8	5·4	2·6	0·8	1045	2	0·9	3083	6·3	0·2±0·1
3	1782	8	4·6	3·4	1·0	849	3	1·4	2631	8·8	0·3±0·1
2	1305	18	3·5	14·5	4·5	637	5	2·3	1942	26·3	1·4±0·3
1·5	877	15	2·2	12·8	4·0	471	9	4·2	1348	30·0	2·2±0·4
1·2	645	10	1·9	8·1	2·5	300	3	1·4	945	15·0	2·4±0·4
1·0	399	14	1·1	12·9	2·1	187	5	1·3	586	21·3	
0·86	327	14	0·8	13·2	—	131	4	—	458	17·2	3·3±0·6
0·75	219	7	0·6	6·4	—	98	2	—	317	8·4	
0·67	132	7	0·3	6·7	—	57	3	—	189	9·7	5·8±1·5
0·60	99	5	0·3	4·7	—	45	5	—	144	9·7	

(1) All particles. (2) Positive particles appearing to stop. (3) Estimated instrumental background. (4) Protons stopped. (5) Estimated number of protons not stopped. (6) Number of protons. (7) Percentage of protons.

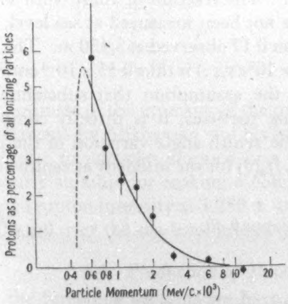

Figure 2.

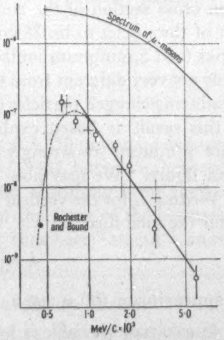

Figure 3. The measured spectrum of protons in the vertical direction at sea level.

● Measurement on slow protons by Rochester and Bound (1940).

○ Sea-level measurements (this paper).

+ Measurements at 30,000 feet after Adams *et al.* (1948) (at arbitrary intensity).

§ 4. DISCUSSION OF RESULTS: DEVELOPMENT

4.1. *The Spectrum of Protons at Sea Level*

The spectrum of the protons is derived immediately by application of the results of Table 5 to the known meson spectrum; for this purpose the meson spectrum given by Rossi (1948) is sufficiently accurate. In Figure 3 we plot on double logarithmic scale the sea-level vertical meson spectrum and the proton spectrum deduced in this way. The slope of the proton curve leads to a differential spectrum of the form $N(p)dp = Kp^{-2\cdot 8}\,dp$, $K = 1\cdot 0 \times 10^{-4}$ cm^{-2} sec^{-1} sterad^{-1} if p and dp are measured in units 10^3 MeV/c. If we assume this momentum spectrum to extend to infinity, the vertical flux of protons with momentum greater than 10^3 MeV/c. is $0\cdot 55 \times 10^{-4}$ cm^{-2} sec^{-1} sterad^{-1}, with about 98% of the particles falling in the measured region $1\text{–}10 \times 10^3$ MeV/c. The spectrum derived from our measurements does not extend to momenta lower than 700 MeV/c., for at lower momenta the results are complicated by the instrumental spread of the meson absorption range. We have therefore no direct evidence of the reduction of proton intensity which must take place when the ionization loss by protons in air becomes large. Rochester and Bound (1940) found a total flux of about $0\cdot 5 \times 10^{-6}$ cm^{-2} sec^{-1} sterad^{-1} of residual range at sea level between 10 and 35 gm.cm^{-2} lead. This spread of range corresponds to a band of momenta about 170 MeV/c. broad at a mean value 450 MeV/c. Their result is therefore shown in Figure 3 at this mean momentum and at proton intensity $0\cdot 3 \times 10^{-8}$ cm^{-2} sec^{-1} sterad^{-1} (MeV/c.)$^{-1}$.

4.2. *Comparison of Total Proton Flux with Data from Photographic Emulsions*

The vertical intensity of protons with momentum greater than 10^3 MeV/c. may be compared with the total flux of star-producing, minimum ionization, charged particles derived from star counts in photographic emulsions and the estimated value of the collision mean free path of these particles in the emulsion. Page (1950) deduces the total flux of star-producing particles at sea level, assuming for the collision cross section of the constituents of the emulsion the geometrical cross section of the nuclei to be 28 cm^{-2} day^{-1}. The fraction of these with charged primaries ($<1\cdot 5$ minimum ionization) has not been measured at sea level, but is probably not very different from the fraction 0·17 observed at 3,450 m. The flux of star-producing charged particles ($p > 0\cdot 98 \times 10^9$ ev/c.) is thus $0\cdot 55 \times 10^{-4}$ cm^{-2} sec^{-1}. Since this result is based explicitly on the assumption that substantially all stars are produced by strongly interacting particles, it is directly comparable with our figure. We may now deduce the zenith angle variation of the proton flux. Writing I_0 for the vertical intensity, $If_0(\theta)$ for the intensity at zenith angle θ, and J for the total flux,

$$J = \int_0^{\pi/2} I_0 f(\theta) 2\pi \sin\theta\, d\theta.$$

If we approximate $f(\theta) = \cos^n\theta$, then

$$\frac{J}{2\pi I_0} = -\int_1^0 \cos^n\theta\, d(\cos\theta) = (n+1)^{-1}.$$

Thus, inserting experimental values of I_0 and J, $n = (2\pi I_0/J) - 1 \sim 5$. This result is, of course, a rough one; using the attenuation mean free path of the protons in the atmosphere deduced later (~ 140 gm.cm^{-2}), the zenith angle effect arising purely from the change of total path length with angle is represented by $n \sim 7$, and the true zenith angle effect is clearly to be expected to be somewhat less sharp.

4.3. *Variation of the Vertical Proton Intensity in the Atmosphere*

The proton spectrum at 30,000 feet may be estimated in a form suitable for comparison with our data from results given by Adams, Anderson, Lloyd, Rau and Saxena (1948). Of 183 counter-controlled cloud-chamber photographs of isolated particles, assuming the positive–negative ratio of the relevant mesons to be 1·25, about 20 are probably due to protons of momentum greater than 10^3 MeV/c.

(30 to protons of lower momentum and about 20 to electrons). The intensity of fast protons is thus about 17% of the meson intensity. We take for the vertical meson flux at 30,000 feet (310 gm. cm^{-2}) $4{\cdot}9 \times 10^{-2}$ cm^{-2} sec^{-1} $sterad^{-1}$, and thus deduce the flux of protons of momentum greater than 10^3 Mev/c. to be $0{\cdot}85 \times 10^{-2}$ cm^{-2} sec^{-1} $sterad^{-1}$.

The proton intensity varies by a factor $(0{\cdot}85 \times 10^{-2})/(0{\cdot}55 \times 10^{-4})$, that is 155, in traversing 720 gm.cm^{-2} of air between 30,000 feet and sea level. The attenuation range is thus 143 gm.cm^{-2}, with an uncertainty mainly arising from the relatively small number of protons observed by Anderson, and their identification by difference. We estimate this number to be 20 ± 8: the range is accordingly 143 ± 13 gm.cm^{-2}.

It is further possible to compare the form of the proton spectrum at sea level and at 30,000 feet. We deduce from the data of Anderson and his co-workers the results of Table 6, and these are plotted at arbitrary intensity in Figure 3. To the rather limited accuracy of the data, Anderson's points conform to the slope of the sea-level spectrum, and to this extent the form of the spectrum appears to be unchanged between 30,000 feet and sea level.

Table 6. Proton Spectrum at 30,000 feet derived from data of Adams *et al.* (1948) (arbitrary intensity)

Curvature range $H \times 10^6$ gauss cm.	10^3 Mev/c.	Proton intensity (arbitrary scale)
0·5–1·5	0·3	0 ± 3
1·5–3·0	0·7	20 ± 6
3–4	1·0	$8{\cdot}5 \pm 4$
4–8	1·8	$2{\cdot}5 \pm 1{\cdot}5$
8–12	3·0	$1{\cdot}0 \pm 0{\cdot}8$

An estimate of the intensity of the proton flux at 3,250 m. can be deduced from measurements by Alikhanian and his co-workers (1948), but since these measurements refer to particles stopped in a rather thin absorbing layer they are not particularly suitable for making a comparison of the form of the spectra. The estimated proton intensity at 3,250 m. is $7{\cdot}7 \times 10^{-4}$ cm^{-2} sec^{-1} $sterad^{-1}$, an increase of $14{\cdot}0 \pm 2{\cdot}0$ over the sea-level intensity.

4.4. *Production of Penetrating Showers by Protons*

In the foregoing sections we have considered exclusively particles of strong nuclear interaction (protons) which are detected by the absence, after interaction, of forward-moving charged particles of range relevant to the method of detection. It is possible that this criterion of selection biases the observations in the sense of failing to identify protons which give rise, after interaction, to penetrating ionizing particles. This problem is discussed again in a later section: here we describe features of the measurements with arrangement (*b*) which might be capable of detecting penetrating showers, that is to say, occasions when two or more fast-charged particles result from the interaction of a proton. Since the deductions made here do not depend critically on the instrumental background inefficiency, more extensive data than those used in Table 2 are available. The occurrence of discharges of two subgroups of counters, either in one of trays UL, BCD, EFG of arrangement (*b*) or in two trays simultaneously, is summarized in Table 7. No examples of double discharges simultaneously in all three trays were encountered.

Column (4) of the Table shows the occurrence of double discharges in one tray only of the arrangement (*b*). Substantially all of these will be due to knock-on electrons produced by mesons, and in fact the percentage of double discharges per tray traversed varies in the way to be expected with meson momentum. We calculate directly from column (4) the corresponding number of simultaneous events in two trays, and this is tabulated in column (6) for comparison with the observed number of simultaneous events (column (5)); while the calculated total number of double counts is 13·2, 18 were actually observed. The difference is not significant, but, in addition, the figure 13·2 is a lower limit, for each momentum category covers a range of momenta, and the mesons leading to detected knock-on electrons in one tray will be derived preferentially from the higher momentum part of that range and will thus be more likely to produce a second double discharge than is indicated in the Table.

Table 7. Multiple Discharge of Counters in Arrangement (*b*)

(1)	(2)	(3)	(4)	(5)	(6)
0	12	705	81	1	3·1
+1	6	908	70	1	2·3
−1		739	74	6	1·9
+2	3	771	66	2	2·8
−2		592	40	3	
+3	2	543	44	1	1·5
−3		464	26	2	
+4	1·5	425	21	0	0·9
−4		298	21	0	
±(6–10)	0·9	838	24	0	0·2
±(>10)	0·5	130	0	0	0
Total double discharges				18±4	13·2

(1) Momentum category. (2) Mean momentum (10^8 Mev/c). (3) Total number of particles. (4) Double discharge of one tray only. Double discharge of two trays: (5) observed, (6) calculated from column (4).

There is thus no statistical indication, to the accuracy of observation set by the knock-on electrons from mesons, of events attributable to showers penetrating the whole absorbing system arising from the stopping of protons. The complete absence of double discharges simultaneously in three trays is in agreement with this conclusion. Some evidence of multiplicity, but comprising particles of rather short range, is, however, indicated by records in which multiplicity is detected in the last counter tray which is discharged by a particle stopped in the absorber.

The number of events of this type due to knock-on electrons should be one-twentieth of the background number of particles appearing to stop (Table 7); the actual record shows twice the expected number. One negative particle from twenty appearing to stop gives a double count in the last tray which it triggers, in agreement with the knock-on rate, but six positive particles from fifty give a double discharge; in two of these events a double discharge occurred in both trays UL and

BCD, and no particle triggered tray EFGH; the probability of such an event arising from the formation of knock-on electrons is about 1/400 of all particles stopping. Taking into account the low efficiency with which the production of secondaries of moderate range will be detected, we estimate that 5–10% of the particles stopped probably give at least two secondary particles of ranges of the order 5–10 cm. lead.

4.5. *Negative Particles stopped in Lead*

In Table 2, of about 2,000 negative particles with momentum greater than 600 MEV/C., four are recorded as stopping in 0–10 cm. lead and none in the following 5 cm. lead (10–15 cm.). Since we have shown that the probability of a particle traversing the counter system failing to discharge counter layers UL and BCD as well as EFGH is about 1/30 of that for failing to discharge layer EFGH alone, and since the apparent rate of stopping, if due to counter inefficiency in the absorption apparatus, should be greater by a fraction of about 5 in the lead layer 10–15 cm. than in the lead layer 0–10 cm., these counts cannot be considered to arise from inefficiency of the absorption apparatus.

It has been shown elsewhere (Hyams *et al.* 1950) that a spurious record of the spectrograph is probably obtained about once for each thousand particles recorded, and that much of this inefficiency arises from the action of extensive electron showers. Such records would clearly be expected, as a rule, to lead to apparent absorption in the first layer of lead, and probably contribute about one-half of the observed effect. The remainder may well represent the contribution of isolated electrons and π-mesons; this remainder amounts to only about 0·1% of the negative beam.

According to Williams (1939) about 1% of cosmic-ray particles of momentum greater than 3×10^8 ev/c. at sea level are electrons, but, to minimize the effect of electrons in our experiment, the particle beam entering the spectrograph is caused to traverse a layer of lead 1·2 cm. thick placed about 30 cm. above the top counter tray of the spectrograph. This layer will strongly degrade in energy electrons falling on the apparatus, which will also be partially excluded from the accepted records by the occurrence of multiple discharges in the top counter tray of the spectrograph. Following the cascade fluctuation calculations of Arley (1949), the probability of an unaccompanied electron of energy greater than 10^3 MEV. emerging from 1·2 cm. lead is of the order 0·20; thus much less than 0·2% of the spectrograph beam is expected to be electronic.

The probable admixture of π-mesons in the beam may be deduced, noting that for proper lifetime $1{\cdot}8 \times 10^{-8}$ sec. the mean range in air at sea level against decay at the relevant momenta would be of the order 3 gm.cm^{-2}, in which less than 5% of existing nuclear interacting particles will make collisions. Since less than 5% of the nucleons are of sufficient energy to produce π-mesons of the observed momentum, the resultant intensity of these can clearly only be of the order 0·005% of the total beam. A contribution of about the same magnitude may be expected to arise from collision in the 1·2 cm. lead screen above the spectrograph.

It is thus probable that the 0·1% fraction of the negative beam which is observed to be readily absorbed is mainly electronic. The measured intensity is essentially a function of the apparatus and not of the free electron flux at sea level, for the apparatus is strongly biased against recording fast electrons.

§ 5. DISCUSSION OF RESULTS: INTERPRETATION

5.1. *The Measured Range of Protons in Lead* 700 MeV/c. $<p<$ 2,500 MeV/c.

The probability that protons entering the lead will give rise to detectable ionizing particles below the absorber is described by the range 160 ± 40gm.cm^{-2}. If, as is probable (see, for example, Bethe 1949), the collision cross section of protons in this range of momentum in lead is the geometrical cross section, $\sigma_{\text{coll}} = 0{\cdot}063 A^{2/3}$ barn, leading to $(1/\lambda)_{\text{coll}} = 156$ gm.cm^{-2}, it must be concluded that very few of these protons give rise to ionizing products of range comparable with the primary collision range.

This result is clearly to be expected at the lower momenta, $p \sim 10^3$ MeV/c. ($E_{\text{kin}} \sim 420$ MeV.), for the scattering cross section per nucleon extrapolated from the Berkeley measurements (0·013 barn per nucleon at 350 MeV.) is still large enough to yield at least one collision in a single heavy nucleus, and any considerable overall loss of energy by the primary proton will leave it with very short ionization range (of the order of 17 gm.cm^{-2} at 100 MeV.). At higher momenta ($p \sim 2{,}500$ MeV/c., $E_{\text{kin}} \sim 1{,}700$ MeV.) there is no clear information about either the total collision cross section or the cross section for meson production. Phenomenologically we would expect our measurement of range to be modified to values greater than the collision range (*a*) by the emission, in the collision, of protons of energy greater than about 200 MeV., (*b*) by the emission of mesons of energy greater than about 100 MeV. The number observed, however, is quite inadequate to determine a separate effective range for these more energetic particles. The evidence available would suggest that the increase of effective range for these particles is not great.

In a recent paper (Camerini *et al.* 1950) protons emitted from stars in a photographic emulsion have been studied, and their range before collision is found to be about 100 gm.cm^{-2} of emulsion, corresponding to a cross section in the emulsion only slightly less than the geometrical cross section. The range of momentum covered in these measurements is similar to that covered by ourselves, namely 0·3 to $1{\cdot}3 \times 10^3$ MeV/c.

In contrast, the reduction of intensity of star production in lead takes place (Bernardini 1948, George and Jason 1949) with a range of greater than 300 gm.cm^{-2}. The difference clearly depends largely on the part played in star production by neutrons of energy comparable with the slowest protons which we measure.

5.2. *Form of the Proton Spectrum and the Attenuation in Air*

That practically the whole of the proton flux measured in our experiments must be of a secondary nature is established by the following results.

(i) The work of Allen and Singer (1950) shows that the differential primary spectrum ($2{\cdot}6 \times 10^3$ MeV. $<p<$ 15×10^3 MeV.) can best be fitted by $dN = 0{\cdot}53(pc/Ze)^{-2{\cdot}1} d(pc/Ze)$. This spectrum is already much flatter than our spectrum, and when allowance is made for the ionization loss of energy in traversing the atmosphere the spectrum would become even flatter, corresponding to an index of about $-1{\cdot}5$, as compared with our value of $-2{\cdot}8$.

(ii) The similarity between the shape of our spectrum at sea level and that determined by Anderson at 30,000 feet again suggests that the particles are of a secondary nature, for

(iii) the Anderson spectrum must be composed entirely of secondary particles since the geomagnetic cut-off momentum at Pasadena is about 5×10^3 MEV/C.

The attenuation of this low energy proton spectrum can be obtained most accurately by comparing the intensities measured by ourselves, Alikhanian, and Anderson at three different heights in the atmosphere. These intensities are

$$0{\cdot}55 \times 10^{-4}\ \text{cm}^{-2}\ \text{sec}^{-1}\ \text{sterad}^{-1} \text{ under } 1{,}030\ \text{gm.cm}^{-2} \text{ air},$$
$$7{\cdot}7 \times 10^{-4}\ \text{cm}^{-2}\ \text{sec}^{-1}\ \text{sterad}^{-1} \text{ under } 690\ \text{gm.cm}^{-2} \text{ air},$$
$$85{\cdot}0 \times 10^{-4}\ \text{cm}^{-2}\ \text{sec}^{-1}\ \text{sterad}^{-1} \text{ under } 310\ \text{gm.cm}^{-2} \text{ air}.$$

Assuming a relationship between the intensity and depth of the form $I = I_0 e^{-\lambda x}$, we obtain the attenuation range $1/\lambda$, 140 ± 10 gm.cm^{-2}.

It is rather difficult to make an adequate comparison of this range with that of energetic, penetrating shower-producing particles in the atmosphere or of the star-producing component, for both of these ranges are determined from measurements for which an application of the Gross transformation is necessary. The range which we have derived, on the other hand, to a first approximation is not subject to the transformation, since measurements at all levels are made with apparatus with a strong bias for the selection of vertical trajectories, this bias being, as is required, strongest for the sea-level measurements. A weak transformation should probably in fact be applied, since our measurements concern particles of such low energy (in terms of the particle rest mass) that diffusion of direction, away from the direction of the primary particles from which our protons are derived, is appreciable.

The exponential range of the particles producing penetrating shower phenomena is 118 ± 2 gm.cm^{-2} in air (Tinlot 1948), and an application of the Gross transformation to this value, bearing in mind the limited aperture of the apparatus used, probably increases this value to 125 or 130 gm.cm^{-2}. The transformed range given by Wataghin (1949) is 119 ± 5 gm.cm^{-2}. The transformed range of star-producing particles, on the other hand, is given by Camerini and his colleagues (1949) as 170 gm.cm^{-2} for all stars, ranging down to 105 gm.cm^{-2} for stars producing six or more fast secondaries. The exponential range equivalent to that given by Camerini for all stars, 135 gm.cm^{-2}, is in accord with other star measurements (Bernardini 1948, George and Jason 1949, Page 1950).

The attenuation of our protons in the atmosphere thus follows more closely that of the energetic primaries of penetrating showers than that of the star-producing component, although the measured protons approximate in energy to the latter. It is probably correct to consider the penetrating shower primaries to be the direct parents of our protons, and it is then necessary to determine whether any large difference of attenuation of the primaries and of their product protons in the atmosphere is to be expected.

Assume, as a simplified model, that the primaries of our protons traverse the atmosphere without change of spectrum (Heitler and Jánossy 1949) with an attenuation coefficient λ_1. The secondary spectrum arising between depths x and $x+dx$ of atmosphere is then $I_s(p, x)\, dp = I_0 \exp(-\lambda_1 x)\, S(p)\, dp\, dx$, where I_0 defines the intensity of the primary beam and $S(p)$ the resultant secondary spectrum arising from the undefined but constant primary spectrum. The observed secondary spectrum at depth X will then be

$$I_{s(\text{total})}(p, X)\, dp = I_0 \int_0^X \exp(-\lambda_1 x) \exp[-\lambda_2 (X - x)]\, S[p + \alpha(X - x)]\, dx\, dp,$$

where λ_2 is the absorption coefficient of the secondary protons in air and α their ionization momentum loss in unit thickness. The total number of secondaries ($p>p_0$) at depth X is accordingly

$$N_s(p_0, X) = I_0 \exp(-\lambda_1 X) \int_{p_0}^{\infty} \int_0^X \exp(\lambda_1 - \lambda_2)(X-x)\, S[p+\alpha(X-x)]\, dx\, dp$$

and the apparent attenuation of the beam, λ_A, is given by

$$\frac{N_s(p_0, X_1)}{N_s(p_0, X_2)} = \exp[-\lambda_1(X_1 - X_2)] \frac{\iint^{X_1} \exp \delta\lambda (X_1 - x)\, S[p+\alpha(X_1 - x)]\, dx\, dp}{\iint^{X_2} \exp \delta\lambda (X_2 - x)\, S[p+\alpha(X_2 - x)]\, dx\, dp},$$

$$= \exp[-\lambda_A(X_1 - X_2)].$$

Ignoring the effect of ionization, this clearly becomes

$$\exp[-\lambda_A(X_1 - X_2)] = \exp[-\lambda_1(X_1 - X_2)] \frac{1 - \exp X_1 \delta\lambda}{1 - \exp X_2 \delta\lambda}.$$

Substituting the values at sea level and 30,000 feet for X_1 and X_2 respectively and taking $1/\lambda_1 = 120$ gm.cm^{-2}, we get the following table of results connecting λ_2 and λ_A:

$1/\lambda_2$ (gm. cm^{-2})	75	100	125	150
$1/\lambda_A$ (gm. cm^{-2})	125	135	155	175

The range of the secondary particles required to give $1/\lambda_A = 140$ gm.cm^{-2} is thus a little greater than 100 gm. cm^{-2}, a value which is necessarily rough but which is quite reasonable. Assuming the above model to give the range for star-producing particles also, we find that in this case the secondary particles must have a range of about 145 gm.cm^{-2}.

Since most of the low energy stars are produced by non-ionizing particles, these particles can be expected to have a longer range than the 100 gm .cm^{-2} given above since, over the momentum range discussed, the ionization energy losses will reduce the effective range of charged particles. Also any particles of the third generation produced will, if charged, have an extremely short ionization range, whereas, if neutral, they will continue until they make a nuclear collision and so help further to increase the effective range of star-producing particles to a value greater than that of the charged nucleons which we have observed.

5.3. *The Form of the Proton Spectrum at Formation*

The above analysis also allows us to estimate the formation spectrum of the protons for which we have given the sea-level spectrum in the form $S(p) \sim p^{-2\cdot 8}$. Assuming for this purpose $\lambda_1 = \lambda_2$,

$$I_{s(\text{total})}(p, X) \sim \int_0^X [p+\alpha(X-x)]^{-\gamma}\, dx \sim \{p^{-(\gamma-1)} - (p+\alpha X)^{-(\gamma-1)}\}.$$

Now αX(sea level) $= 2 \times 10^3$ Mev/c.: fitting to the observed spectrum at $p = 10^3$ Mev/c. and $p = 3 \times 10^3$ Mev/c.,

$$\frac{I_{s(\text{total})}(1, X)}{I_{s(\text{total})}(3, X)} = 17 \text{ (experimental)} \quad \text{and so } \gamma \sim 3\cdot 3.$$

Thus $S_{\text{formation}}(p)\,dp \sim p^{-3\cdot 3}\,dp$. This result can be compared with that measured directly by Camerini and his co-workers (1950) in photographic emulsion exposed at an altitude of 3,500 m. Transforming Camerini's results from a kinetic energy scale to a momentum scale, $S_{\text{formation}}(p)\,dp \sim p^{-3\cdot 1}\,dp$; the agreement is then satisfactory.

ACKNOWLEDGMENTS

We are grateful to Professor P. M. S. Blackett for his constant encouragement and interest throughout the whole project of which this work forms part, and to Dr. B. G. Owen for advice on many of the technical problems involved.

One of us (M. G. M.) is indebted to the Department of Scientific and Industrial Research for a Maintenance Grant.

REFERENCES

Adams, R. V., Anderson, C. D., Lloyd, P. E., Rau, R. R., and Saxena, R. C., 1948, *Rev. Mod. Phys.*, **20**, 334.

Alikhanian, A., Alikhanov, A., and Weissenberg, A., 1948, *J. Exp. Theor. Phys., U.S.S.R.*, **18**, No. 8, 673.

Allen, J. A., and Singer, S. F., 1950, *Phys. Rev.*, **78**, 819.

Arley, N., 1949, *Stochastic Processes and Cosmic Radiation* (New York : Wiley).

Bernardini, G., 1948, *Phys. Rev.*, **74**, 845.

Bethe, H. A., 1949, *Proc. Echo Lake C.R. Symposium* (Washington: Office of Naval Research), p. 117.

Camerini, U., Coor, T., Davies, J. H., Fowler, P. H., Lock, W. O., Muirhead, H., and Tobin, N., 1949, *Phil. Mag.*, **90**, 1073.

Camerini, U., Fowler, P. H., Lock, W. O., and Muirhead, H., 1950, *Phil. Mag.*, **91**, 413

George, E. P., and Jason, A. C. 1949, *Proc. Phys. Soc.* A, **62**, 243.

Heitler, W., and Jánossy, L., 1949, *Proc. Phys. Soc.* A, **62**, 374.

Hyams, B. D., Mylroi, M. G., Owen, B. G., and Wilson, J. G., 1950, *Proc. Phys. Soc.* A, **63**, 1053.

Lheritier, M., Peyrou, C., and Lagarrigue, A., 1947, *C. R. Acad. Sci., Paris*, **225**, 1304.

Page, N., 1950, *Proc. Phys. Soc.* A, **63**, 250.

Rochester, G. D., and Bound, M., 1940, *Nature, Lond.*, **146**, 745.

Rossi, B., 1948, *Rev. Mod. Phys.*, **20**, 537.

Tinlot, J., 1948, *Phys. Rev.*, **74**, 1197.

Wataghin, G., 1949, *Suppl. Nuovo Cim.*, **6**, 559.

Williams, E. J., 1939, *Proc. Soc. Roy.* A, **172**, 194.

Further Measurements of the Charge Ratio of μ-Mesons at Sea Level

By B. G. OWEN and J. G. WILSON
Physical Laboratories, University of Manchester

Communicated by P. M. S. Blackett; *MS. received* 23rd *November* 1950

ABSTRACT. Extended measurements of the charge ratio (positive/negative) of near-vertical μ-mesons at sea level show that it increases with meson momentum from about $1\cdot17$ at 10^3 Mev/c. up to about $1\cdot26$ at 4×10^3 Mev/c. At higher momenta the statistical accuracy of the measured charge ratio is limited by the instrumental rate of collection, and it cannot yet be definitely decided whether the charge ratio decreases with increasing momentum, although the evidence now available favours a slow decrease.

The general implications of the form of variation of charge ratio with momentum are indicated.

§ 1. INTRODUCTION

Previous measurements of the charge ratio of vertical sea-level mesons made with the Manchester magnetic spectrograph have been reported by Owen and Wilson (1949) and Wilson (1949). A further discussion of this work is now given because the data available are considerably more extensive, and particularly because the parallel investigation of the proton component in the vertical beam (Mylroi and Wilson 1951) has now yielded adequate information for the reduction of the crude measured charge ratios at the lower momenta to values strictly applicable to μ-mesons.

A considerable volume of work by other groups has now been reported, and it is also useful to review existing information, to determine whether serious discrepancies exist among the various values, and to give as far as possible a unified picture of present knowledge.

No important modifications of the technique described in an earlier paper (Owen and Wilson 1949) have been made, and the procedure of measurement, field reversals and other measures, will not be discussed again. In particular, the angular distribution of particles considered is unchanged.

§ 2. EXPERIMENTAL RESULTS

The crude ratios are summarized in Table 1. These require correction for two factors: the presence of the proton component, which is of appreciable intensity at the lower momenta, and the contamination of measurements in momentum category 1 with particles of the opposite sign. The detailed results of Table 1 are collected into six momentum ranges and corrected accordingly.

Table 1. The Crude Ratios of Positive to Negative Particles in the Vertical Beam at Sea Level

Deflecting field (gauss cm.)	Momentum categories	Log (mean momentum) (10^3 MeV/c.)	Observed no. of particles		Ratio
			+ve	−ve	
$2{\cdot}9 \times 10^5$	1	0·81	3248	2600	1·249
	2	0·54	1687	1388	1·215
	2+3*	0·46	1959	1523	1·286
	3+4*	0·30	2068	1639	1·262
	>3*	0·11	1896	1522	1·246
	>4*	0·02	2201	1802	1·221
$3{\cdot}35 \times 10^5$	1	0·85	3382	2815	1·201
	2	0·62	3204	2544	1·259
	3+4	0·35	4287	3348	1·280
	>4	0·07	4553	3639	1·233
$5{\cdot}8 \times 10^5$	1	1·06	2624	2161	1·214
	2+3	0·76	5544	4333	1·279
	4+5+6	0·48	5178	4181	1·238
	>6	0·21	4492	3548	1·238

* Separate sections of the records were summarized in different ways; there is no overlap of data.

The proton component is taken as given in Figure 2 of the paper by Mylroi and Wilson (1951). The correction for high momentum contamination is not quite so straightforward, for it must be based on the charge ratio of the contaminating particles, which are of decidedly higher momentum (mean about 80×10^3 MeV/c.)

than the main measured group. The mechanism by which the contaminating particles appear in category 1 measurements is explained in Figure 1 (and its legend). There seems little indication that the charge ratio is falling off rapidly with increasing momentum, and none at all that it is rising. We have therefore made the correction on the assumption that the charge ratio does not change significantly between 12×10^3 Mev/c. and 80×10^3 Mev/c., and since in fact a slow fall of charge ratio is, on balance, seen to be probable, the corrected ratios are probably very slightly too high. The collected values in their crude form and after correction are given in Table 2.

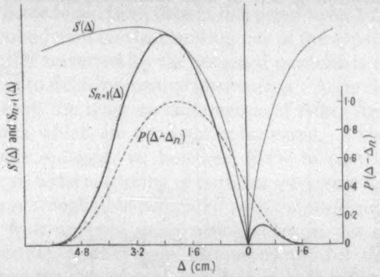

Figure 1. Illustrating the way in which the measured momentum category 1 includes some particles (about 3%) of opposite sign to the nominal sign of the group. (Notation as in Hyams *et al.* 1950.) $S(\Delta)$ is the deflection spectrum of mesons falling on the apparatus, while $P(\Delta-\Delta_n)$ is the collecting efficiency function of the spectrograph drawn, relative to the deflection spectrum, in the position appropriate to momentum category 1. The deflection spectrum of particles accepted by the spectrograph, $S_1(\Delta)$ is then given by the product $S(\Delta)P(\Delta-\Delta_n)$ and this curve will be seen to extend through $\Delta=0$ to include deflections in the direction opposite to the nominal deflection.

Table 2. Collected Groups of Charge Ratio Data for the Vertical Beam at Sea Level

Log (mean momentum) (10^3 Mev/c.)	Observed no. of particles		Crude charge ratio	Corrected charge ratio (μ-mesons)
	+ve	−ve		
1·06	2624	2161	1·214	1·229±0·036
0·83	6630	5415	1·224	1·240±0·023
0·69	10435	8265	1·263	1·263±0·019
0·44	11424	9052	1·262	1·251±0·018
0·28	10847	8535	1·271	1·241±0·018
0·06	8650	7017	1·233	1·172±0·019

§ 3. COMPARISON WITH OTHER OBSERVATIONS

In Table 3 we summarize the measurements of other workers who have measured the charge ratio near sea level. These measurements are plotted together with our present results (column 5 of Table 2) in Figure 2. The early cloud chamber observations of Blackett (1937), Jones (1939) and Hughes (1940) which were quoted separately in the earlier paper are now combined.

The majority of the results reported elsewhere are in good agreement with our measurements, and taking these into account according to their statistical weights does not significantly alter our values. It is particularly satisfactory to note the confirmation which we give to Nereson's low value near 10^3 Mev/c.

This is of comparable weight to our result but is obtained by a completely different method.

Some comment is necessary, however, on the measurement by Brode* and on the high momentum group of the values reported by Caro, Parry and Rathgeber.

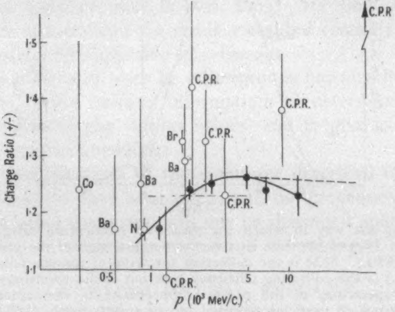

Figure 2. Charge ratio of vertical μ-mesons at sea level as a function of momentum. ● the results reported in this paper, ○ measurements of other workers. Co, Conversi (1949) Ba, Bassi, Clementel, Filosofo and Puppi (1949); N, Nereson (1948); Br, Brode (1949), C.P.R., Caro, Parry and Rathgeber (1950). The light horizontal broken line is the average value given in cloud chamber measurements. —— adopted form of the variation of charge ratio. - - - - obtained by including results of Caro *et al.* at their normal statistical weight (momenta $>5\times10^3$ Mev/c.).

Table 3. Values of Charge Ratio at Sea Level reported by other Workers

Reference	Method	Log (momentum)	Charge ratio
Blackett 1937 Jones 1939 Hughes 1940	Cloud chamber	$\bar{1}\cdot6$–$1\cdot3$	1·225±0·049
Conversi 1949	Relative decay rates in C and S	$\bar{1}\cdot48$	1·24 ±0·26
Bassi *et al.* 1949	Deflection in air	$\bar{1}\cdot74$	1·17 ±0·13
		$\bar{1}\cdot93$	1·25 ±0·15
		0·25	1·29 ±0·10
Nereson 1948	Detection of decay electrons (deflection in iron)	$\bar{1}\cdot95$	1·170±0·020
Brode 1949	Deflection in iron	0·23	1·320±0·020
†Caro *et al.* 1950	Deflection in air	$\bar{1}\cdot48$	0·97 ±0·23
		$\bar{1}\cdot78$	1·24 ±0·20
		$\bar{1}\cdot90$	1·07 ±0·14
		0	0·95 ±0·10
		0·11	1·09 ±0·12
		0·30	1·42 ±0·18
		0·40	1·32 ±0·09
		0·54	1·23 ±0·10
		0·95	1·38 ±0·10
		1·54	1·60 ±0·20

---

* We were fortunate to have an opportunity of discussing this measurement with Professor Brode in September 1950.

† The figures quoted are derived from a published graph. In particular the mean momenta tabulated have been estimated from the block limits of momentum indicated in the original and from the known meson spectrum.

The result quoted by Brode is obtained using an iron core deflection system in which, unlike the earlier apparatus of Bernardini and his co-workers (1941), the selecting counters are out of alignment, the measured effect therefore not being diluted by the slightly deflected particles of high momentum. The crude measurement may be deduced from data in this paper to be 1·22; this is increased to 1·32 by a correction based on the counting rate of the apparatus when the field in one half of the iron traversed by the recorded particles is reversed. All such counts are attributed to field-insensitive phenomena. Accordingly, this counting rate is subtracted from the main measurements (of either sign) and the ratio of the remaining counts which are accepted is increased. This correcting count, with deflecting fields opposed, is, however, likely to contain a field sensitive element arising because the scattering of particles traversing a piece of iron of the dimensions used is not negligible compared with the magnetic deflection. That part of the count with opposed fields which arises in this way should not be applied as a correction to the main measurements, for the probability that scattering will reverse the direction of deflection in both halves of the iron system simultaneously is negligible. It is therefore likely that Brode's measurement is overcorrected, and that the charge ratio is really smaller than the quoted value. This view is supported by the fact that the collected cloud chamber data (Blackett, Jones, Hughes) while covering a large range of momenta draws a large fraction of particles from the region 10^3 Mev/c. $<p<5\times10^3$ Mev/c. The charge ratio so measured ($1\cdot225\pm0\cdot049$) is in excellent agreement with our measurements but does not fit well with any large particle group of high charge ratio.

We therefore consider that the measurement given by Brode does not provide grounds for adopting a value of charge ratio, in the region 10^3 Mev/c. $<p<2\times10^3$ Mev/c., different from that given in our work.

The results (Table 3) given by Caro and his co-workers (1950) are made with an apparatus similar in principle to our own. They are characterized by generally low values of charge ratio up to about $1\cdot5\times10^3$ Mev/c. and then much higher values at greater momenta. The statistical weight of the results is, however, generally rather low, and up to 4×10^3 Mev/c. there is no significant discrepancy with our measurements. The two values at mean momenta about 9×10^3 Mev/c. and 35×10^3 Mev/c. are of importance, for the second occupies a momentum range which we do not reach in our work, while the two together suggest a rather rapid increase of charge ratio with momentum continuing at least to 35×10^3 Mev/c. However, the detailed account of the experiments upon which these points are based is not yet available, and it may be that freedom from systematic errors has not been completely achieved in the relatively small number of particles recorded; we therefore again regard the curve drawn through our points as the best available. Even if we assume the measurements of Caro and his co-workers to be free from systematic error and draw the best linear variation of charge ratio with $\log p$ by the method of least squares, fitting to the low momentum part of our curve at 5×10^3 Mev/c. (broken curve, Figure 2), the general form of the variation of charge ratio with momentum at the higher momenta is not greatly altered.

§ 4. DISCUSSION

Our conclusions refer to the full line of Figure 2, which, for the reasons given in the previous section, we regard as that most consistent with existing information. The increase of charge ratio from about 1·17 at $p=10^3$ Mev/c. to about

1·26 at $p = 5 \times 10^3$ MeV/c. seems well established, but although the results favour rather strongly a decrease of charge ratio at higher momenta, this cannot be regarded as decisively established. The decrease, if real, does not appear to be very rapid.

The data necessary to clarify this important region of the curve (Figure 2) cannot be expected quickly. To halve the statistical uncertainty of our point at 11×10^3 MeV/c. would require continuous operation (24 hours per day) of the Manchester spectrograph for one year, and for a longer period with the Melbourne instrument, the operating rate of which is not as great. From neither apparatus will results in fact be available so quickly, for other work will require the spectrographs to be operated for considerable periods under conditions unsuitable for high momentum charge ratio determinations.

Interpretation. The interpretation of the form of the measured charge ratio variation with momentum, in terms of the encounters at which meson formation takes place, has been examined by many authors * and no comparison of the models set up and the conclusions reached will be attempted here. It will be useful, however, to examine the general features which are indicated by the curve shown in Figure 2.

We may assume that all nucleon–nucleon collisions at the relevant energies are free and independent whether the bombarding particle is a single nucleon or a small nucleus (α-particle). The *first collision* of a cosmic-ray primary reaching the earth is then made by protons and neutrons in a proportion determined by the relative numbers of protons and α-particles in the primary beam (the proportion of heavier nuclei in the primary beam is small, and their composition is substantially the same as that of the α-particles). No evidence has yet been given of any change in the relative numbers of primary protons and α-particles as a function of momentum.

Since at moderate energies the ratio of protons to neutrons in the primary particle beam is roughly 3/1 (80% protons, 20% α-particles), it follows, because the meson charge ratio arising is of the order 1·2 to 1·25, that overall, several charged mesons are produced for each incident primary cosmic-ray particle. In the simplest model we assume that the whole charge excess of the incident beam goes to mesons; there is then clearly an overall multiplicity of meson production of the order 7. This multiplicity may arise either because about seven mesons are formed in the single nucleon–nucleon encounter of a first collision, or because a smaller number of mesons, perhaps one only, is formed in the first collision but that others are formed by subsequent collisions of one or both of the nucleons concerned in the first collision, and of nucleons in their turn arising in the later collisions. We examine the form of the charge ratio variation to determine whether it distinguishes in any way between these alternatives.

There is abundant evidence that nucleons formed in first and later encounters do take part in further meson forming collisions. We refer to these events as *secondary collisions* and in them the bombarding particles are mainly free nucleons, with roughly equal numbers of protons and neutrons. It is to be observed that the *first collision* is the first *nucleon–nucleon* collision of a primary nucleon, and that it may well be that secondary collisions leading to fast mesons often take place within the same air nucleus as the first collision.

---

* In particular, Clementel and Puppi (1948), Caldirola (1949), Bassi, Clementel, Filosofo and Puppi (1949), Cini and Wataghin (1950), Caldirola and Loinger (1950).

We therefore expect ***first collisions*** to lead to mesons with a charge ratio determined by the relative number of protons and neutrons in the primary cosmic-ray beam and by the average number of mesons formed in each first collision, while ***secondary collisions*** will lead to mesons with a small charge ratio because those mesons arise from a component containing similar numbers of protons and neutrons. The contribution from secondary collisions thus dilutes the charge ratio arising in first collisions.

There is no reason to expect that the momentum spectrum of primary and secondary nucleons will be the same, and there is in fact evidence that the secondary nucleon spectrum contains a relatively larger number of low energy particles. For example, Mylroi and Wilson (1951) show that the differential momentum spectrum of protons between 1 and 5×10^3 Mev/c. at sea level is of the form $p^{-2\cdot8}$ and a similar conclusion, for protons produced in emulsion stars at high altitude, may be drawn from the results of Camerini and his co-workers (1950). On the other hand the spectrum of primary protons does not, according to Winckler, Stix, Dwight and Sabin (1950), approach this index at momenta less than about 25×10^3 Mev/c.

It is accordingly plausible to identify the well-established decrease of charge ratio at low momenta with strong dilution of the ratio by mesons formed in secondary collisions, and to assume that the products of secondary collisions become relatively less important at the high momenta. If this view is correct, the reduction of charge ratio at momenta greater than 5×10^3 Mev/c. must depend upon variations of charge rtaio in first collisions. While we cannot at present exclude the possibility that the reduction arises because the proportion of α-particles (and so of neutrons) in the primary cosmic-ray beam increases with momentum, it is more probable that it is variation characteristic of the detailed production of mesons in nucleon–nucleon collisions, and as such must be taken as evidence that the average number of mesons formed in a first collision increases with the energy of the mesons produced.

The limitations of measurement in the spectral region for which the high-momentum reduction of charge ratio takes place are sufficiently serious to make any more detailed deductions very uncertain.

ACKNOWLEDGMENTS

The authors have pleasure in recording their indebtedness to Professor P. M. S. Blackett for his constant interest in this problem, and to M. G. Mylroi and G. M. D. B. Jones who have supervised the operation of the spectrograph during much of the recording time. Assistance in computing the detailed results has been made possible from grants to the laboratory by the Nuffield Foundation and by the Department of Scientific and Industrial Research.

REFERENCES

Bassi, P., Clementel, E., Filosofo, I., and Puppi, G., 1949, *Nuovo Cim.*, **6**, 484.
Bernardini, G., Conversi, M., Pancini, E., and Wick, G. C., 1941, *Ric. Sci.*, **20**, 1227.
Blackett, P. M. S., 1937, *Proc. Roy. Soc.* A, **159**, 1.
Brode, R. B., 1949, *Nuovo Cim.*, **6** (Suppl.), 465.
Caldirola, P., 1949, *Nuovo Cim.*, **6**, 565.
Caldirola, P., and Loinger, A., 1950, *Nuovo Cim.*, **7**, 161.
Camerini, U., Fowler, P. H., Lock, W. O., and Muirhead, H., 1950, *Phil. Mag.*, **91**, 413.
Caro, D. E., Parry, J. K., and Rathgeber, H. D., 1950, *Nature, Lond.*, **165**, 689.
Cini, M., and Wataghin, G., 1950, *Nuovo Cim.*, **7**, 135.
Clementel, E., and Puppi, G., 1948, *Nuovo Cim.*, **5**, 529.

Conversi, M., 1949, *Phys. Rev.*, **76**, 311.
Hughes, D. J., 1940, *Phys. Rev.*, **57**, 592.
Hyams, B. D., Mylroi, M. G., Owen, B. G., and Wilson, J. G., 1950, *Proc. Phys. Soc.* A, **63**, 1053.
Jones, H., 1939, *Rev. Mod. Phys.*, **11**, 235.
Mylroi, M. G., and Wilson, J. G., 1951, *Proc. Phys. Soc.* A, **64**, 404.
Nereson, N., 1948, *Phys. Rev.*, **73**, 565.
Owen, B. G., and Wilson, J. G., 1949, *Proc. Phys. Soc.* A, **62**, 601.
Winckler, J. R., Stix, T., Dwight, K., and Sabin, R., 1950, *Phys. Rev.*, **79**, 656.
Wilson, J. G., 1949, *Nuovo Cim.*, **6** (Suppl.), 523.

LETTERS TO THE EDITOR

The Electron Voltaic Effect

We have observed that photovoltaic cells are sensitive to electron bombardment. In a particular series of experiments a Westinghouse selenium cell was bombarded with a stream of electrons accelerated by a potential difference of up to 80 kv., after the varnish protecting the cell had been removed. The electrons were slightly concentrated so that they impinged on to a circle of 14 mm. diameter and both the bombarding current and the circulating current were observed. In the Figure the ratio of circulating current to bombarding current (gain) is shown for a primary current of $1{\cdot}5 \times 10^{-8}$ amp., corresponding to about 10^{-8} amp/cm^2. The load of the circulating current was about 700 ohms. It is seen that the gain has a maximum at a value of 500 in the neighbourhood of 50 kv. At higher current densities the gain is lower.

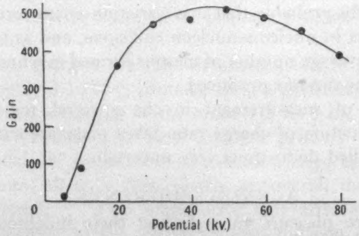

At low voltages the gain rises rapidly with voltage, thus appearing to be proportional to the number of ion pairs produced in the selenium. The maximum may be understood on the basis that the sensitive region of the cell is near the surface : with increasing voltage the electrons penetrate to greater depths, and the number of ion-pairs formed in the sensitive region decreases.

On copper oxide cells, an effect was observed only after the oxide layer had been reduced in thickness by grinding and re-metallized by evaporated gold. Then a small gain was first observed at 60 kv.; at 90 kv. this had risen to about 150. The high threshold voltage confirms the view that the sensitive layer in copper oxide cells is situated at the oxide-copper boundary.

The experiments are being continued. They appear to have theoretical interest and they indicate a new way of measuring electron beams.

Birkbeck College Research Laboratories,
University of London.
16th January 1951.

W. Ehrenberg.
Chi-Shi Lang.
R. West.

Calculation of Oscillator Strengths for certain Electronic Transitions in B_2 and Na_2

In this Letter the oscillator strengths for certain molecular electronic transitions in B_2 and Na_2 are computed using the quantum mechanical one-electron approximation (see Bates 1949, Shull 1950, Stephenson 1951).

The constants of the transitions are given in Table 1 (see Herzberg 1950) where R(A.) represents the equilibrium internuclear distance in Ångström units and $R(a_0)$ the same distance in terms of the radius a_0 of the first Bohr orbit. The wavelengths appropriate to the electronic transitions are also given in Table 1.

Table 1

	Transition	λ_e (A.)	R (A.)	$R(a_0)$
B_2	${}^3\Sigma_g^- - {}^3\Sigma_u^-$	3271	1·589	3·00
Na_2	${}^1\Sigma_g^+ - {}^1\Sigma_u^+$	6812	3·078	5·83

Expressing these transitions in the form of molecular orbitals (Mulliken 1932, 1939), it is found that the boron transition reduces to the form $(\sigma_u 2s)-(\sigma_g 2p)$ and the sodium transition to $(\sigma_u 3s)-(\sigma_g 3p)$. The wave functions of these reduced transitions may be written as suitable linear combinations of the atomic wave functions in the usual way. Table 2 gives the values of the appropriate integrals (as given by Stephenson 1951). These integrals were evaluated using Slater type atomic wave functions with an effective nuclear charge Z and principal quantum number n^* (see Slater 1930).

Table 2

$n^*=3;\ Z=2{\cdot}02_5$		$n^*=2;\ Z=2{\cdot}42_5$	
Na_2 ${}^1\Sigma_g^+ - {}^1\Sigma_u^+$		B_2 ${}^3\Sigma_g^- - {}^3\Sigma^-$	
P(3, 0, 0; 3, 1, 0)	2·99	P(2, 0, 0; 2, 1, 0)	1·19
T(3, 0, 0; 3, 1, 0)	2·26	T(2, 0, 0; 2, 1, 0)	0·48
S(3, 0, 0)	0·46	S(2, 0, 0)	0·52
S(3, 1, 0)	−0·15	S(2, 1, 0)	−0·28

Making use of the expression for the dipole moment factor D

$$D=\frac{[\mathrm{P}(n,0,0;\ n,1,0)-\mathrm{T}(n,0,0;\ n,1,0)]^2}{[1-\mathrm{S}(n,0,0)][1-\mathrm{S}(n,1,0)]}$$

and the relation $f=304D/\lambda_e$, where f is the oscillator strength and λ_e the wavelength in A., we finally obtain the following results.

Table 3

	Transition	λ_e (A.)	D	f	Lifetime (sec.)
† Na_2	${}^1\Sigma^+ - {}^1\Sigma_u^+$	6812	0·87	0·039	$1{\cdot}8\times10^{-7}$
B_2	${}^3\Sigma_g^- - {}^3\Sigma_u^-$	3271	0·83	0·077	$2{\cdot}1\times10^{-8}$

† The value given by Stephenson, *Nature*, 1950, **166,** 191, is in error owing to the use of an inaccurate value for the internuclear distance.

It is to be noted that in these calculations hybridization of the states has been neglected.

Department of Physics,
Imperial College, London S.W.7.
24th January 1951.

G. Stephenson.

Bates, D. R., 1949, *Proc. Roy. Soc.* A, **196,** 586.
Herzberg, G., 1950, *Molecular Spectra and Molecular Structure*, Vol. I (New York: Van Nostrand).
Mulliken, R. S., 1932, *Rev. Mod. Phys.*, **4,** 1; 1939, *J. Chem. Phys.*, **7,** 20.
Shull, H., 1950, *Astrophys. J.*, **112,** 352.
Slater, J. C., 1930, *Phys. Rev.*, **36,** 57.
Stephenson, G., 1951, *Proc. Phys. Soc.* A, **64,** 99.

On the Elimination of Divergencies from Quantum Electrodynamics

It has now been well established that all divergencies in any arbitrary process in quantum electrodynamics may be reduced to three quantities : the self-energy of the electron, the self-charge of the electron, and the self-energy of the photon. According to Schwinger (1949) and Tomonaga (Fukuda, Miyamoto, and Tomonaga 1949) the self-energy and the self-charge of the electron may be removed by a renormalization of the mass and the charge of the electron, while, following Schwinger (1949), the self-energy of the photon may be taken as zero on account of the gauge invariance of electrodynamics. Further, it has been shown by Dyson (1949) that this procedure can be applied to the collision problems in any approximation. Thus, the work of Tomonaga, Schwinger, Dyson and others has produced a scheme by which all divergencies in quantum electrodynamics may be removed, and a finite result obtained for any physical process. In this way it has also been found possible to give a satisfactory explanation for the observed hydrogen-line shift and the anomalous magnetic moment of the electron.

The aim of the present note is to show that the above programme may also be carried out in a somewhat different way, which involves a more symmetrical treatment of the matter and the radiation fields. We choose the Lagrangian density for an electrodynamic system as

$$L=L_{\mathrm{E}}+L_{\mathrm{P}}+L'+L_1+L_2, \qquad \ldots\ldots(1)$$

where L_{E} and L_{P} are the usual Lagrangian densities for the uncoupled electron and radiation fields respectively, L' is the interaction term given by $L'=A_\mu j_\mu$, and L_1 and L_2 are Lorentz-invariant counter-terms given by

$$L_1=\delta m\overline{\psi}\eta\psi, \qquad L_2=\tfrac{1}{4}\delta f F_{\mu\nu}{}^2, \qquad \ldots\ldots(2)$$

the constants δm and δf to be determined by an investigation of the self-energy of the electron and the polarization of vacuum. After obtaining the Hamiltonian density from (1) in the usual way, and passing over to the interaction representation by transforming away the parts belonging to the uncoupled electron and radiation fields, we obtain for the Hamiltonian density in the 'natural' coordinate system :

$$\begin{aligned}H&=-A_\mu j_\mu-\delta m\overline{\psi}\eta\psi-\tfrac{1}{4}\delta f F_{\mu\nu}{}^2-\frac{(\delta f)^2}{2(1-\delta f)}F_{4i}{}^2\\ &=-A_\mu j_\mu-\delta m\overline{\psi}\eta\psi-\tfrac{1}{4}\delta f F_{\mu\nu}{}^2-\tfrac{1}{2}\{(\delta f)^2+(\delta f)^3+\ldots.\}F_{4i}{}^2. \qquad \ldots\ldots(3)\end{aligned}$$

For practical purposes, it is most convenient to use the Feynman–Dyson form of the invariant perturbation theory, and it can be shown by an argument due to Matthews (1949) that instead of (3) we can take the Hamiltonian density in the interaction representations as

$$H=-A_\mu j_\mu-\delta m\overline{\psi}\eta\psi-\tfrac{1}{4}\delta f F_{\mu\nu}{}^2, \qquad \ldots\ldots(4)$$

provided we always take effectively

$$\left\langle P\left(\frac{\partial A_\nu(x)}{\partial x_\mu}, \frac{\partial A_\varrho(x')}{\partial x_\lambda'}\right)\right\rangle_0=\frac{\partial^2}{\partial x_\mu\partial x_\lambda'}\langle P(A_\nu(x), A_\varrho(x'))\rangle_0. \qquad \ldots\ldots(5)$$

In order to prove that the present approach will remove all divergencies from the S-matrix in quantum electrodynamics, we can follow the treatment of Dyson (1949) with the only difference that the factor Z_3 should now be put equal to unity, for the contribution of the last term in (4) for a photon of momentum k_μ is given by

$$-\delta f A_\mu(-k)[\delta_{\mu\nu}k^2-k_\mu k_\nu]A_\nu(k), \qquad \ldots\ldots(6)$$

which cancels the entire divergency in the 'photon self-energy part' after the requirements of gauge invariance have been satisfied. Moreover, since the contribution of Z_1 is cancelled by that of Z_2 (Ward 1950), *no charge renormalization is necessary in the present treatment.*

In conclusion, we add a few remarks about the correspondence in the elimination of divergencies from classical and quantum electrodynamics. It is well known that in order to carry out a mass renormalization, it is necessary to show that the self-energy W of an electron with momentum $\mathbf{p}$ can be expressed in the form

$$W=\delta m\{m/(m^2+p^2)^{1/2}\}, \qquad \ldots\ldots(7)$$

where δm is a Lorentz-invariant quantity. Since it does not seem possible to express the classical self-energy of the electron in the form (7), a mass renormalization may not be possible in classical electrodynamics. However, this does not matter, for the mass renormalization may not be taken too literally, but we may regard this procedure simply as a covariant subtraction of the *physically meaningless* self-energy of an isolated electron. It can then be shown that a covariant subtraction of the self-energy of the electron is also possible in classical electrodynamics by means of a suitable counter-term (Gupta 1951).

I would like to express my thanks to Dr. N. Kemmer and Mr. A. Salam for helpful discussions.

Cavendish Laboratory,
Cambridge.
22nd January 1951.

SURAJ N. GUPTA.*

* State Scholar of the Government of India.

DYSON, F. J., 1949, *Phys. Rev.*, **75**, 1736.
FUKUDA, H., MIYAMOTO, Y., and TOMONAGA, S., 1949, *Progr. Theor. Phys.*, **4**, 47, 121.
GUPTA, S. N., 1951, *Proc. Phys. Soc.* A, **64**, 50.
MATTHEWS, P. T., 1949, *Phys. Rev.*, **76**, 684.
SCHWINGER, J., 1949, *Phys. Rev.*, **75**, 651, **76**, 790.
WARD, J. C., 1950, *Phys. Rev.*, **78**, 182.

On the Elimination of Divergencies from Classical Electrodynamics

In a recent paper with the above title Gupta (1951) obtains for the force density at the world-line of the rth electron in an assembly of n electrons the expression

$$k'^{(r)}_{\mu} = [(F_{\mu\nu} - f^{(r)}_{\mu\nu,\,\mathrm{sym}}) j'^{(r)}_{\nu}]/c, \qquad \ldots\ldots (1)$$

where $F_{\mu\nu}$ is the sum of the retarded fields of all the electrons (including the rth), $f^{(r)}_{\mu\nu,\,\mathrm{sym}}$ is the mean of the retarded and advanced fields of the rth electron, and $\mathbf{j}^{(r)}$ is the current density due to the rth electron, all quantities being evaluated at the world-line of the rth electron. From (1) Gupta derives an equation of motion for the electron which, he observes, is just that obtained by Dirac (1938).

This note is to point out that the equivalence with Dirac's theory can be seen directly from (1), without actually deriving the equation of motion. To do this we write $F_{\mu\nu}$ as $f^{(r)}_{\mu\nu,\,\mathrm{ret}} + \sum_{s \neq r} f^{(s)}_{\mu\nu,\,\mathrm{ret}}$ and $f^{(r)}_{\mu\nu,\,\mathrm{sym}}$ as $\frac{1}{2} f^{(r)}_{\mu\nu,\,\mathrm{ret}} + \frac{1}{2} f^{(r)}_{\mu\nu,\,\mathrm{adv}}$. Substitution in (1) then gives immediately

$$k'^{(r)}_{\mu} = \frac{1}{c}\left\{\tfrac{1}{2}(f^{(r)}_{\mu\nu,\,\mathrm{ret}} - f^{(r)}_{\mu\nu,\,\mathrm{adv}}) + \sum_{s \neq r} f^{(s)}_{\mu\nu,\,\mathrm{ret}}\right\} j'^{(r)}_{\nu}. \qquad \ldots\ldots (2)$$

The first term in the braces is recognizable as the Dirac self-field of the rth electron, and the second is the sum of the retarded fields of all the other electrons at the world-line of the rth electron; in other words (2) is exactly the force density at the world-line given by Dirac's theory. This argument is unaffected by the inclusion in $F_{\mu\nu}$ of an arbitrary external field which Gupta denotes by $f_{\mu\nu,\,\mathrm{ex}}$ and which for simplicity has here been taken as zero.

The procedure of substracting out the symmetrical field (which diverges quadratically at the world-line of the electron) to obtain a finite self-field is not of course limited to Dirac's theory. Eliezer (1947) has reviewed a number of theories which retain this feature, while modifying the self-field in the attempt to obtain an equation of motion for the electron which does not give the non-physical behaviour of Dirac's equation. However, Gupta's choice of the form of $F_{\mu\nu}$ ensures that his formulation corresponds unambiguously with Dirac's theory; for in the alternative theories the force exerted by an electron on other charges in its field would be determined by a mixture of its retarded and advanced fields. Gupta's view that this force must not involve the advanced field, since the latter cannot be a measurable quantity, leads immediately to his adoption of the Lorentz–Dirac field tensor for $F_{\mu\nu}$.

School of Theoretical Physics,
Dublin Institute for Advanced Studies.
5th February 1951.

J. W. GARDNER.

DIRAC, P. A. M., 1938, *Proc. Roy, Soc.* A, **167**, 148.
ELIEZER, C. J., 1947, *Rev. Mod. Phys.*, **19**, 147.
GUPTA, S. N., 1951, *Proc. Phys. Soc.* A, **64**, 50.

Radioactive ^{159}Dy

In an earlier paper (Butement 1950) the preparation of a long-lived radioactive ^{159}Dy was mentioned. This letter describes a detailed investigation of this isotope.

The stable isotopes of dysprosium are given in the Table (Inghram, Hayden and Hess 1949):

Mass number	156	158	160	161	162	163	164
Abundance (%)	0·0524	0·0902	2·294	18·88	25·53	24·97	28·18

The shorter-lived activities produced by neutron capture are 140-minute ^{165}Dy and, by capture of a second neutron by this isotope, some 82-hour ^{166}Dy.

A sample of 10 mg. of dysprosium oxide was irradiated in a neutron flux of 10^{12} cm^{-2}sec^{-1} for 20 days and the dysprosium purified by means of an ion-exchange resin column. After waiting 60 days for complete decay of the ^{166}Dy, the decay of the long-lived activity was followed for 400 days, and showed a half-life of 132 days (see Figure).

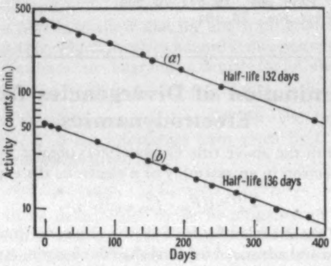

Decay of ^{159}Dy (*a*) from pile irradiated dysprosium, and (*b*) from deuteron irradiated terbium.

A sample of 14 mg. of very pure terbium oxide was given 70 microampere-hours irradiation with 9 Mev. deuterons, and the ^{159}Dy produced by the reaction ^{159}Tb (d, 2n) isolated by the ion-exchange method. Its activity decayed with a half-life of 136 days (see Figure).

Both the above dysprosium samples emitted only electromagnetic radiations with energies (determined by absorption measurements in copper and aluminium) of 6·6 and 44 kev., corresponding to the L and K x-rays of terbium. Positron emission, if any, was less than one per thousand disintegrations. It is concluded that the only long-lived product of neutron capture by dysprosium is ^{159}Dy. Ketelle (1949) has independently found that neutron irradiation of dysprosium gives a 140-day activity, which is evidently this isotope.

The author thanks Mr. R. L. Evans for assistance with the counting, and Professor J. Rotblat for arranging the cyclotron irradiation.

Atomic Energy Research Establishment,
Harwell, Didcot, Berks.
23rd January 1951.

F. D. S. Butement.

Butement, F. D. S., 1950, *Proc. Phys. Soc.* A, **63**, 532.
Inghram, M. G., Hayden, R. J., and Hess, D. C., 1949, *Phys. Rev.*, **75**, 693.
Ketelle, B. H., 1949, *Phys. Rev.*, **76**, 1256.

Isotope Effect in Hydrocarbon Flame Bands

Though there have been reasonable grounds to believe that the hydrocarbon flame bands have to be attributed to HCO, there has been so far no direct proof. An attempt has now been made to determine the emitter by utilizing isotope effect through deuterium substitution. The source used for obtaining the isotope shifts was the glow of deutero-acetylene interacting with atomic oxygen at a pressure of 3 mm. Hg.

In the original analysis (Vaidya 1939) the hydrocarbon flame bands were divided into three groups, A, B, A′, A″. The A group contained most of the bands, while the B bands appeared under special circumstances. The v', v'' numbering of the A bands was provisional. The stronger bands belonged to $v'=0$ and $v'=1$ progressions.

In Table 1 are shown the isotopic bands and the shifts. From the order of diminution of the shifts, the position which would be occupied by the (0,0) band was determined.

An independent check on the location of the (0,0) band was made by giving longer exposures in order to determine the extent of the spectrum in the ultra-violet. This resulted in better photographs of the spectrum near λ2550 and from a careful examination of the spectrum it was concluded that the (0, 0) band was missing. That the system did not extend farther was also concluded from the absence of the band which was expected to appear at $v'=2$ and $v''=0$ on the Condon intensity parabola.

Thus, by fixing the position of the (0, 0) band, the vibrational constants of the A system could be determined. The A bands are represented by the formula

$$\nu=39849+[1075(v'+\tfrac{1}{2})-6(v'+\tfrac{1}{2})^2]-[1883(v''+\tfrac{1}{2})-9{\cdot}4(v''+\tfrac{1}{2})^2].$$

The isotopic bands can be represented by

$$\nu^{1}=39843+[1062(v'+\tfrac{1}{2})-5{\cdot}7(v'+\tfrac{1}{2})^2]-[1855(v''+\tfrac{1}{2})^2-8{\cdot}7(v''+\tfrac{1}{2})^2].$$

There were two sets of extra bands which did not belong to the main A system; they were denoted B bands and A′, A″ bands. By locating shifts corresponding to these it has been possible to understand their significance. Unfortunately, owing to overlapping, observations were possible on only a few of them. The isotopic bands of these two sets are shown in Table 2.

Table 1

Ordinary (cm^{-1})	Isotopic (cm^{-1})	Shifts (cm^{-1})	Old (v', v'')	New (v', v'')
ν 39476			0, 3	0, 0 missing
37600	37630	30	0, 4	0, 1
35741	35793	52	0, 5	0, 2
33909	33978	71	0, 6	0, 3
*	*	*		
30302	30423	121	0, 8	0, 5
28541	28682	141	0, 9	0, 6
26798	26955	157	0, 10	0, 7
25071	25249	178	0, 11	0, 8

Table 2

B bands			Associated A bands		
Ordinary (cm^{-1})	Isotopic (cm^{-1})	Shift (cm^{-1})	Normal (cm^{-1})	Isotopic (cm^{-1})	Shift (cm^{-1})
ν 29762	29892	130	29500	29734	134
26290	26447	157	26137	26298	161

A′, A″ bands

	Ordinary (cm^{-1})	Isotopic (cm^{-1})	Shift (cm^{-1})
A′	ν 36333	36420	87
A″	27498	27764	266

The near equality of the shifts of the B bands and the associated A bands suggests that the B bands are the R heads. The shifts of the A′ and A″ bands are, however, much larger than for the A bands in the same region.

In extending the spectrum in the ultra-violet a set of new bands appeared which have been interpreted as being due to the bending frequency of the emitter. Their wavelength and the quantum numbers are given below.

The small change in the vibrational frequency of the A band system suggests that though H is present in the emitter, the vibration which gives rise to the hydrocarbon flame bands is such that H is not directly taking part in it. As regards the likely nature of the other vibration concerned in the emission of the band system, the recent experiments of Dyne and Style (1947), where they obtained the A bands by fluorescent excitation of formaldehyde, suggest that the vibrator must be C=O. Thus, the emitter has to be HC=O. The other combination C—OH is very unlikely since the vibrational frequency of single bond C—O is very much smaller.

The discovery of bands corresponding to the bending frequency whose value is of the right order, assuming that the emitter is HCO, also supports the assignment to this emitter.

Table 3

		Quantum numbers					
λ	ν	v_1'	v_2'	v_3'	v_1''	v_2''	v_3''
2420·5(1)	41301	2	1	0	0	1	0
2436·5(2)	41030	2	2	0	0	2	0
2447·8(1)	40841	2	0	0	0	1	0
2463·8(1)	40575	2	1	0	0	2	0
2480·0(1)	40310	2	2	0	0	3	0

In an ordinary diatomic molecular spectrum, one can calculate the mass factor $(\rho-1)$ from the isotope effect and this enables the reduced mass of the emitter to be determined. A similar calculation has been made assuming that HC moves as a unit against O; this gives $(\rho-1)=-0{\cdot}015$, using ground frequencies while theoretically it is $-0{\cdot}0198$.

Further details will be published in due course.

National Physical Laboratory,
New Delhi, India.
17th January 1951.

W. M. Vaidya.

Dyne, P. S., and Style, D. W. G., 1947, *Disc. Faraday Soc.*, **2**, 159.
Vaidya, W. M., 1934, *Proc. Roy. Soc.* A, **147**, 513.

Emission Band of the Cd_2 Molecule at $\lambda 2212$

Certain diffuse bands and continua in the visible and near ultra-violet regions, ascribed to the Cd_2 molecule, have been variously observed in emission, absorption and fluorescence by a number of workers. Relevant data have been summarized by Cram (1934), who made new observations and interpreted the collated material in terms of the potential energy curves to be expected when account is taken of van der Waals interactions. It is worth mentioning that Cram acknowledges that he has taken the general form of the potential energy curves from theoretical predictions of Van Vleck, to appear in a later paper of the latter; the paper concerned is by King and Van Vleck (1939), and in it Cram's work is cited as lending support to the theory.

Important features of Cram's interpretation depend on the behaviour of a diffuse band at about $\lambda 2212$. This band had been observed to occur readily in absorption by several workers, notably Mohler and Moore (1927) and Winans (1929). An emission band having the same location was reported by Robertson (1932) as present when cadmium vapour at low pressure was excited in a ring discharge. Both Winans (1929) and Cram (1934) reported the absence of the band in emission, using Tesla coil excitation. Cram considers Robertson's band as probably due to an impurity. It is obvious that in interpreting a spectrum of this kind importance attaches to the case of a band appearing strongly in absorption but absent in emission.

Recently, plates exposed by members of an undergraduate class at Imperial College were being examined. On a picture of the spectrum of the cadmium arc in air, obtained on an Ilford Q/1 plate with the Hilger medium quartz spectrograph, there was noticed a prominent diffuse emission feature in the 2200 A. region. Investigation has shown this band to be centred on 2212 A., and subsequent exposures have proved that it appears regularly. On the reproduction of a typical plate, here shown, the λ2212 emission band is plainly visible at X. The strongly reversed singlet resonance line at λ2288 can also be seen with its associated continuous emission band. The λ2212 band is unmistakably separated from the latter. There seems little doubt that it is identical with Robertson's band. Examination of the plate shows impurity lines to be few and weak, the strongest being the Cu doublet $\lambda\lambda$3274, 3247, and a few feeble Pb lines.

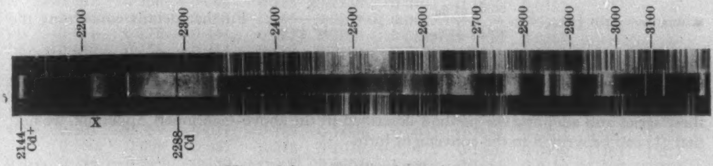

Ultra-violet spectrum of cadmium arc.

That the λ2212 band has not been previously reported in these conditions is perhaps in part due to the relatively infrequent use of Ilford Q emulsions with medium-quartz spectrographs. The failure of Cram to observe the band in emission may be partly due to the fact that he was working at high vapour pressures, at which it is apparent in Robertson's pictures that the band had disappeared, possibly either through change in excitation conditions or re-absorption in the vapour, or both.

It thus appears that the λ2212 emission band is readily excited in emission in cadmium vapour, and Cram's interpretations need reconsideration, perhaps in the light of further experiments.

Department of Astrophysics,
Imperial College, London S.W.7.
9th February 1951.

W. R. S. Garton

Cram, S. W., 1934, *Phys. Rev.*, **46**, 205.
King, G. W., and Van Vleck, J. H., 1939, *Phys. Rev.*, **55**, 1165.
Mohler, F. L., and Moore, H. R., 1927, *J. Opt. Soc. Amer.*, **15**, 74.
Robertson, J. K., 1932, *Phil. Mag.*, **14**, 795.
Winans, J. G., 1929, *Phil. Mag.*, **7**, 555.

Free Energy of the Double Layers of Two Plates at Large Separations

In a recent paper (Levine and Suddaby 1951) we developed an expansion for the interaction of the electric double layers of two parallel (colloidal) plates at large separations, when immersed in an electrolyte of the binary symmetrical type. In this note we shall obtain the next term in this expansion. Although the derivation of this term is very laborious, the final result is not complicated, and is suitable for numerical computations. Let R be the separation of the plates, n the density of positive (or negative) ions in the interior of the electrolyte, v the valency of a positive ion, D the dielectric constant of the electrolyte (aqueous) medium, ϵ the electronic charge, $\boldsymbol{k}$ Boltzmann's constant, T the temperature, $\kappa^2=8\pi nv^2\epsilon^2/D\boldsymbol{k}T$ the Debye–Huckel parameter, ψ_{m} and ψ_0 the potentials at the median plane (between the plates) and at the plate surfaces respectively, $\eta_0=\epsilon\psi_0/\boldsymbol{k}T$, $\eta_{\mathrm{m}}=\epsilon\psi_{\mathrm{m}}/\boldsymbol{k}T$, $k=\exp(-v\eta_{\mathrm{m}})$ and $\sin\phi_0=k^{-1/2}\exp(-\frac{1}{2}v\eta_0)$. Then the solution of the Poisson–Boltzmann equation yields the relation

$$\tfrac{1}{4}\kappa R=k^{1/2}\{F(k,\pi/2)-F(k,\phi_0)\}, \qquad \ldots\ldots(1)$$

where $F(k,\phi_0)$ is the elliptic integral of the first kind. The free energy $2F$ of the double layers is obtained from the force equation

$$2(dF/dR)=-n\boldsymbol{k}T(k+k^{-1}-2), \qquad \ldots\ldots(2)$$

assuming that the surface potential ψ_0 is independent of R.

We first expand $F(k, \phi_0)$ in a Taylor series about $k'^2=0$, where $k'^2=1-k^2$, namely

$$F(k, \phi_0)=-\tfrac{1}{2}\ln\gamma-\tfrac{1}{8}k'^2\ln\gamma+\frac{1}{128}(\delta-9\ln\gamma)k'^4$$
$$+\frac{5}{512}(\delta-5\ln\gamma)k'^6+\frac{1}{2(128)^2}(335\delta+6\mu-1225\ln\gamma)k'^8+\ldots, \qquad \ldots\ldots(3)$$

where $\gamma=\tanh\tfrac{1}{4}v\eta_0$, $\delta=\dfrac{\cosh\frac{1}{2}v\eta_0}{\sinh^2\frac{1}{2}v\eta_0}$ and $\mu=\dfrac{\delta}{\sinh^2\frac{1}{2}v\eta_0}$. Further details concerning the method of determining this power series in k'^2 are given in Appendix I of the earlier paper (Levine and Suddaby 1951). The corresponding expansion of $F(k, \pi/2)$ is given, for example, by Jahnke and Emde (*Tables of Functions*, 3rd edition, p. 73). Making use of these series and adopting the method described in the above-mentioned Appendix, we find that (1) can be written in the convenient form

$$k'^2=\chi\Psi(k'^2), \qquad \ldots\ldots(4)$$

where

$$\Psi(k'^2)=\exp\left[-\frac{1}{2}k'^2-\frac{1}{64}(13+2\ln 4\gamma^{1/2}+\delta)k'^4-\frac{1}{64}\left(\frac{43}{6}+2\ln 4\gamma^{1/2}+\delta\right)k'^6\right.$$
$$\left.-\frac{1}{(128)^2}\left(\frac{2341}{2}+462\ln 4\gamma^{1/2}+231\delta+6\mu\right)k'^8+\ldots\right],$$

an analytic function of k'^2, and

$$\chi=\chi_0\exp\left[\frac{1}{64}k'^4\left(1+k'^2+\frac{231}{256}k'^4+\ldots\right)\ln k'^2\right], \quad \chi_0=16\gamma\exp(-\tfrac{1}{2}\kappa R). \qquad \ldots\ldots(5)$$

The relation (4) can be inverted by Lagrange's theorem, so that k'^2 is obtained as a power series in χ. Substituting this latter series into (5), we use the method of successive approximations to express χ as a series in χ_0. In this way we derive that

$$k'^2=\chi_0-\tfrac{1}{2}\chi_0^2+\frac{1}{128}(22-\kappa R-2\delta)\chi_0^3+\frac{1}{128}(-6+\kappa R+2\delta)\chi_0^4$$
$$+\frac{1}{2(128)^2}\{359+5(\kappa R)^2+(20\delta-135)\kappa R-270\delta+20\delta^2-12\mu\}\chi_0^5+\ldots \qquad \ldots\ldots(6)$$

Finally, we expand (2) as a power series in k'^2, substitute (6) for k'^2 and then integrate (2) with respect to R, obtaining for the interaction

$$V(R)=2F-2F_\infty=V_1(R)(1+\mathscr{C}_1+\mathscr{C}_2+\ldots), \qquad \ldots\ldots(7)$$

where*

$$V_1(R)=nkT\chi_0^2/4\kappa, \qquad \ldots\ldots(8)$$

$$\mathscr{C}_1=-\frac{1}{256}\chi_0^2(2\kappa R-3+4\delta), \qquad \ldots\ldots(9)$$

$$\mathscr{C}_2=\frac{1}{96\times 256}\chi_0^4\{3(\kappa R)^2+3\kappa R(4\delta-\tfrac{5}{2})+3-15\delta+12\delta^2-6\mu\}$$
$$=2\mathscr{C}_1^2-\frac{1}{128}\mathscr{C}_1\chi_0^2-\frac{\chi_0^4}{4(16)^3}(1+4\mu), \qquad \ldots\ldots(10)$$

and $2F_\infty$ is the free energy at infinite separation. We have checked the expression (10) for $\mathscr{C}_2$ by expanding $2F$ in a double series in powers of η_0^2 and $\exp(-\tfrac{1}{2}\kappa R)$ and comparing with the same double series which can be derived from the formula for $2F$ at moderate potentials, as given by Levine and Suddaby (1951). A different method of determining (7) will be published later.

In the Table, we compute the values of $\mathscr{C}_1$ and $\mathscr{C}_2$ for various $v\eta_0$ and κR and also the values of κR at which $\mathscr{C}_1=0$ and $\mathscr{C}_2=0$. (The equation $\mathscr{C}_2=0$ is quadratic in κR, but we need only consider the larger root.) For $\kappa R=2$ the three terms in (7) yield an accuracy of about 1 or 2% for all $v\eta_0$. When $v\eta_0\leqslant 5$, say, then we can still use (7) for values of κR as low as 1·5, the maximum error at $\kappa R=1{\cdot}5$ being about 4%. However, when $\kappa R=1{\cdot}0$,

---

* We wrote $\mathscr{C}_1$ as $\mathscr{C}(v\eta_0, \kappa R)$ in the earlier paper.

(7) only gives a qualitative answer, and for still smaller κR it is of little use. Indeed, the question of convergence arises at small κR. According to Verwey and Overbeek (1948), the region $\kappa R \geqslant 2$ is the important one in determining stability properties of colloids, and

	$\mathscr{C}_1$	$\mathscr{C}_2$	$\mathscr{C}_1$	$\mathscr{C}_2$	$-\mathscr{C}_1$	$\mathscr{C}_2$	$-\mathscr{C}_1$	$\mathscr{C}_2$	$\mathscr{C}_1=0$	$\mathscr{C}_2=0$
κR \ $v\eta_0$	0·5	0·5	1	1	1·5	1·5	2·0	2·0	κR	κR
0	−0·607	0·368	−0·368	0·135	0·2231	0·0498	0·1353	0·0183	—	—
0·5	−0·588	0·345	−0·362	0·135	0·2231	0·0527	0·1374	0·0206	—	—
1·0	−0·531	0·275	$-0{\cdot}344_5$	$0{\cdot}131_5$	0·2223	0·0603	0·1430	0·0268	—	—
1·5	−0·440	0·158	−0·314	0·117	0·2193	0·0683	0·1504	0·0356	—	—
2·0	−0·320	0·003	−0·273	0·087	0·2129	0·0721	0·1581	0·0449	—	0·488
2·5	−0·176	−0·171	−0·220	$0{\cdot}036_5$	$0{\cdot}2019_5$	0·0689	0·1641	0·0527	0·028	0·844
3·0	−0·018	−0·339	−0·160	−0·030	0·1868	0·0562	0·1679	0·0573	0·462	1·102
3·5	0·143	−0·477	−0·095	−0·106	0·1683	0·0355	0·1692	0·0584	0·739	1·293
4·0	0·301	−0·569	−0·031	−0·183	$0{\cdot}1480_5$	0·0093	0·1683	0·0563	0·928	$1{\cdot}456_5$
5·0	0·580	−0·609	0·087	−0·316	0·1076	−0·0472	0·1626	0·0460	1·165	1·671
6·0	0·794	−0·519	$0{\cdot}180_5$	$-0{\cdot}408_5$	$0{\cdot}0733_5$	−0·0966	0·1554	0·0334	1·299	1·801
7·0	0·945	−0·387	0·247	$-0{\cdot}464_5$	0·0479	−0·1330	$0{\cdot}1489_5$	0·0225	1·379	1·879
8·0	1·045	−0·266	0·292	−0·497	0·0304	−0·1576	0·1442	0·0146	1·427	1·927
9·0	1·109	−0·174	0·321	−0·515	0·0190	−0·1734	0·1410	0·0092	1·456	1·956
10·0	1·149	−0·111	0·339	−0·526	0·0117	−0·1833	0·1388	0·0057	1·473	1·973
∞	1·213	0	0·368	−0·541	0	−0·1991	0·1353	0	1·500	2·000

therefore series (7) should be quite useful. In a later paper we shall apply it when developing further the incorporation of the Stern theory of the double layer into a theory of interaction of colloidal plates (see Levine 1951).

Department of Mathematics,
The University, Manchester.
S. Levine.

Sir John Cass College, London.
A. Suddaby.

13th February 1951.

Levine, S., 1951, *J. Colloid Science*, in the press.
Levine, S., and Suddaby, A., 1951, *Proc. Phys. Soc.* A, **64**, 1.
Verwey, E. J. W., and Overbeek, J. Th. G., 1948, *Theory of the Stability of Lyophobic Colloids* (Amsterdam and New York : Elsevier), p. 129.

REVIEWS OF BOOKS

The Meaning of Relativity, by Albert Einstein. 4th Edition, containing an Appendix on the Generalized Theory of Gravitation. Pp. v + 145. (London : Methuen and Co., Ltd., 1950.) 7*s*. 6*d*.

This well-known book, originally published in 1922, is based on the text of Einstein's Stafford Little Lectures delivered at Princeton University in May 1921. In 1946 the author added an appendix ' On the " Cosmologic Problem " ' in which he reviewed advances since 1921, and in particular rejected the cosmological constant, which he had himself originally introduced in 1917. The present edition is noteworthy for a second appendix on the author's new generalization of General Relativity, and it is to this appendix which most readers will immediately turn when they obtain this edition. The translation of this appendix was made by Sonja Bargmann.

Newtonian physics was founded on the associated concepts of ' particle ' and ' action at a distance ', concepts which until recently were considered fully adequate for a theory of gravitational phenomena, although in order to explain electromagnetic phenomena Faraday and Maxwell introduced the ' field ' concept. Einstein, who has more than once paid tribute to the genius of Maxwell, has striven to extend the field concept so that it embraces both gravitation and electromagnetic phenomena in a ' unified field theory '. A first version was published by him in 1929, and this latest theory may be regarded as the fruit of thirty years' reflection by the most famous mathematical physicist of the century. For this reason alone, it must be read with respect even by the most critical.

At the outset a fundamental limitation of the new theory will strike most readers, for it is clear that in no sense is it a quantum theory. The most that the author sets out to achieve is a new unification of macroscopic phenomena. It is too soon to say whether any new experimentally verifiable effects will be predicted by the new theory. The General Theory of 1916, however, was much less fruitful in this respect than the Special Theory of 1905. Of the three famous tests of the General Theory only the first is now regarded as fully confirmed, and then strictly speaking only for a single planet. Despite the startling agreement with observation in the case of Mercury, the appeal of the General Theory is primarily epistemological and aesthetic. The derivation of a more accurate law of gravitation than that of Newton from axioms of 'minimum arbitrariness' was in itself a major intellectual achievement. That the whole of physics can likewise be contained in some such compact and 'epistemologically primitive' form is at best still a dream and some may think a mirage, but *any* extension of General Relativity which covers a wider class of phenomena without introducing more than the bare minimum of new arbitrariness would be full justification for the time which Einstein has devoted to the problem.

The core of General Relativity is comprised in the standard equation relating the tensor g_{ik}, which represents the metric properties of space–time, and the material–energy tensor T_{ik}. In this theory the tensor g_{ik} is symmetrical, and Einstein's new theory is his answer to the problem: to find a natural generalization of this tensor and an associated system of field equations which will be the most logically satisfactory generalization of the equations of pure gravitation, the only clue from experience being 'the vague perception that something like Maxwell's electromagnetic field has to be contained within the total field'.

The main steps in Einstein's answer to this problem may be summarized very briefly as follows. First, the symmetrical g_{ik} (ten components, corresponding to the gravitational field) is replaced by a general non-symmetrical g_{ik} with six additional components (corresponding to the electromagnetic field). It is then shown how an absolute differential calculus can be constructed for such a non-symmetrical field. The notion of affine parallel displacement is introduced into the new theory, and by means of it a general curvature tensor is defined and a contracted form R_{ik} obtained. The analysis gives rise to three Hermitian tensors which can be combined to form a new tensor U_{ik} with certain special properties. A variational principle $\delta\{\int g^{ik}U_{ik}\delta\tau\}=0$ is then shown to imply a system of equations (laws) 'of utmost simplicity', including $R_{ik}=0$, which may be regarded as 'the natural extension' of the equation $G_{ik}=0$ of (pure gravitational) General Relativity. In so far as the new laws can be compared to Maxwell's electrodynamics, they involve a special postulate which corresponds to the assertion that the magnetic current density vanishes, but they automatically imply 'conservation of electricity'. Although Einstein believes that his latest solution of the unified field theory problem is 'highly convincing', he admits that formidable mathematical difficulties will have to be overcome before it is possible to consider testing the theory experimentally. G. J. WHITROW.

Classical Mechanics, by HERBERT GOLDSTEIN. Pp. 399. (Cambridge, Mass.: Addison-Wesley Press Inc., 1950.) $6.50.

There has long been a need for a textbook of classical mechanics written with the needs of the physicist in mind. The book under review tulfils this need admirably.

The field covered is in the main the familiar one of the mechanics of particles and of rigid bodies, of the Lagrange and Hamiltonian equations. Particular attention is paid to the latter, three chapters being devoted to Hamiltonian equations, canonical transformations and Hamiltonian–Jacobi theory. What is to some extent a novel feature is a chapter on relativistic mechanics and on the Hamiltonian and Lagrangian formulations for continuous systems and for fields. Oscillations of a system are dealt with in some detail, including the transformation to principal axes, normal modes, and the calculation of eigenfrequencies.

Some acquaintance with vector algebra is assumed, but special sections are devoted to the explanation of the properties of tensors, dyadics and matrices, of which full use is made. The illustrative examples, both in the text and at the ends of chapters, are in the main chosen from physics instead of being, to quote a phrase of the author, "the usual pedantic museum pieces". For instance, the normal modes of a triatomic molecule are used to illustrate the theory of small oscillations, and the transformation to laboratory coordinates of the scattering cross section is discussed in connection with the theory of the collision of particles. An excellent set of references is included at the end of each chapter, with comments on these textbooks. This is a novel and rather intriguing feature. The comments are occasionally pungent—" a formidable treatise which often manages somehow to make the elegant simplicity of vector and tensor methods appear quite complicated and repellant ". As a contribution to this process of brightening scientific textbooks the reviewer would like to draw attention to a comment of Tawney (*Religion and the Rise of Capitalism*) on a mediaeval historical treatise—" a comprehensive but completely unreadable account of the subject".

The book is written in a pleasant style and is a pleasure to read. Occasionally the author tends to assume a surprising knowledge of theoretical physics on the part of the reader, though this usually occurs in ' asides ' or footnotes. Very few students will appreciate the point of the remark that the cross section for Coulomb scattering is infinite in quantum mechanics, nor, by the way, is the author correct in stating that " all fields that fall off faster than a Coulomb field produce a finite scattering cross section in quantum mechanics ".

There is hardly any need to add that all physicists are strongly recommended to lose no time in acquiring this textbook. M. BLACKMAN.

Practical Applications of Spectrum Analysis, by H. DINGLE. Pp. x+245. (London: Chapman and Hall, 1950.) 40*s*.

The main theme is qualitative chemical analysis using arc spectra. On the instrumental side the general principles of prismatic and grating spectrographs are given, and the various factors influencing dispersion, resolution and light-gathering power are discussed. Methods of taking comparison spectra and measuring photographic plates for the determination of wavelengths are dealt with. This is all quite elementary, and intended for readers without previous spectroscopic training. The principles underlying the excitation of spectra and the various factors influencing the strength of spectrum lines are similarly dealt with in an elementary way.

There are two chapters on qualitative analysis, mainly using arc spectra, in which much valuable information gained during thirty years of experience in this type of work at Imperial College, London, is included. This is the most valuable part of the book. The most sensitive lines of the various elements are considered in detail, and especially the influence of other possible constituents in masking or interfering with the sensitive lines. It is stressed that lines of the same multiplet usually vary in strength in a similar way, and the various multiplets among the sensitive lines are grouped so that they may be picked out for study together. The need for careful criticism of results before final acceptance is stressed. In Professor Dingle's words, " It is no exaggeration to say that in my experience more than half of the spectrographic analyses which have been published during the last thirty years are untrustworthy ". Application of the principles and detailed information supplied here should help to prevent a continuation of such a state of affairs.

One brief chapter is devoted to quantitative work, mostly using the Foster arc. Professor Dingle appears to think that this small amount of space given to quantitative work reflects the present state of achievement in this field. There will probably be many who will differ from him.

The book contains useful tabular matter on the sensitive lines of the elements, on Burns wavelengths of iron arc lines, and wavelengths of lines from a *raies ultimes* mixture containing practically all the spectroscopically sensitive elements except rare earths. There are several good plates, including a set of the spectrum of the *raies ultimes* mixture. The book is written in Professor Dingle's usual clear style, and is excellently produced, especially the plates; in some of the tables there is a little difficulty in following along the table from the line to its identification.

It should be clearly understood that this book does not give a comprehensive account of the subject. It is essentially a record of personal experience. No mention is made of recent developments in quantitative analysis elsewhere in this country, and in Germany and America. The new photoelectric methods using photon multipliers are not described, and subjects such as the quantitative estimation of vitamins by absorption spectra are omitted. One may even doubt whether the title has been well chosen, for it is not the applications at all but a single method, that of the arc, which is the theme. However, within these limits the book does give a new approach to the subject, and includes so much valuable experience that it may be recommended. A. G. G.

An Introduction to Luminescence of Solids, by H. W. LEVERENZ. Pp. xv+569. 1st Edition. (New York: John Wiley and Sons; London: Chapman and Hall, 1950.) 96*s*.

This book is published in the 'Structure of Matter' series, and the author's intention is to provide "an orderly introduction to a growing field" for scientists of other interests. He also attempts to systematize the terminology of the subject and to provide a general coordination of luminescence phenomena, using specific materials as examples. The book begins with two introductory chapters, the first of which covers the elementary concepts of modern physics but includes rather irrelevant topics, such as Dirac's theory of positrons and pair production. Chapter II is more useful as it provides an introduction to the crystalline state with some specific reference to the crystal structure of typical luminescent solids. Chapter III is concerned with syntheses of well-known types of phosphors and the system of notation for defining the final products. Chapter IV discusses phosphor constitution, crystal structure, impurity activators and the electronic energy states of phosphors; it includes a very brief discussion of photoconductivity.

Chapter V consists of more than two hundred text pages and covers all the physical phenomena encountered in the study of luminescence in solids. The space given to each topic is rather inadequate, and better treatment of such important aspects of the subject might have been possible by affording them the space occupied elsewhere in the text by more speculative discussions. It will be difficult for those 'not skilled in the art' to distinguish the processes of luminescence treated in this chapter with respect to their relative importance, as the author's style is not very lucid. The next chapter provides a summary of phosphor characteristics, or, as the author terms it, 'a capsulized description of phosphors', while the last chapter is concerned with the various applications of phosphors. Five appendices and a glossary of symbols follow. Only the first appendix, dealing with the preparation of pure zinc and cadmium sulphides and selenides, and the third, giving useful conversion factors for photometric units, appear to be of definite usefulness. Some six hundred text references and a supplementary list of references to very recent publications are given which, apart from one or two important omissions, provide a valuable guide to the literature of luminescence since the titles of individual papers are included. The book concludes with adequate formulae, author and subject indexes.

Taken as a whole, the book contains a large amount of information on phosphors, particularly those of commercial interest, but its arrangement does not appear to be the best that could have been chosen. The reader may well object to the many cumbersome phrases suggestive of the jargon of luminescence laboratories but not helpful to the average scientific worker. Such phrases as 'consciously added activator', 'difficultly eradicable complex absorptions' and 'energy *transmittal* in solids' may be included with the above. For the industrial scientist the book may be of considerable interest as it represents the contribution of a recognized worker in applications of luminescence who has set very high standards of purity and control in the production, and faithful reproduction, of phosphors of high quality to meet the stringent demands of commercial users. G. F. J. GARLICK.

Photons and Electrons, by K. H. SPRING. Pp. 108. 1st Edition. (London: Methuen and Co., Ltd., 1950.) 7*s*. 6*d*.

This monograph gives a simple account of the theoretical results which have been obtained for the main high energy processes involving photons and electrons, viz. the photoelectric effect, Compton scattering, bremsstrahlung, and pair production. The theoretical cross sections are in every case compared with the experimental values, and particular emphasis is placed on the angular distributions of the various outgoing particles. The last chapter contains an elementary account of the results of the cascade theory of the soft component of cosmic radiation, including a discussion on the lateral spread of the showers.

The discussion of the physical ideas is restricted to brief accounts of the radiation emitted by an accelerated (classical) electron, Einstein's explanation of the photoelectric effect, Compton's theory of scattering, and the Dirac 'hole' theory. The mathematical development of these ideas is avoided, and there is no attempt to introduce the concepts of a quantized field theory. It is perhaps a pity that the idea of a collision parameter is not used in discussing the effect of atomic shielding in the bremsstrahlung process.

The variation of the cross sections with energy and angle is fully illustrated, and there are useful tables of data. The book should be of considerable value in presenting the results of quantum-electrodynamics to those who are not specialists in theory, or in cosmic-ray work.

It is regrettable that in a monograph which is intended for a wide public many errors in the formulae have escaped the proof reader. In some instances, also, economy of words has been carried too far. For example, on page 95 the Rutherford scattering formula is given, without any reference to the fact that the scattering potential is of the Coulomb type. The use of the word ' gaussianly ' (page 97) could have been avoided.

J. HAMILTON.

Faraday's Discovery of Electromagnetic Induction, by THOMAS MARTIN. Pp. 160. (London : Edward Arnold & Co., 1949.) 9*s*.

As is well known, Faraday kept a detailed diary covering his years of mature research at the Royal Institution, that is, from 1820 to 1862. This was first published at intervals between 1932 and 1936, edited by Thomas Martin from the manuscript in the possession of the Royal Institution. So voluminous a work—it is in seven volumes—is, however, accessible to comparatively few, so that all who are interested in Faraday's work and in the early history of electromagnetism will welcome the appearance of Mr. Martin's new book.

Faraday's published papers and the *Experimental Researches in Electricity* give in a masterly manner the results of his researches ; but the steps by which he was led to his epoch-making discoveries, the little revealing touches that show how his mind was working, these are to be found only in the Diary itself. Mr. Martin, by a judicious choice of extracts, has succeeded in conveying much of the charm and intimacy of the Diary. His book is not, however, merely an abridged version of the relevant portions of the larger work, but gives a connected account of the early history of electromagnetism from the announcement in 1820 of Oersted's discovery to the conclusion of Faraday's electromagnetic researches in the spring of 1832, the period covered by the first volume of the Diary in its printed form.

A brief survey of the main developments in electricity arising out of Galvani's discovery provides the historical setting for Faraday's work. This is followed by an account of Faraday's own early experiments in electricity—those on electromagnetic rotations, made in the latter part of 1821. After the successful conclusion of these experiments ten years elapsed before Faraday was again free to give his full attention to electricity, though scattered references in the Diary show how his thoughts dwelt on the subject. Then, between the end of August 1831 and the beginning of March, 1832, came that amazing series of experiments and observations ' which may be said to constitute the discovery of electromagnetic induction '. Mr. Martin, in describing these researches, makes frequent use of Faraday's own words ; the diagrams are, with few exceptions, reproductions of Faraday's freehand sketches. At the same time much is to be found here that is not to be found in the Diary itself. For instance, we read (p. 59) that the art of covering copper wire with silk or cotton was apparently a monopoly in the hands of the opticians, who charged exorbitant prices ; that experimenters were advised to take their own copper wire to a bonnet-wire coverer living in Spitalfields, who worked at much lower rates; iron wire could be obtained cotton-covered and was probably bonnet-wire used for stiffening ladies' bonnets.

We have nothing but praise for this modest little volume, and hope that Mr. Martin will deal in a similar manner with other aspects of Faraday's work.

N. H. DE V. HEATHCOTE.

CONTENTS FOR SECTION B

PAGE
Dr. W. D. Wright. The Role of Convergence in Stereoscopic Vision . . . 289
Mr. D. C. Pack and Dr. W. M. Evans. Penetration by High-Velocity (' Munroe ') Jets : I 298
Dr. W. M. Evans and Mr. D. C. Pack. Penetration by High-Velocity (' Munroe ') Jets : II 303
Dr. F. F. Evison. An Electromechanical Source of Elastic Waves in the Ground . 311
Dr. R. Bechmann. Contour Modes of Square Plates excited Piezoelectrically and Determination of Elastic and Piezoelectric Coefficients 323
Dr. F. E. Hoare and Mr. J. C. Walling. An Absolute Measurement of the Susceptibility of Tantalum and other Metals 337
Dr. E. Billig. Thermal Instability of Contact Rectifiers : The Effect of the Constituent Materials on the Efficiency of a Rectifying Junction . . . 342
Dr. P. C. Thonemann and Mr. W. T. Cowhig. The Role of the Self Magnetic Field in High Current Gas Discharges 345
Mr. H. Edels. The Relationship between the Radial Concentration Variations of excited Atoms and Electrons in a Discharge in Thermal Equilibrium . . 354

Letters to the Editor :

Dr. R. H. Kay. The Interpretation of Radiosonde Data in Relation to Cosmic-Ray Intensity Variation 359
Mr. H. A. Gebbie and Mr. E. W. Saker. Properties of Amorphous Selenium in the Infra-Red 360
Dr. E. Billig and Dr. K. W. Plessner. A Note on the Dielectric Dispersion in Polycrystalline Materials 361
Prof. E. N. da C. Andrade and Dr. A. J. Kennedy. A Surface Effect in the Creep Behaviour of Polycrystalline Lead 363
Contents for Section A 366
Abstracts for Section A 367

ABSTRACTS FOR SECTION B

The Role of Convergence in Stereoscopic Vision, by W. D. Wright.

ABSTRACT. An apparatus for testing stereoscopic acuity has been constructed in which the distance of a reference aperture P is compared with that of a test aperture Q selected from one of a tapering series of aperture plates. The apertures are seen as illuminated discs in a black field and all monocular aids to depth perception are eliminated. The observer has to state whether Q is in front or behind P, and the acuity is derived by plotting the percentage estimates against the distance of Q. Observations have been made for condition A, in which the observer is allowed to look first at P and then at Q, and for condition B, in which the observer fixates on P and views Q extra-foveally. From a comparison of the acuity for the two conditions for various angular separations θ between P and Q, deductions can be made about the relative contributions to stereoscopic vision of convergence and retinal disparity. The results suggest that convergence makes a significant contribution and has become the predominant factor at $\theta=20°$. For $\theta=14°$, the acuity for condition A is due entirely to convergence, since the blind spot interferes with the retinal disparity. Tests with flash exposures suggest that small eye movements do not play any important part in depth perception. The presence of depth perception under conditions of gross diplopia was confirmed, indicating that fusion is not an essential item for three-dimensional vision.

Penetration by High-Velocity ('Munroe') Jets: I, by D. C. Pack and W. M. Evans.

ABSTRACT. By means of certain simplifying assumptions a formula is developed for the penetration into a ductile target by a high-velocity (' Munroe ') jet. The action of the jet is divided into two stages, each making its contribution to the total penetration. In the first stage a hole is formed by the lateral compression of the target as the jet penetrates it; the second stage begins when the last particle of the jet has ceased to act, the hole continuing to deepen until the residual energy in the target has been spent. At the high pressures set up by a Munroe jet the strength of the target plays only a subsidiary part in the phenomenon.

Penetration by High-Velocity ('Munroe') Jets: II, by W. M. Evans and D. C. Pack.

ABSTRACT. Work is described in which the two stages of penetration by a high-velocity ('Munroe') jet were separated experimentally. The large penetrations measured in lead targets are shown to result from the flow which takes place in the metal after the jet itself has been consumed. For a given jet at a given stand-off it is possible to predict the penetration into a combination of targets from the results of a very small number of standard experiments. The method depends upon the calculation of a certain quantity which is constant for a given jet at a given stand-off, and examples are given of the determination of this quantity from experimental data.

An Electromechanical Source of Elastic Waves in the Ground, by F. F. Evison.

ABSTRACT. In order to extend the study and use of the elastic properties of geological bodies to include effects involving the amplitude and frequency of elastic radiation, a new source of energy is needed.

A large moving-coil transducer is described which, when attached rigidly to the rock, radiates sinusoidal vibrations of controllable amplitude, frequency and duration. The operation of the vibrator is analysed in detail by the method of electromechanical analogy.

For experiments in a chalk-mine, energy at each of the frequencies 300, 600 and 1,000 c/s. was radiated in the form of a square-enveloped pulse, of 20 msec. duration. Vibrations were detected in the rock by means of a piezoelectric microphone, amplifiers and an oscillograph, with an overall magnification of about 10^9. Oscillograms show the complex disturbances produced by the arrival of direct and reflected energy, at distances out to the limit of the mine at 450 ft. Measurements of amplitude at 130 ft. are used to examine the mechanism of the transfer of energy from the vibrator to the rock.

The power radiated was about 0·05 watt at 600 c/s., of which about one-sixth was in the compressional mode and five-sixths in the shear mode; but this power may readily be increased.

Contour Modes of Square Plates excited Piezoelectrically and Determination of Elastic and Piezoelectric Coefficients, by R. Bechmann.

ABSTRACT. The suitability of square plates, vibrating in contour modes, for the determination of piezoelectric coefficients is considered. Piezoelectric measurements on such plates provide checks for the theoretical solution of the various modes and in particular for the distribution of displacement. The recently published solutions for square plates form a basis for this work and the reliability of these solutions is discussed. The materials used were sodium chlorate, sodium bromate, quartz, ammonium dihydrogen phosphate and ethylene diamine tartrate (EDT). New determinations of the elastic and piezoelectric coefficients of these materials have been made, with the exception of EDT, the data for which were published in a previous paper.

An Absolute Measurement of the Susceptibility of Tantalum and other Metals, by F. E. Hoare and J. C. Walling.

ABSTRACT. The magnetic susceptibility of tantalum has been determined absolutely, the value obtained for the mass susceptibility being $\chi_{\mathrm{Ta}} \times 10^6 = 0{\cdot}8490 \pm 0{\cdot}0006$ at 20° c. Small specimens of tantalum have been used to determine, by a comparative method, the susceptibilities of specimens of platinum, palladium and rhodium at 20°c. The values obtained are : $\chi_{\mathrm{Pt}} \times 10^6 = 0{\cdot}9712 \pm 0{\cdot}0007$, $\chi_{\mathrm{Pd}} \times 10^6 = 5{\cdot}231 \pm 0{\cdot}004$, $\chi_{\mathrm{Rh}} \times 10^6 = 0{\cdot}9903 \pm 0{\cdot}0008$. All specimens were prepared from spectrographically standardized materials.

Thermal Instability of Contact Rectifiers: The Effect of the Constituent Materials on the Efficiency of a Rectifying Junction, by E. Billig.

ABSTRACT. If due allowance is made for the lowering by the image force of the height of the potential barrier in contact rectifiers, current–voltage characteristics can be calculated which are in good agreement with observed characteristics. On application of a voltage in the blocking direction, electrons (or holes) pass over the barrier owing to their thermal energy, the number of successful passes, i.e. the leakage current, being exponentially dependent on temperature. As the applied voltage is increased and the barrier lowered, the power loss corresponding to the increased leakage current will eventually raise the temperature in the thin barrier layer sufficiently to increase the current in turn until the cooling arrangement provided cannot cope with the increased power loss and the rectifier becomes thermally unstable. The conditions for this instability to arise are investigated quantitatively. Amongst other parameters such as mode of operation, cooling, etc., the conductivity of the semiconductor, and in particular the height of the potential barrier, have a paramount effect on the maximum voltage that can be withstood. The simultaneous requirements for large resistivity and barrier height severely restrict the choice of materials which can be used for efficient rectifiers.

The Role of the Self Magnetic Field in High Current Gas Discharges, by P. C. Thonemann and W. T. Cowhig.

ABSTRACT. It is shown that the self magnetic field of a high current discharge plays an important part in determining the radial electron density distribution. The effect of this magnetic field can be treated by adding a 'magnetic potential' term, $V_{\mathrm{m}} = \int_0^r \overline{w} H \, dr$ to the electrostatic potential V_{s} in the Boltzmann equation for the radial electron density distribution, $\overline{w}$ being the longitudinal electron drift velocity. The drift of electrons and ions to the tube walls is equalized at low arc currents by a radial electric field. Since the magnetic field reduces the drift of electrons to the wall whilst having little influence upon the ions, increasing the arc current leads to a progressive reduction of the radial electric field. Probe measurements in an arc at low pressures show that at currents over 50 amperes, the radial electric field is zero except for a narrow sheath at the wall. The axial density is then mainly determined by the self magnetic field. A theoretical expression is derived for the equilibrium density distribution assuming a balance between the diffusion rates due to the concentration gradient and the magnetic forces. Experiments in a mercury vapour arc at high currents support this theory.

The Relationship between the Radial Concentration Variations of excited Atoms and Electrons in a Discharge in Thermal Equilibrium, by H. Edels.

ABSTRACT. The excitation and Saha equations applicable to gaseous electrical discharges in thermal equilibrium are used to obtain convenient expressions for calculating the radial concentration variations of electrons and excited atoms when the radial intensity variation of one spectral line is known, and when the temperature on the axis of the discharge can be estimated.

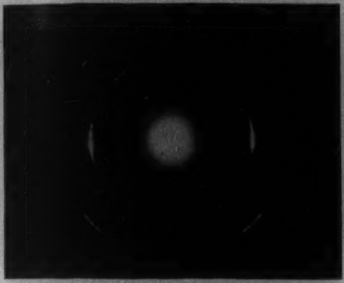

Figure 5. Cu foil, nearly normal transmission.

Figure 6. Annealed rolled Cu; reflection after etching.

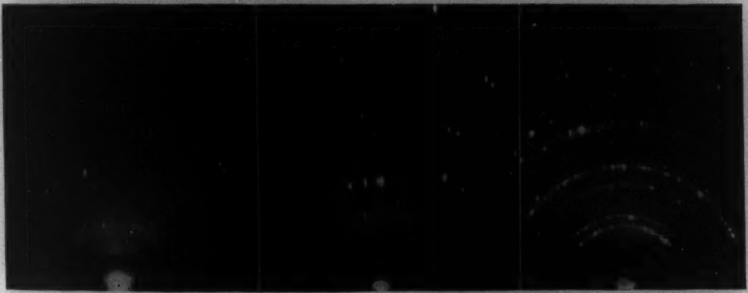

Figures 7, 8, 9. Recrystallized rolled Cu; reflection after etching.

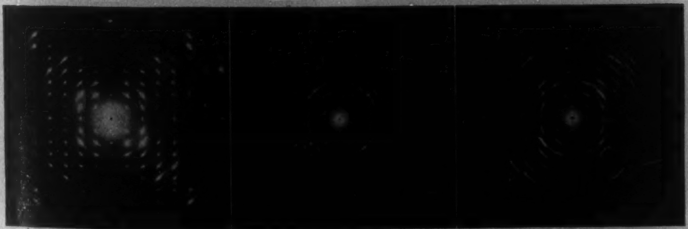

Figures 50, 51, 52. 5.6 Cyclo-penteno-1.2 Benzanthracene.

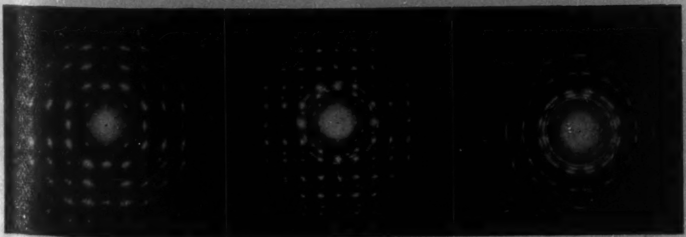

Figures 53, 54, 55. 1.2 Benzpyrene.

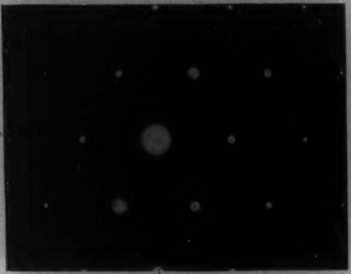

Figure 10. One CdI$_2$ crystal.

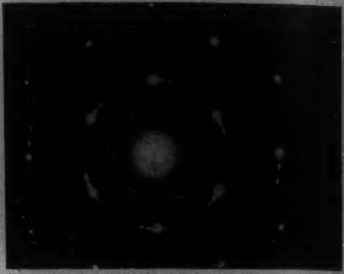

Figure 11. CdI$_2$ triplet; $\delta=6° 40'$.

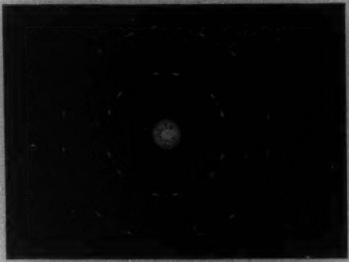

Figure 12. CdI$_2$ triplet; $\delta=9° 26'$.

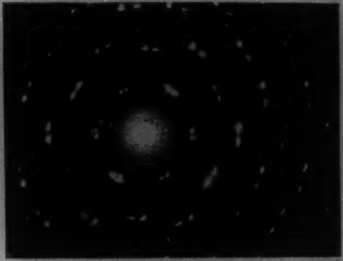

Figure 13. CdI$_2$ doublet.

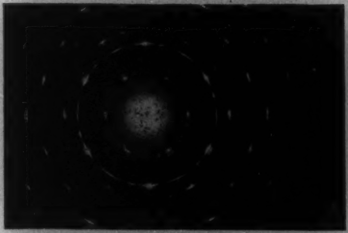

Figure 14. CdI$_2$.

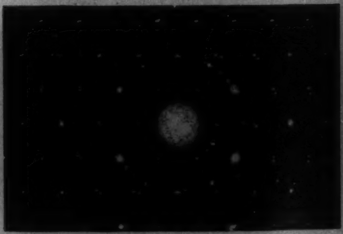

Figure 15. CdI$_2$.

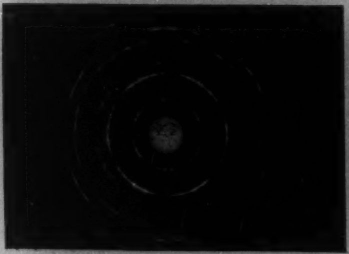

Figure 16. CdI$_2$ quintuplet.

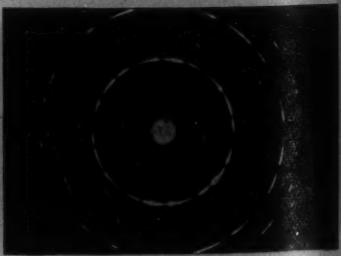

Figure 17. CdI$_2$ tailed arcs.

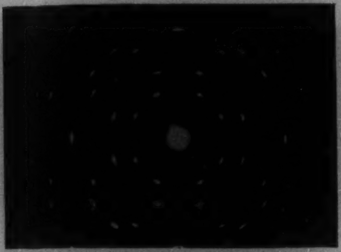
Figure 18. NaCl {001} doublet.

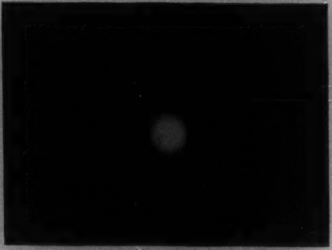
Figure 19. CuO flakes.

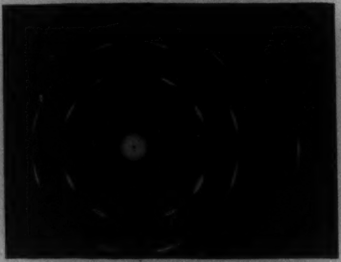
Figure 20. Pd leaf (arced doublet).

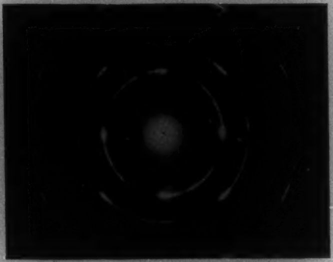
Figure 21. Pd leaf 'tadpole' arcs.

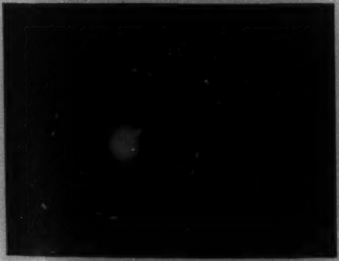
Figure 22. Al leaf, recrystallized.

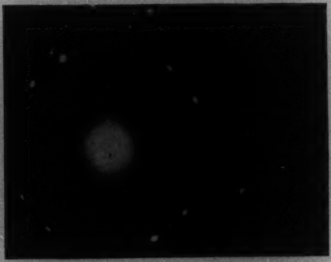
Figure 23. Al leaf, recrystallized.

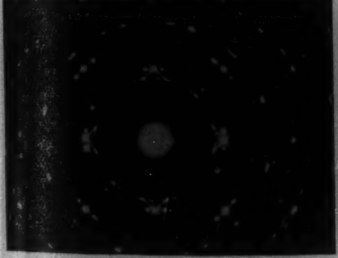
Figure 24. {111}-twinned Ag triplet.

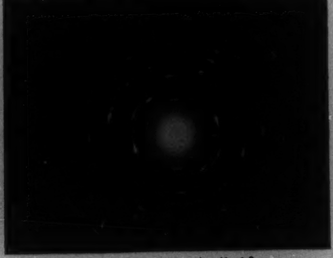
Figure 25. $NaNO_3$, 'tailed' arcs.

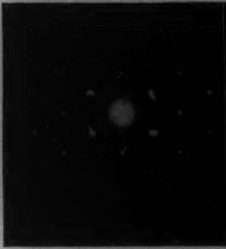

Figure 26 *a*. $C_{32}H_{66}$ doublet.

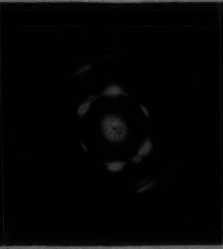

Figure 27. Paraffin wax.

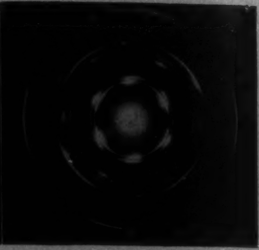

Figure 28. $C_{24}H_{42}$ (+Au rings).

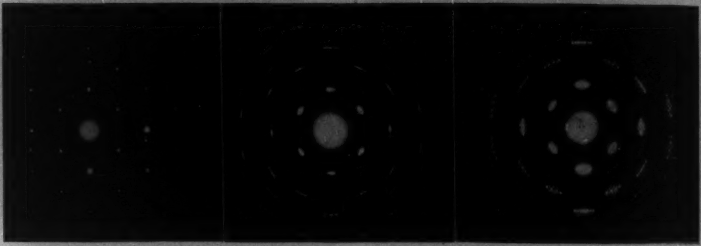

Figures 29, 30, 31. n-$C_{16}H_{33}OH$.

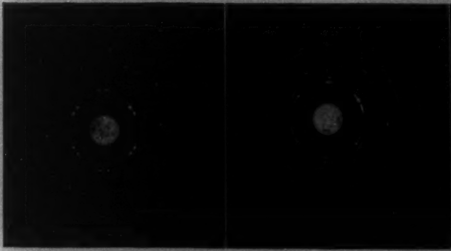

Figures 32, 33. n-$C_{16}H_{33}OH$.

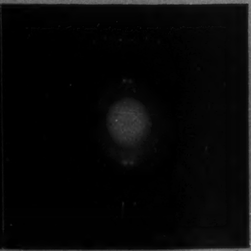

Figure 34. n-$C_{17}H_{35}I$.

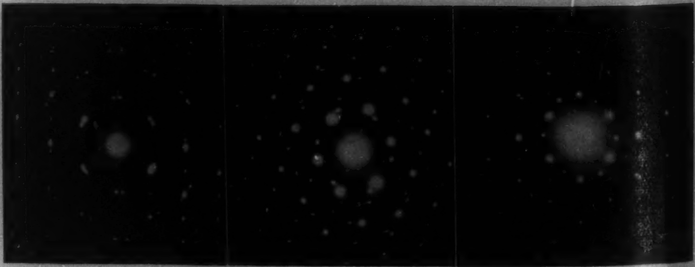

Figures 35, 36, 37. n-$C_{18}H_{37}OH$.

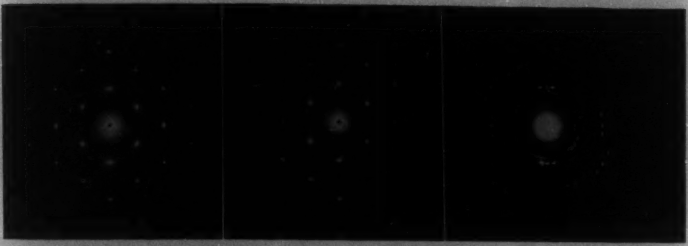

Figures 38, 39, 40. A long-chain wax.

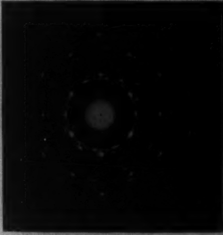

Figure 41. Elaïdic acid.

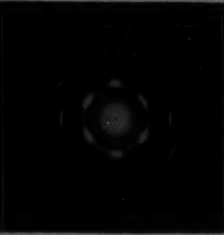

Figure 42. Fe^{+++} stearate.

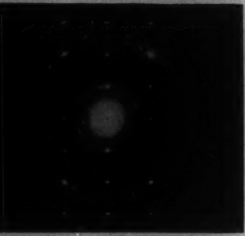

Figure 43. Urotropine.

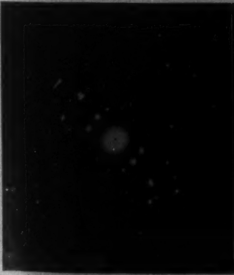

Figure 44. Anthracene.

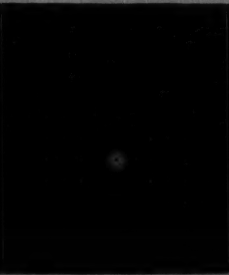

Figure 45 *a*. 1.2, 5.6-diB.A.

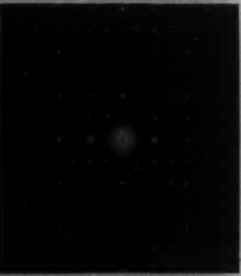

Figure 46. Chrysene.

Figure 47. 5Me . 1.2 B.A.

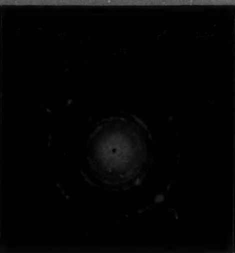

Figure 48. Naphthacene.

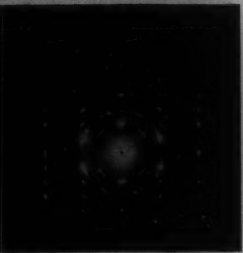

Figure 49*a*. Dispersol fast scarlet.

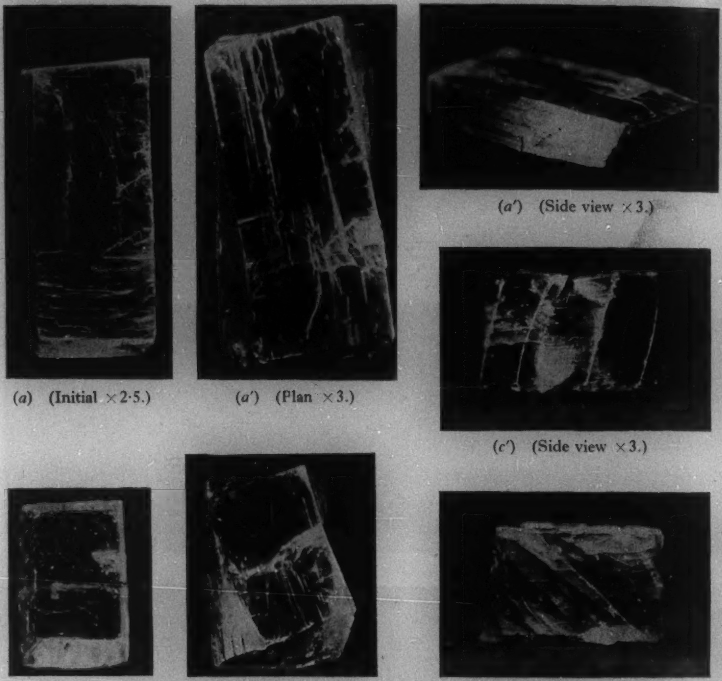

(*a*′) (Side view ×3.)

(*a*) (Initial ×2·5.) (*a*′) (Plan ×3.)

(*c*′) (Side view ×3.)

(*b*) (Initial ×2·5.) (*b*′) (Plan ×3.) (*d*′) (Side view ×3.)

Figure 56. Rotational slip in potassium ferrocyanide trihydrate; four crystals, *a*–*d*.

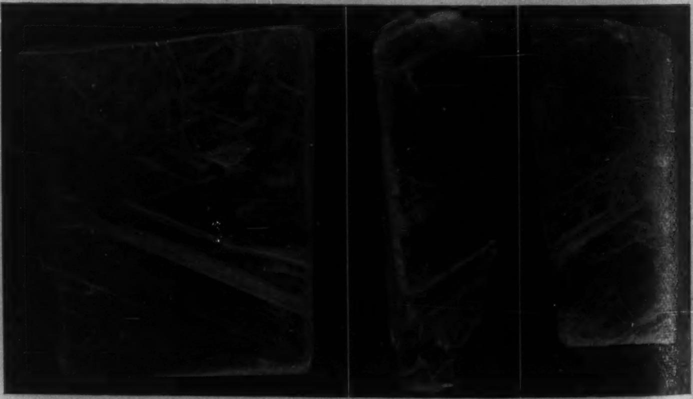

(*a*′) (× 5·5.) (*b*′) (× 5·5.) (*c*′) (× 5·5.)

Figure 57. Rotational slip in gypsum (plan views of three crystals).